Biomechanics of Lateral Hip Impacts: the Influence of Measurement Technique and Contact Area

by

Shivam Bhan

A thesis
presented to the University of Waterloo
in fulfillment of the
thesis requirement for the degree of
Master of Science
in
Kinesiology

Waterloo, Ontario, Canada, 2014

AUTHOR'S DECLARATION

I hereby declare that I am the sole author of this thesis. This is a true copy of the thesis, including any required final revisions, as accepted by my examiners.

I understand that my thesis may be made electronically available to the public.

Shivam Bhan

Abstract

The experiments presented in this thesis provide novel insight into two scarcely studied areas in the field of lateral hip impact biomechanics. The high energy nature of hip impacts requires high sampling rates for accurate study of hip impact dynamics. However, to date only optical motion capture, with relatively lower sampling rates (240-400 Hz), has been used to measure pelvic deflection during hip impact experiments with human participants. As such, the results from the first study compared the differences between two measurement systems (3D optical motion tracking and 2D high speed videography) in measuring common variables of impact biomechanics (peak force, time to peak force, peak deflection, time to peak deflection and energy absorbed). Although significant differences were seen between systems in measuring T_{Fmax} and E_{max}, the magnitude of differences were at or below 5% of the total magnitude of each measured variable. Furthermore, averaging impacts within a subject reduced the differences between systems for E_{max}. Furthermore, this study showed the effect of sampling rate on measuring hip impact dynamics, and how sampling at lower frequencies affects the aforementioned variables. Tests on the effect of sampling rate found differential effects contingent on the dependent variable measured. Sampling as low at 300 Hz, significantly reduced measures of F_{max} and D_{max}, but only by on average 0.7 and 0.5 %, respectively. Whereas measures of T_{Fmax} and T_{Dmax} increased by on average 9.5 and 6.8 %. Sampling E_{max} at 500 Hz and 300 Hz increased measures of impact absorption by 2.2 and 2.8 % respectively. Sampling at 4500 Hz was the lowest sampling rate that was not significantly different from 9000 Hz across all dependent variables.

The second study in this thesis investigates the influence of contact area on load distribution during lateral hip impacts. In summary, this study shows that all three time-varying signals ($F_{t,}$ FT_t and D_t) were significantly correlated with time-varying contact area (C_t). These results lend support to the possibility of modeling lateral hip impacts with contact models, but provide little support for a Hertzian model adaptation. Analysis on the relationships between body mass and BMI found both anthropometric measures to correlate significantly with peak impact force, but not with peak impact force directed to the greater

trochanter. These results bring into question the feasibility of modeling hip fracture risk with body mass or BMI as inputs, without further investigating the distribution of impact force to the greater trochanter. In this study only contact area was significantly correlated with all measures of GT specific loading, and has never before been implemented in predictive modelling of hip fracture risk. Finally, this study found that although effective mass, total body mass and BMI were significantly correlated with the contact area at peak force, they only accounted for 21, 22 and 33% of the variance in *CA.* Altogether, this study sheds new light on the role that contact area plays in lateral hip impact loading and the importance of understanding load distribution during lateral hip impacts. It also highlights the importance of moving towards predictive models that incorporate more robust estimate of body composition and geometry, with hopes that these will better help estimate the risk of hip fracture.

Overall, this thesis provides insight into the expected differences between measuring hip impact dynamics with two, relatively different measurement techniques. In addition, it highlights the need for further study on the relationship between contact geometry and hip fracture risk, something not currently implemented in most hip fracture risk models.

Acknowledgements

"Give me six hours to chop a tree, I will spend the first four sharpening my axe."
-Abraham Lincoln

I gained a true understanding of preparation during my time at the University of Waterloo. Preparation for work, preparation for play, and preparation for life. My experience at this institution has been, to date, the single best decision I have made in my life. I would sincerely like to thank everyone who I have had the pleasure of meeting at UW. I hope that this school, especially the Department of Kinesiology, continues to be the fostering and inspiring place that it is for many years to come.

In particular, I would like to thank my supervisor, Dr. Andrew Laing for his constant support, insights and mentorship during my graduate education. I have improved myself both as a researcher and a student of science as a result of your guidance and tutelage. I would also like to thank my committee members Dr. Jack Callaghan and Dr. Richard Wells for their advice and guidance during the course of this project, and for making my graduate education an absolute pleasure. Thank you as well to Jeff Rice, who is the back bone of all the great research in the Department of Kinesiology.

I would also like to thank my friends and family for all the support and memories during my time at UW. Thanks to Tom, Jason, Nick, Laura and Bryan you are all better friends than you are scientists (zing). Lastly, to my mom, dad and sister, I love you and thank you for everything you have ever done for me.

Table of Contents

AUTHOR'S DECLARATION ii
Abstract iii
Acknowledgements v
Table of Contents vi
List of Figures viii
List of Tables xiii
Chapter 1 Thesis Overview 15
Chapter 2 Literature Review 21
2.1 Fall Related Injuries in Older Adults 21
2.2 Factors that Modulate Hip Fracture Risk 24
2.2.1 Mechanics of Falls from Standing and Age-related Changes 24
2.2.2 Hip Fracture Type In Relation to Bone Geometry and Quality 26
2.2.3 Tolerance of the Proximal Femur 29
2.2.4 Loads Applied to Proximal Femur 31
2.3 Variables that Modulate Hip Fracture Load 33
2.3.1 Pelvic Stiffness, Strain and Load Distribution 34
2.3.2 Contact Pressure during Lateral Pelvic Impact 38
2.4 Characterizing Pelvic Deflection and Contact Area 39
2.4.1 Quantifying Deflection during Impact 40
2.4.2 Contact Area 44
2.4.3 Conclusions 49
Chapter 3 The Effect of Motion Capture Technique and Sampling Rate on Biomechanical Measures of Lateral Hip Impact Response 50
3.1 Introduction 50
3.2 Methods 55
3.2.1 Participants 55
3.2.2 Experimental Protocol 56
3.2.3 Camera Calibration 59
3.2.4 Data Analysis 65
3.2.5 Statistics 68
3.3 Results 70

3.3.1 Effects of Motion Capture System 70
3.3.2 Effects of Sampling Rate 73
3.4 Discussion 76
3.4.1 Effects of Motion Capture System 79
3.4.2 Effects of Sampling Rate 86
3.4.3 Limitations 91
3.4.4 Conclusions 92
Chapter 4 Contact Area in Lateral Hip Impact Mechanics 93
4.1 Introduction 93
4.2 Methods 98
4.2.1 Participants 98
4.2.2 Experimental Protocol 99
4.2.3 Data Analysis 103
4.2.4 Statistics 104
4.3 Results 105
4.3.1 Time-varying Contact Area 105
4.3.2 Contact Area and Force Distribution 107
4.3.3 Contact Area and Anthropometrics 109
4.4 Discussion 111
4.4.1 Time-varying Contact Area 112
4.4.2 Contact Area and Force Distribution 116
4.4.3 Contact Area and Anthropometrics 122
4.4.4 Limitations 125
4.4.5 Conclusions 126
Chapter 5 Thesis Summary 127
References 129
Appendix A Synchronization and Drift Between OPT and HSV 148
Appendix B Empirical Cumulative Distributions 151
Appendix C Contingency Table Analysis 152
Appendix D Non-constant Errors in Deflection and Trapezoidal Integration 153

List of Figures

Figure 2.1: World-wide hip fracture incidence rates (women). Adapted from Kanis, Oden et al. (2012) 22

Figure 2.2 Hip fractures are specifically referred to as proximal femur fractures. Within the subset of proximal femur fractures are cervical, intertrochanteric and subtrochanteric classifications. Cervical neck fractures are those occurring at the femoral neck; intertrochanteric are those occurring between the greater and lesser trochanter; subtrochanteric are fractures which occur distal to both trochanters. 28

Figure 2.3: Biomechanical testing of the load capacity of the proximal femur is typically done in the simulated fall configuration. The specimen being tested is affixed to the apparatus at either the greater trochanter (shown) or the femoral head, and a lateral load is applied until failure. 29

Figure 2.4: Parameters of interest in mechanical strength testing of biological materials and structures. 30

Figure 2.5: Regional variation in soft tissue stiffness of the lateral pelvis in an older adult woman. Stiffness was measured with a hand held device with rigid surface area, that measured the deflection (and load) as the device was loaded to areas of the lateral pelvis. Adapted from Laing and Robinovitch (2008c).....37

Figure 2.6: Example peak pressure profiles from trials in the unpadded condition between participants of low (A) and high (B) BMI. For a low BMI participant in the unpadded condition, pressure centered over the GT and the contact area was small. For a high BMI participant in the unpadded condition, peak pressure occurred over the GT and contact area was larger compared to the low BMI participant in the same condition. the magnitude of pressure is indicated by a color scale. Pressure unit on a color bar is N/cm2 (1 N/cm2 = 10 kPa). Note the different pressure ranges in the scales for parts A and B (Choi et al., 2010a). 38

Figure 2.7: Example force vs. deflection traces from two individuals with varying BMI. Low BMI < 22.5 and high BMI > 28. Notice differences in the initial non-linear loading, followed by transition to linear and marked increase in stiffness, until a plateau near peak force.....43

Figure 2.8: Theoretical force-deflection curve for lateral pelvis release. This illustrates how the change in contact area (from 1 to 2) might potentially modulate the non-linear effective stiffness of the pelvis. 46

Figure 2.9: Hertz contact theory approximates the interaction of two elastic contact surfaces, whose curvature is defined by the inverse of the surface radius (R_1,R_2). The surfaces are depicted as axisymmetric about the axis S_A-S_B, with material properties defined by E_1 and E_2. Note for contact with a flat (planar) surface R = ∞. 48

Figure 3.1 The effect of sampling rate on the number of data points theoretically collected during various time to peak force durations seen in lateral hip impact studies. Solid traces indicate impact durations commonly seen during in-vivo “lateral pelvis release experiments. The dashed traces indicate impact durations seen

commonly during lateral impact studies conducted at higher impact velocities, with stiffer, cadaver specimens (3-4 m/s). The horizontal dashed line at 200 data points signifies the suggested number of data points for impact testing of materials (America Kessler and ASTM Committee D-20 on Plastics. 1987).....54

Figure 3.2: The participant was positioned on their left side with their pelvis supported by the nylon sling. The upper torso and shoulder, as well as the lower legs were contacting the ground, but not the force plate.....57

Figure 3.3: Visibility of the greater trochanter optical marker from the perspective of the HSV and OPT camera. The placement was determined to ensure the complete visibility of the marker throughout the entire impact trial by both motion capture systems.....58

Figure 3.4: Design of rigid body for HSV camera. To ensure that the OPT and HSV systems were tracking the same marker motion, this rigid body was used to align the HSV to the OPT system's global co-ordinate system. The difference in angle between the corresponding axes of the HSV rigid body and the global co-ordinate system of the OPT were minimized to below 0.5 degrees. 61

Figure 3.5: Birds eye view of the experimental set up. Labeled are four OPT camera banks (1-4), the HSV camera, the force plate, and the two computer systems needed to collect both systems (CPU). Dotted lines show the theoretical field of view of each camera. With the force plate centered in the middle of the capture volume, four OPT camera banks were used to allow for proper alignment of OPT and HSV. The second OPT camera bank (OPT 2) was aligned to view the HSV camera rigid body. This allowed for proper calibration of the HSV with respect to the OPT system, and subsequently, the impact event. 62

Figure 3.6: This figure illustrates the theoretical alignment of two cameras tracking a vertical displacement vector (light grey line). Since the intersection of two planes is a line, minimizing rotations about the x and y axis would assure the best alignment between the two camera systems. The OPT and HSV camera system were aligned to reduce rotations between the x and y-axes of the HSV rigid body and the OPT global co-ordinate system. 63

Figure 3.7: Steps to calibrating the HSV system with the OPT system, and also the image plane.....65

Figure 3.8: Example of spatial representation of object B in the object space, and it's corresponding representation (A) in the image plane of the high speed camera.....68

Figure 3.9: Time varying data showing trials which had the lowest differences between systems. A) Time-varying force for the same impact trial. B) Time-varying deflection for one impact trial. C) Force deflection trace for one impact. Black data traces are measured by the high speed videography system (HSV), while grey traces are data measured by the Optotrak system (OPT). 77

Figure 3.10: Time varying data showing trials which had the greatest differences seen between systems in this study. A) Time-varying force for the same impact trial. B) Time-varying deflection for one impact trial. C) Force deflection trace for one impact. Black traces are data measured by the high speed videography system (HSV), while grey traces are data measured by the Optotrak system (OPT).....78

Figure 3.11: Relationship between difference in time to peak force and the difference in energy absorption measured by each system. Difference was calculated by subtracting the respective value measured by the Optotrak system (OPT) from that measured by the high speed video system (HSV)..... **Error! Bookmark not defined.**

Figure 3.12: Time-varying difference traces calculated for the deflection signals measured by both systems from impact initiation until peak force. These traces were calculated by subtracting the deflection measured by the high speed video system (HSV) from the deflection measured by the Optotrak system (OPT) or every time point, for every impact. Different colours represent different impact trials. Of interest is the time varying bias that occurs as the impact trial propagates between the two systems. This can lead to significant differences between systems upon integration to calculate energy.....85

Figure 3.13: Mean percent difference in calculated dependent variable of interest at various sampling rates. Positive percent difference means the value increased compared to the value at 9000 Hz. A negative percent difference means the value decreased. Values are labelled with the standard errors for the percent difference. Not confidence intervals, which are shown in Table 3-4. * denotes sampling rates that were significantly different from the control 9000Hz level, as determined from the confidence intervals (Table 3-4). 88

Figure 3.14: The effect of sampling force deflection response of the pelvis at 300 Hz (black), compared to sampling it at 9000 Hz (grey) for two separate impact trials (separate participants). Panel A shows very little change in the force-deflection curve measured at 300 Hz, whereas data in in panel B is markedly different. The shape of the loading history has a large effect on how well reduced sampling can represent the underlying biological signal. 89

Figure 3.15: Percent difference from data measured at 9000 Hz to those measured at 4500, 1500, 500 and 300 Hz. Data for every trial analyzed is shown. Panel on the left is energy absorbed (E_{max}) and on the right is time to peak force (T_{Fmax}). Of interest is the variability that reduced sampling rates can have on estimates of energy absorbance, compared to time to peak force. Both variables increase in variability as data sampling is reduced to 300 Hz, but the trend is more apparent for time to peak force.....90

Figure 4.1: Visibility of the greater trochanter optical marker from the perspective of the HSV and OPT camera. The placement was determined to ensure the complete visibility of the marker throughout the entire impact trial by both motion capture systems. The participant was positioned on their left side with the pelvis supported by the nylon sling. The upper torso and shoulder, as well as the lower legs were contacting the ground, not impacting the pressure plate.....102

Figure 4.2: Selected deflection and contact area traces for four separate participants. The top two panels show participants from opposite ends of the BMI spectrum. A) Lower BMI participant (BMI=20.7 kg/m^2); B) higher BMI participant (BMI=30.8 kg/m^2). The bottom two panels show two participants with the highest two highest peak contact areas measured. A) lower BMI participant (BMI=22.5 kg/m^2) with a peak contact area of 251.3 cm^2; B) higher BMI participant (BMI=33.2 kg/m^2) with a peak contact area of 237.8 cm^2.....114

Figure 4.3: Selected force and contact area traces for four separate participants. The top two panels show participants from opposite ends of the BMI spectrum. A) Lower BMI participant (BMI=20.7 kg/m^2); B) higher BMI participant (BMI=30.8 kg/m^2). The bottom two panels show two participants with the highest two highest peak contact areas measured. A) lower BMI participant (BMI=22.5 kg/m^2) with a peak contact area of 251.3 cm^2; B) higher BMI participant (BMI=33.2 kg/m^2) with a peak contact area of 237.8 cm^2.....115

Figure 4.4: Correlations between loading parameters and contact area. The shade of each dot varies by the BMI of the participant according to the shade bar associated with each plot. 119

Figure 4.5: Load distribution images at peak force for six participants. The top three images are from three separate participants with a lower BMI (below 21 kg/m^2). The bottom three images are from three participants with a higher BMI (above 28 kg/m^2). Note the differences in contact area between participants of lower and higher BMI. Also of interest are the differences in the range of loads measured by each sensor in the pressure plate (evidenced from the range of the colour bars to the right of each image) between lower and higher BMI participants. Units for the colour bars are in Newtons, images depict each sensor of the pressure plate (64 x 64 =4096 sensors of 0.762 x 0.508 cm dimensions). 120

Figure 4.6: Pressure at peak force for two subjects who had relatively differing body mass indices (A=22.5 kg/m^2, B=33.2 kg/m^2), but similar contact area (A=247.1 cm^2, B=237.8 cm^2). Units for the colour bars are in Newtons, images depict each sensor of the pressure plate (64 x 64 =4096 sensors of 0.762 x 0.508 cm dimensions). 121

Figure 4.7: Correlations between body mass (*Mass*), body mass index (*BMI*) and effective mass (m_{eff}), with contact area (measured at peak force). 124

Figure 4.8: Representative square wave trial used to assess the synchronization of the OPT and HSV system by external trigger. Black tracing shows the square wave as measured by HSV, while the grey tracing shows that measured by the OPT. 148

Figure 4.9: Representative derivatives of the square wave trials shown in Figure 5.1. The spikes indicate where the square wave changed levels. Numbers indicate the difference in time of pulse measured between systems (by frame). Positive numbers indicate that the HSV measured a change in the square wave later than the OPT. Black tracing shows the square wave as measured by HSV, while the grey tracing shows that measured by the OPT. 149

Figure 4.10: Change in agreement between systems as a function of collection duration. Each trace is from a separate pilot trial (colour coded). Positive values indicate that HSV measured a change in square wave voltage later than the OPT (vice versa for the negative values). Notice how drift increases as a function of time, but the direction of the drift is not systematic, meaning in some trials the OPT was faster (negative values), while in other the HSV was faster. 150

Figure 4.11: Empirical cumulative distributions for each dependent variable of interest. The abscissa of each plot is logarithmic to allow for better visualization of the

differences between systems at end ranges. Dark black lines depict measurements from the HSV system, and grey lines depict the OPT.....151

Figure 4.12: Three difference traces that were created to simulate non-constant difference between systems. Separately, each one of these traces was added to an actual collected deflection trial from a participant. Subsequently, the energy absorbance was calculated. This was then compared to the energy calculated for the unadjusted force deflection trial (See Figure 4.13). 154

Figure 4.13: Force deflection tracings for four separate trials. The black trial is an actual impact trial measured in this study. The rest of the trials (three in total) are hypothetical force deflection tracings if the deflection had an additional error in it. The peak deflection error for each force deflection trace corresponds with the trace in Figure 4.12. Values in the legend are energy calculations for that corresponding force deflection trace. 129

List of Tables

Table 3-1 Anthropometrics for thirteen participants recruited in study. 55

Table 3-2: Mean and bootstrapped bias-corrected and accelerated 99% confidence intervals (BCa) for the difference in the measurement of the dependent variable of interest between the HSV and OPT systems (HSV value minus the OPT value). BCa intervals were calculated over 5000 iterations. A significant difference between systems was concluded if the confidence interval did not include zero mean difference. Significantly different variables, by this definition, are denoted by *. 71

Table 3-3: Subject level dependent variables measured for the HSV and OPT systems, at two drop heights tested. Main effect of height was ignored, but significant effects of system and a height by system interaction was evaluated. Data presented in parentheses are standard deviations. Variables that were deemed significantly different ($p < 0.05$) are denoted by *.....72

Table 3-4: Average and bootstrapped bias-corrected and accelerated 99% confidence intervals (BCa) for the mean difference in the measurement of the dependent variable of interest between 9000 Hz and the subsequent sampling rate in question. Positive values indicate the measured value increased compared to that measured at 9000 Hz. BCa intervals were calculated over 5000 iterations. Significant difference between systems were determined likely if the confidence interval did not include zero mean difference. Significantly different variables are denoted by *. 74

Table 3-5: Subject level dependent variables measured across five sampling rates. Numbers in parentheses are standard deviations of the means above them. P-values denoted are for overall main effect of sampling rate tested for that variable. Sampling rate had a significant main effect on every variable measured, and variables measured that were significantly different compared to the 9000 Hz condition (pairwise post-hoc analyses) are denoted by *. All significance levels were evaluated at $\alpha < 0.05$.....75

Table 4-1: Anthropometrics for twenty female participants recruited in study.....99

Table 4-2: Correlations between time-varying contact area with time varying-force, transformed time-varying force, and time varying deflection. Correlations were calculated for every impact trial, and then averaged within participants. Bootstrapped mean correlations (bias corrected and accelerated) were calculated through 5000 iterations to determine the 95% confidence interval. A significant correlation was concluded if the confidence interval did not include zero, and is denoted by *. 106

Table 4-3: Mean values for impact force measures in this study. Also reported are standard deviations (SD) and coefficient of variations (COV).....107

Table 4-4: Pearson product-moment correlations calculated between previously cited measures of hip fracture risk and five dependent variables of load distribution.....108

Table 4-5: Mean contact area and body anthropometry measured across twenty participants. Also shown are standard deviations and coefficient of variations. 109

Table 4-6: Correlations between contact area at peak force (CA) and three common variables associated with hip fracture risk: body mass (*Mass*); body mass index (*BMI*); effective mass (m_{eff}). Pearson correlations significant at the 0.05 level are denoted by *.....110

Chapter 1
Thesis Overview

Annually, there are an estimated nine million osteoporotic fractures worldwide. Of these nine million, 1.6 million are of the hip (Cummings and Melton, 2002). The majority of these hip fractures are caused by direct lateral-falls on the greater trochanter (Courtney et al., 1994; Hayes et al., 1996; Nevitt and Cummings, 1993), with the estimated economic burden of these injuries topping $2 billion annually in Canada (SMARTRISK, 2009). As a result, an extensive amount of research has focused on the mechanics of falls in efforts to better predict and reduce the risk of fracture for a given individual.

From an engineering perspective, the risk of failure for any structure is fundamentally modelled as the ratio of applied load to load capacity. In the case of hip fracture, this refers to the ratio of the load applied to the greater trochanter during a fall, to the capacity of that hip to withstand such a load. If load surpasses capacity, the structure will fail.

The efficacy of any risk predicting model depends heavily on the inputs for that model. If inputs such as contact area, material stiffness, strain or applied stress are inaccurate or even nonexistent, estimating hip fracture risk becomes meaningless. Thus, any benefit from the use of predictive models in hip fracture research depends on sufficient and accurate characterization of the variables that best estimate the dynamic response of the pelvis to impact loads, and understanding how variations in these inputs can cause changes in predicted loads.

This thesis attempted to address the unknowns relating to measuring inputs commonly used in the field of hip fracture mechanics, as well as explore understudied ones.

Specifically, the first study focused on the methods of quantifying the dynamics response of the pelvis, and the effects of sampling rate on measuring that response. The second study focused on contact area, and how it varies with force, deflection and body anthropometry. In addition, it investigated the extent to which body anthropometry and contact area explain the variability in impact load distribution.

STUDY 1

In-vivo studies of fall related hip impacts by Laing and Robinovitch (2010) directly measured the force-deflection response of the pelvis during low velocity "pelvis release experiments" (Robinovitch et al., 1991). This method involved tracking a marker on the opposite greater trochanter of the impacting hip, during the compressive phase of impact. In their study, pelvic deflection was measured with an eight-camera optical motion tracking system, sampling at 240Hz, whereas subsequent studies using this method have sampled pelvic deflection at 400Hz (Bhan et al., 2013; Levine et al., 2013; Levine, 2011). Elsewhere, blunt lateral impact studies by Viano and colleagues (1989a; 1989b; 1983) used load cells, accelerometry and high-speed videography, sampling at 500 to 2000Hz, to quantify the load, compression and force-deflection response of cadaver specimens (hip and thorax) to impact loads in simulated automobile collisions. Similar studies of side-impact vehicle collisions, have measured pelvic deflection at 500 and even 1000 Hz sampling rates. The varied use of videography and optical motion capture raises obvious concerns of the comparability between seemingly different methods, and whether previously used sampling rates have been sufficient. Sampling pelvic deflection at higher rates provides two advantages: 1) lower

sampling rates might not accurately capture peak pelvic deflection (a popular biomechanical variable), as the high frequency nature of impacts might result in underestimation of peak pelvic deflection; 2) higher sampling rates allow for a greater number of data points to define the force-deflection curve of the pelvis, which allows for more accurate modelling of the system (characterizing stiffness, energy absorption). Currently, technological limitations require the use of high speed videography to obtain these higher sampling rates (i.e. over 1500 Hz). Unfortunately, high-speed videography has never been used with lateral pelvis release experiments and therefore it would be beneficial to compare high speed video to previously used methods.

Accordingly, the purpose of the first study of this thesis was two-fold: 1) to determine the effects of motion capture system (3D optical motion tracking vs. 2D high speed videography) on five commonly reported measures of impact severity (peak force, time to peak force, peak deflection, time to peak deflection and energy absorbed); and 2) to determine the effect of sampling rate on the five aforementioned discrete measures of impact severity. Thirteen participants were recruited for lateral pelvis release experiments, where pelvic impact force and deflection were measured simultaneously with the two different motion tracking systems, at two drop heights (1.5 cm and 5cm). Data collected with high speed videography system was then used to determine the effect of sampling rate (9000 Hz compared to 4500, 1500, 500 and 300 Hz) on measures of impact severity.

It was hypothesized that there would be no significant difference in any of the dependent measures of impact severity (peak force, time to peak force, peak deflection, time to peak deflection and energy absorbed) between the two motion capture systems (3D optical

motion tracking and high-speed videography) sampling at 1500 Hz, for either drop height (1.5cm and 5cm). Furthermore, it was hypothesized that sampling at lower rates would reduce the measured peak force, peak deflection and energy absorbed, while increasing the time to peak force and time to peak deflection when compared to the "gold-standard" at 9000 Hz.

STUDY 2

Direct impact on the trochanteric area of the hip during a sideways fall is particularly detrimental in the event of a fall (Hayes et al., 1996). As a result, many biomechanical interventions have been engineered to mitigate the force directed to the greater trochanter during an impact. Previous research has shown a positive correlation ($r = 0.86$) between BMI and soft tissue depth above the greater trochanter (Maitland et al., 1993), and it has been suggested that the additional soft tissue helps to reduce total pelvic stiffness and subsequently reduces the force transmitted to the greater trochanter (Laing and Robinovitch, 2008b; Robinovitch et al., 1995b). Interestingly, confounded within BMI (calculated as the mass of a person in kg divided by the square of their height in meters) is mass, which is directly related the impact energy (kinetic energy = $1/2mv^2$, where m = mass and v = linear velocity). Therefore, the increased mass typically associated with higher BMI would be expected to increase impact energy (and potentially increasing impact force). Mass has been used as a predictor of impact load previously (Dufour et al., 2012) and one finite element study suggests a detrimental effect of body mass, independent of BMI, on risk of pelvic fracture

(Kim et al., 2013). Nevertheless, epidemiological literature continues to affirm a reduced risk of hip fracture for the elderly with high BMI (Armstrong et al., 2011; Morin et al., 2009). Although, a single-degree-of-freedom system approach has been beneficial in furthering our understanding of the mechanics of hip impacts, and predicting impact forces (Laing and Robinovitch, 2010; Robinovitch et al., 1991, 1997b), no literature exists on the spatial distribution (i.e. contact area) of loads on lateral pelvis during hip impact. Additionally, little is known about how this load distribution changes as a function of individual anthropometries (ex. mass, BMI etc.), and how it relates back to hip fracture risk. It remains unknown if the reduced risk of hip fractures associated with higher BMI, is correlated with the load distribution in the geometry of this population.

Accordingly, there were three primary objectives to this study, with the overall purpose to investigate the relationships between contact area and load distribution with respect to impact force, pelvic deflection and three anthropometric variables associated with hip fracture risk. Specifically, the second study of my thesis investigated whether: 1) time-varying force (F_t) and deflection (D_t) were significantly correlated (Pearson product-moment correlation) with time-varying contact area (C_t) during the compressive phase of a lateral hip impact (from impact initiation to peak force), and if transformation of the impact force (power law transformation, FT_t) was more highly correlated with contact area; as suggested by Hertzian contact theory; 2) if contact area at peak force was significantly correlated with different anthropometric variables associated with hip fracture risk (effective mass, total body mass, BMI); and 3) how contact area at peak force was associated with force distribution, specifically total peak force and force within a 5cm radius circle surrounding the

greater trochanter (*GT relevant force*). Particularly, how peak impact force (F_{max}), normalized peak impact force (F_{max}/m_{eff}), GT relevant peak force (F_{GT}), normalized GT relevant peak force (F_{GT}/m_{eff}) and the percent of total peak force directed to the GT relevant area ($F_{GT\%}$) correlated with the total contact area at peak force (*CA*), total body mass and BMI.

It was hypothesized that: 1) time varying contact area would be positively correlated with time-varying impact force and deflection, with power-law transformation of impact force being correlated to a greater degree with time varying contact area; 2) contact area at peak force would be positively correlated with effective mass, total body mass and BMI; and 3) peak impact force (F_{max}) would be positively correlated with total body mass, BMI and *CA*. Normalized peak impact force (F_{max}/m_{eff}) would not be significantly correlated total body mass, BMI or *CA*. GT relevant force (F_{GT}), normalized GT relevant force (F_{GT}/m_{eff}) and the percent of total peak force directed to the GT relevant area ($F_{GT\%}$) would be correlated with the total contact area at peak force (*CA*), total body mass and BMI.

Chapter 2
Literature Review

2.1 Fall Related Injuries in Older Adults

Hip fractures in older adults are a major public health concern. The lifetime risk of hip fracture for white, American women, from 50 years of age and onwards, is approximately 17% (Melton, 2000). The majority of hip fractures, as determined by post-fracture patient reports, are caused by direct lateral falls impacting the greater trochanter (Courtney et al., 1994; Hayes et al., 1996; Nevitt and Cummings, 1993). Recent numbers from the province of Ontario show that 1548 (per 100,000) hip and thigh injuries, resulting from falls, required hospital visits for adults over 80 years of age (OIDR 2011). In Canada, these falls and the catastrophic fractures they cause, represent the greatest economic burden on health care resources associated with incident fractures (Hopkins et al., 2012; Leslie et al., 2011).

There are approximately 23,000 incidents of hip fracture every year in Canada, with associated treatment costs of about $1 billion (Papadimitropoulos et al., 1997). Some studies estimate hip fractures cost the public Canadian healthcare system, $45,715 (per patient) in excess costs, when compared to matched controls (Hopkins et al., 2012). The costs are even higher in the U.S. with nationwide annual treatment costs approximated at $10 billion (Melton, 1993). Without improvements in prevention, hip fracture incidence is expected to increase 4-fold by the year 2041 due to the demographic shifts towards a more aged population, and the exponential increase in fracture risk that accompanies advancing age (Jaglal et al., 1996, Papadimitropoulos et al., 1997, Wiktorowicz et al., 2001).

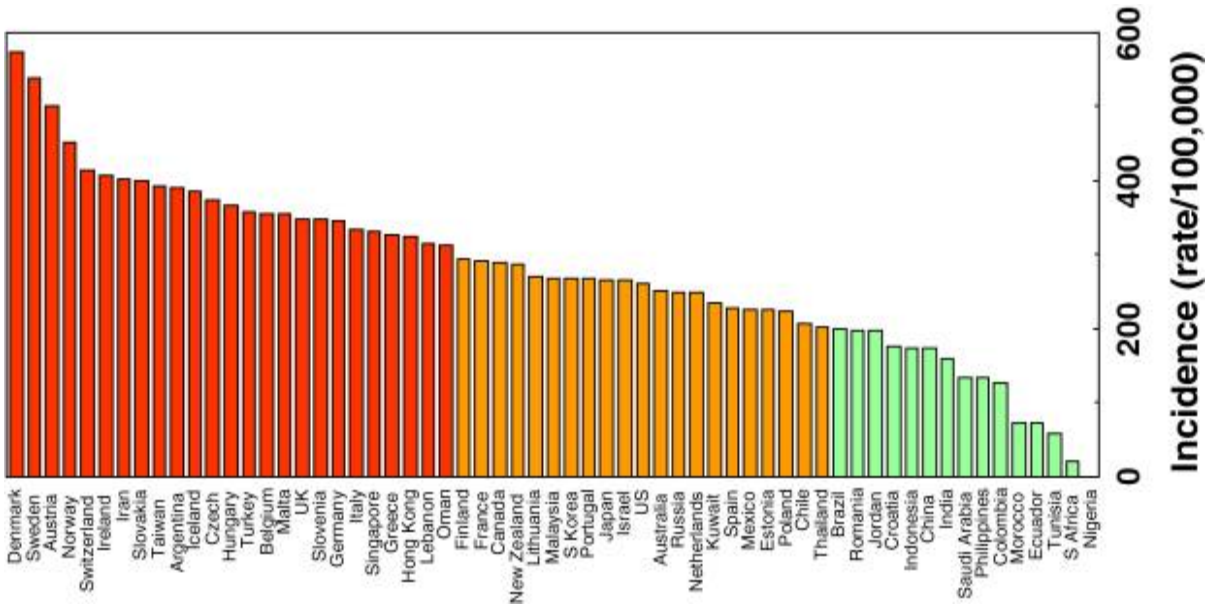

Figure 2.1: World-wide hip fracture incidence rates (women). Adapted from Kanis, Oden et al. (2012)

Recent evidence suggests that current screening strategies and pharmaceutical interventions have tempered the expected rate of increase in hip fracture incidence in Canada where all seniors have universal access to medical treatment (Leslie et al., 2009). However, globally, the reduction in incidence is less definitive (Kanis et al., 2012). In Norway and Sweden, where hip fracture rates are amongst the highest in the world (Figure 2.1), there has been a decrease in incidence over the past decade (Nilson et al., 2012; Omsland et al., 2012). Contrastingly, certain Asian countries are reporting an increase in the rate of hip fractures (Arakaki et al., 2011; Yoon et al., 2011). It is speculated that this increasing trend will continue as the demographics in certain Asian nations shift towards an increasingly aged population (Dhanwal et al., 2010; Dhanwal et al., 2011). Although the global variation in hip

fracture incidence is pronounced, the debilitating effect a hip fracture has on an individual's quality of life is more so.

Hip fractures cause increased mortality (Empana et al., 2004; Ioannidis et al., 2009; McColl et al., 1998; Meyer et al., 2000; Wolinsky et al., 1997) and declines in mobility, physical activity, and functional independence (Norton et al., 2000; Wolinsky et al., 1997). Even when injuries do not occur following a fall, the subsequent 'fear of falling' that develops can trigger a cascade of diminished mobility, activity, strength, coordination, and independence (Howland et al., 1998; Jellesmark et al., 2012; Visschedijk et al., 2010).

The need for additional prevention efforts to reduce the burden of these hip fractures is immense. Passive biomechanical interventions such as wearable hip protectors (i.e. protective padding systems built into garments) have shown a capability to reduce the severity of an impact (Ishimaru et al., 2012; Koike et al., 2009; Laing and Robinovitch, 2006b; Laing and Robinovitch, 2008a; Nabhani and Bamford, 2002), and to reduce the risk of hip fractures in frail older adults (Kannus et al., 1999; Lauritzen et al., 1993). Similarly, compliant flooring systems have shown the capacity to absorb impact energy from a fall on the lateral pelvis (Casalena et al., 1998; Laing and Robinovitch, 2009; Laing et al., 2006; Maki and Fernie, 1990; Simpson et al., 2004; Sran and Robinovitch, 2008). The effectiveness of these intervention strategies stem from their ability to modulate the load response characteristics of the impacting hip. Furthermore, the designs of these interventions are based off a large volume of literature defining parameters which modulate the impact load and subsequent risk of fracture.

2.2 **Factors that Modulate Hip Fracture Risk**

Predicting the likelihood that a fall will result in a hip fracture is a complex problem. From a structural engineering perspective, the risk of structural failure can be reduced to two simple variables; applied load and load tolerance. If the load applied to a structure exceeds its capacity to withstand that load, the structure will fail, or in the case of bone, fracture (Sellier, 1965). In the field of hip fracture research, this requires accurately characterizing the factors that modulate loads applied to hip (geometry, impact velocity, deformation, stiffness) during a lateral fall and the tolerance of the hip (incorporating loading direction and loading rate) (Courtney et al., 1994; Ford et al., 1996; Pinilla et al., 1996).

2.2.1 **Mechanics of Falls from Standing and Age-related Changes**

Typically, the available energy from a standing-height fall exceeds that required to fracture the proximal femur (Courtney et al., 1995; Lotz and Hayes, 1990; Robinovitch et al., 1991). Yet, almost counter-intuitively, only 1-2% of falls in older adults result in a hip fracture (Sattin, 1992; Tinetti et al., 1988). Variations in fall bracing strategies have been a proposed explanation for this discrepancy. Upper-limb bracing strategies (Feldman and Robinovitch, 2007; Hsiao and Robinovitch, 1998) and energy absorption in the lower limbs (Sandler and Robinovitch, 2001) are suspected to cause the lower impact velocities measured in experiments of young subjects falling from standing, when compared to those predicted by free-fall assumptions (Hsiao and Robinovitch, 1998; Robinovitch et al., 1991; van den Kroonenberg et al., 1996). Hsaio and colleagues (1998) found that during unexpected sideways falls initiated by sudden translation of a support surface, young adults tended to

avoid hip impact by rotating their trunk forward during descent to land on both outstretched hands. Feldman and colleagues (2007), also testing young adults, found that the hand impacted before the hip in a vast majority (about 95% of the 39 trials conducted) of falls initiated by a translating floor surface, and that the knee impacted (in 57% of trials) before the hip. Furthermore, they found that impact velocity of the pelvis decreased when the time interval between hand and pelvis impact increased (presumed to be result of greater upper extremity energy absorption). Even though sideways falls can produce a wide range of impact configurations (Robinovitch et al., 2009), some studies have even shown bracing strategies to reduce hip impact velocities to as low as 0.8 m/s (Feldman and Robinovitch, 2007).

The benefit of reducing the impact velocity of the hip can be explained by simple impact models, where the body is considered to be a damped single-degree-of-freedom mass-spring system with a linear spring constant. During an impact of this model, it is assumed that all of the kinetic energy of the mass ($E_{KE} = 1/2mv^2$) is converted into elastic strain energy ($E_{SE} = 1/2kx^2$) upon compression (where m = mass of object, v = velocity of mass, k = spring stiffness, x = linear deflection). This means that the energy at impact increases with the square of the velocity at impact. Thus, reducing impact velocity is an important factor that reduces impact energy, and presumably impact loads, as well as the risk of hip fracture.

Interestingly, some evidence suggests that these same bracing mechanisms that reduce impact velocity in young adults, are diminished in the older adults. In terms of upper limb bracing, reduction in movement time has been shown in groups of older adult (> 70 years of age) women when compared to young women (18-35 years of age) as they moved

their hands to a protective position in preparation for sideways fall (DeGoede et al., 2001; Robinovitch et al., 2005).With regards to lower limb bracing, Wojcik and colleagues found, when examining single-step recoveries from forward-fall tether release experiments, that younger women completed a step an average 60 ms faster than older adult women (Thelen et al., 1997; Wojcik et al., 1999, 2001). This suggests that the way a person braces for an impact plays a substantial role in mitigating injury risk, and aging related changes in mobility and movement time diminish the ability of the faller to reduce impact velocity of the body; which might contribute to the increased incidence of fracture in older adults.

2.2.2 **Hip Fracture Type In Relation to Bone Geometry and Quality**

Hip fractures, or more specifically fractures of the proximal femur are categorized by their anatomical location. The most common, fall related, proximal femur fractures are categorized as cervical, intertrochanteric, or subtrochanteric. Cervical neck fractures are those occurring at the femoral neck; intertrochanteric are those occurring between the greater and lesser trochanter; and subtrochanteric are fractures which occur distal to both trochanters (Figure 2.2) (Marks et al., 2003).

Post-fracture mortality rates have been correlated to fracture type; with some studies reporting intertrochanteric (between the lesser and greater trochanter) fractures having a higher mortality risk compared to cervical fractures (Haentjens et al., 2007; Keene et al., 1993; Lawton et al., 1983) and some reporting no difference (Aharonoff et al., 1997; Kenzora et al., 1984). Elsewhere, studies have shown that women more frequently suffer cervical fractures compared to men ($p = 0.002$), and that bone structural geometry, including femoral

neck axis length or hip axis length, femoral neck-shaft angle and cortical thickness, vary between fracture types (Dincel et al., 2008; Gnudi et al., 2002; Mautalen and Vega, 1993; Partanen et al., 2001; Pulkkinen et al., 2006). A recent experimental finite element study by Koivumaki (2010) evaluated the predicted principal strain distributions of 13 cervical and 13 trochanteric (intertrochanteric and subtrochanteric) fractures. They found a significant difference in the two-dimensional strain ratio (compression to tension) between the two fracture types, and that their model could predict the fracture type based off of the local estimated strains (for 22 out of 26 specimens).

Some studies have shown that reduced bone mineral density (BMD) has been correlated with an increased chance of hip fracture (Bruyere et al., 2009; Cheng et al., 1997; Pande et al., 2000). Others suggest that age-related declines in BMD and the increased incidence of falls does not fully account for the exponential rise in hip fracture incidence with aging (Horsman et al., 1985; Pinilla et al., 1996; Wainwright et al., 2005). Over 80% of low trauma fractures occur in people who do not have bone-degrading diseases like osteoporosis (Siris et al., 2004). This suggests that after accounting for bone quality, age-related changes in neuromuscular function might contribute more to the higher incidence of these fractures in older adults (Cummings and Nevitt, 1989, 1994; Jarvinen et al., 2008).

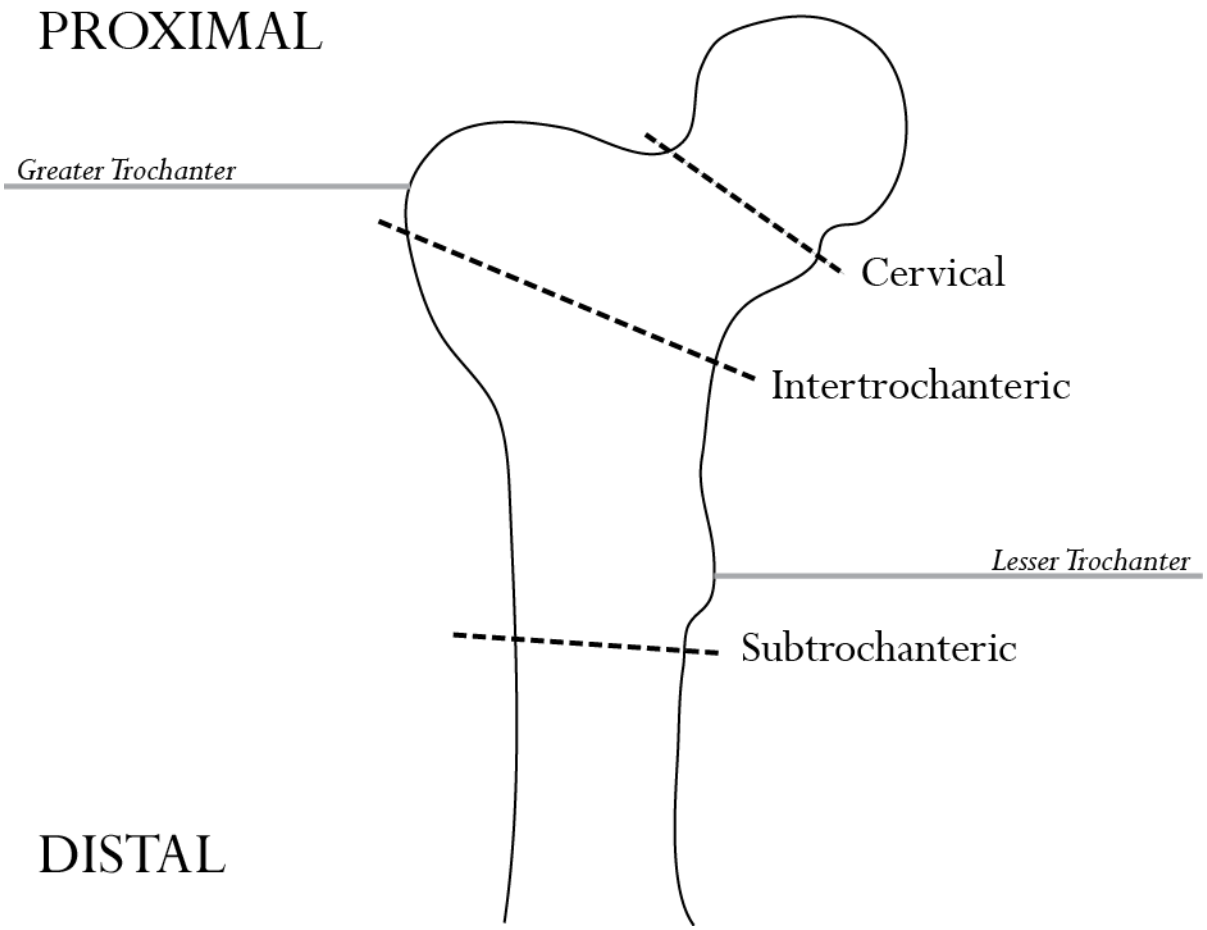

Figure 2.2 Hip fractures are specifically referred to as proximal femur fractures. Within the subset of proximal femur fractures are cervical, intertrochanteric and subtrochanteric classifications. Cervical neck fractures are those occurring at the femoral neck; intertrochanteric are those occurring between the greater and lesser trochanter; subtrochanteric are fractures which occur distal to both trochanters.

2.2.3 **Tolerance of the Proximal Femur**

To experimentally measure femoral neck strength, the proximal end of the femur is mounted in a loading fixture, either by embedding it in plastic resin or clamping it in place, and a force is applied to the femoral head until the femoral neck fractures. When considering lateral falls, a simulated fall configuration is normally used to test the strength of the proximal femur under more realistic loading conditions (Figure 2.3) (Hayes et al., 1991).

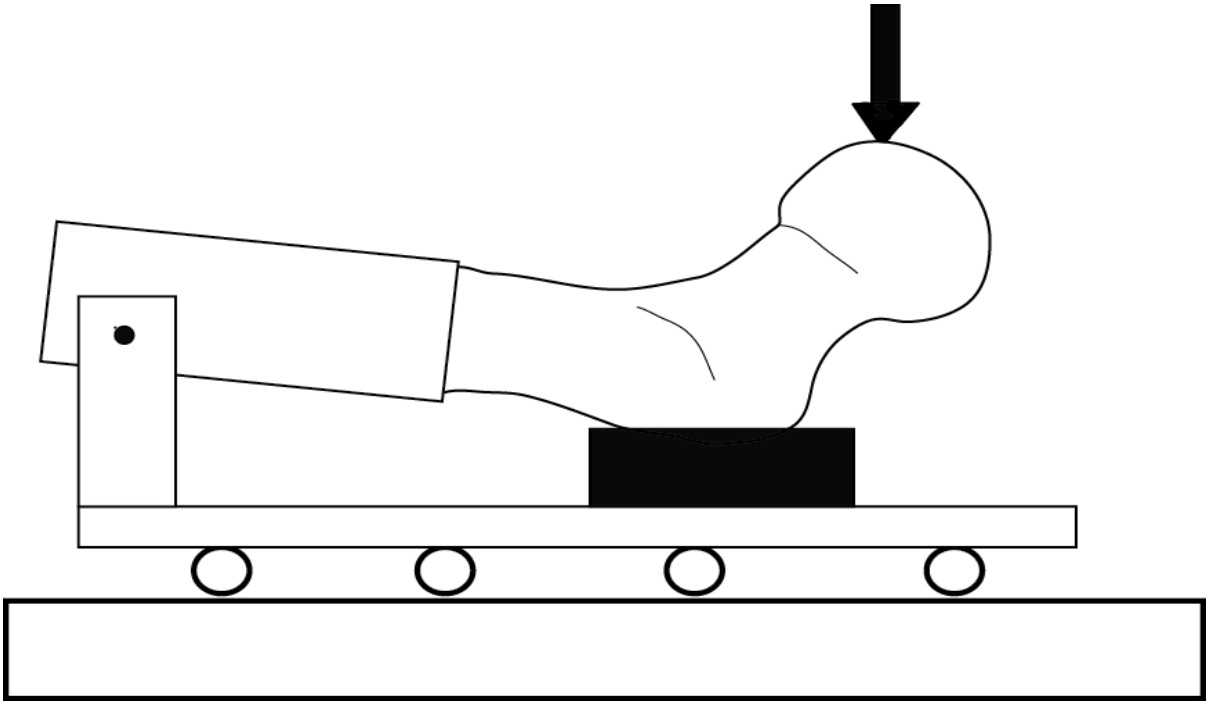

Figure 2.3: Biomechanical testing of the load capacity of the proximal femur is typically done in the simulated fall configuration. The specimen being tested is affixed to the apparatus at either the greater trochanter (shown) or the femoral head, and a lateral load is applied until failure.

The outcome measures of interest from mechanical testing come from the load (or force) applied to the structure and the resulting displacement (or deflection). The stiffness, ultimate load (force at failure), work to failure (area under load-displacement curve) and ultimate displacement are all parameters that reflect a different property of the structure (Figure 2.4).

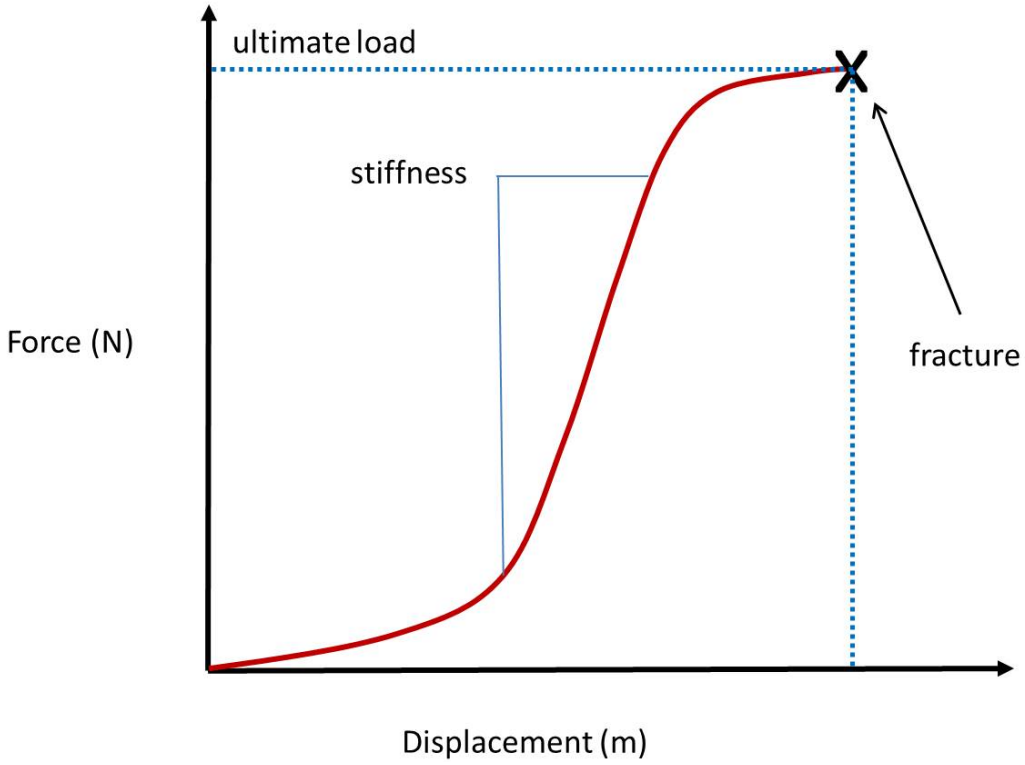

Figure 2.4: Parameters of interest in mechanical strength testing of biological materials and structures.

In-vitro mechanical failure testing of excised cadaveric human femurs have shown variable fracture-energy values across age groups. For example, Courtney et al. reports the mean (SD) energy to fracture to be significantly lower for older specimens (5.5 ± 3.0 J) compared to younger ones (18.0 ± 8.3 J) (1995). Additional studies have found energy-to-fracture values ranging from 5 to 104 J (Courtney et al., 1994; Esses et al., 1989; Lotz and Hayes, 1990), with bone mineral density, rate of loading and loading direction all showing to have significant influence on the amount of energy the proximal femur can absorb (Beason et al., 2003; Courtney et al., 1994). With regards to hip fracture risk, this suggests that the energy required to fracture the proximal femur can be an order of magnitude smaller than the potential energy available during a fall from standing (Courtney et al., 1995; Lotz and Hayes, 1990; Robinovitch et al., 1991).

In terms of force at failure, the fracture threshold for the proximal femur has been measured to range between 778 to 4040 N, with mean (SD) maximum loads, adjusted for total BMD, were 4050 (900) N (Lotz and Hayes, 1990). The mean (SD) fracture threshold for older, adult women reported by Cheng et al. was 3140 (1240) N (Cheng et al., 1997). Whether using energy or force as a measure of mechanical exposure, the proximal femur of older adults results in significant decreases in ability to resist fracture.

2.2.4 **Loads Applied to Proximal Femur**

Predicting the loads applied to the pelvis during a lateral impact on the hip is dependent on accurately recreating the intimal parameters of a fall (and pelvis) from standing height. Ideally, measuring the impact forces associated with falls from standing height, in the

laboratory would be done without protective padding. However, the inherent risk of injury with such an experiment becomes unethical and dangerous. Regardless, some studies have tried to quantify impact forces using padded force plates, and low severity (low velocity) hip impact simulations.

The average (SD) peak force applied to the hip during self-initiated sideways falls onto a 13 cm foam mattress overlying a force plate, has been reported to be 2252 (442) N (Nankaku et al., 2005). A study on hip loading during side jumps/dives by soccer goalkeepers found that peak vertical impact forces ranged between 3000 N to 8000 N, and were highly correlated with the vertical impact velocity (r^2=0.74) (Schmitt et al., 2010).

In attempts to simulate the end-stage impact of the pelvis under lower severity conditions, Robinovitch and colleagues (1991) used "lateral pelvis release" experiments to measure the impact response of the pelvis to a low velocity (~1.0 m/s) impact. They used a simple nonlinear viscoelastic model (a mass above parallel spring and non-linear damper elements) created from free-fall data from "pelvis release experiments" to predict impact force from a fall from standing height. The average peak force predicted by their model (a free-fall of 0.7m), was on average 5600 N. Subsequent improvements to their model parameters (mass-spring model to eliminate the minimal contributions of damping and muscle contraction level) predicted peak forces ranging from 1150 to 5288 N (Robinovitch et al., 1997a). A study by van den Kroonenberg et al. (1995) also used a mass-spring model to predict peak forces of 2900, 3580, and 4260 N for 5, 50, and 95 percentile females during sideways falls from standing height. Laing et al. (2010) predicted average peak impact force to be 1846, 2649 and 3434 N for falls with hip impact velocities of 2, 3 and 4 m/s,

respectively. Experimental testing using a surrogate mechanical pelvis (simulated trochanteric soft tissue and proximal femur) at an impact velocity consistent with a fall from standing height, produced total peak hip impact forces of 4,000 N and femoral neck impact forces of 2,500 N (Majumder et al., 2007; Robinovitch et al., 1991). In addition, a finite element model produced by Majumder et al. simulating impact force following a sideways fall from standing height, estimated a peak force of 8331 N (2007). Indicating that these forces might be higher than currently measured or predicted. Overall, it is generally accepted that the force applied to the hip during a sideways fall from standing in an older adult is likely in the range of 3-8,000 N.

2.3 **Variables that Modulate Hip Fracture Load**

As with most biological structures, the complexity of materials that compose them underscore the difficulty in characterizing their response to external loads. Considering the pelvis, bone, muscle, fat and skin are only some of the biological tissues that make up the lateral hip. Evidently, determining the mechanical properties of the pelvis can be difficult, but fair insight can be garnered from simple approximations.

Revisiting the conservation of energy formulas presented previously (section 2.2.1), it can be seen that during the compressive phase of impact (from impact onset until when the relative velocity of the mass reaches zero), the total kinetic energy of the falling mass ($E_{KE} = 1/2mv^2$) is converted into elastic strain energy ($E_{SE} = 1/2kx^2$). Or equivalently $E_{SE} = 1/2F^2k^{-1}$, where F is the average force of the impact. Accordingly, the average compressive force generated during impact can be estimated as $F = v(mk)^{1/2}$. These equations demonstrate that the fundamental variables influencing load applied to the pelvis are impact velocity

(dependent on fall height), effective mass, and effective stiffness of the impacting pelvis. The most difficult of these to measure is the effective stiffness, as it requires measuring how much the pelvis deforms in response to applied load (i.e. stiffness). As such to better estimate impact forces applied to the pelvis during a fall from standing, accurate methods of characterizing pelvis deformation and stiffness are required.

2.3.1 **Pelvic Stiffness, Strain and Load Distribution**

In considering the stiffness of the entire pelvis an approximation can be derived by considering the hip as a system of springs in-series. The soft tissues (k_1), in series with the bony pelvis (k_2), produce the effective stiffness (k_*) of the impacting pelvis, which can be predicted as:

$$k_* = \left(\frac{k_1 k_2}{k_1 + k_2}\right) \tag{1}$$

Thus the force applied to the hip equates to,

$$F = v\sqrt{mk_*} \tag{2}$$

Equation (2), in conjunction with equation (1), shows that any attenuation in peak impact force provided by biomechanically tuned devices, such as hip protectors or compliant flooring, depends on not only the stiffness of the device, but also the stiffness of the body and its soft tissues.

Mechanically, soft tissues act as shock absorbers by decreasing system stiffness and absorbing energy during impact (Bouxsein et al., 2007; Etheridge et al., 2005; Laing and Robinovitch, 2006a; Laing and Robinovitch,2008b; Lauritzen and Askegaard, 1992;

Majumder et al., 2008; Robinovitch et al., 1995b; van Schoor et al., 2006). Robinovitch et al. (1995b) observed that the peak load applied to the proximal femur decreased by 71 N for each additional mm of cadaveric soft tissue incorporated into a mechanical test system of hip fractures. Similarly, van Schoor observed a 31% decrease in peak force applied to a mechanical hip impact simulator when surrogate soft tissues (foam) were increased from 12.7 to 25.4 mm (2006). Although both the aforementioned studies saw reductions in force with increasing soft tissue depth, van Schoor and colleagues measured force applied to the lateral hip at the surface of impact, while Robinovitch et al. measured the force applied to the proximal femur. This discrepancy in measurement is very important when considering the risk of fracture from a fall. To truly estimate fracture likelihood, the exact loading on the proximal femur is desirable, but in most in-vivo experiments, the external reaction force is all that is available (from load cells or force plates). Thus, interpreting the risk of fracture from and impact force that develops during a fall, is dependent on understanding how the geometrical and anatomical variations in the pelvis modulate force distribution upon impact.

How impact force is distributed spatially to the lateral pelvis depends on the structural composition of the lateral pelvis. Studies by Laing and Robinovitch (2008c) and Robinovitch and Hayes (1995a) reported regions directly overlying the greater trochanter to be two to three times stiffer than the tissues anterior or posterior. Using a customized indentation device composed of a 3.8 cm diameter cylindrical probe, Laing and Robinovitch (2008d) measured the localized force-deflection properties of the lateral hip from nine locations (3 x 3 grid) centered about the greater trochanter. They found that soft tissue stiffness varied across pelvic locations (Figure 2.5), being stiffest directly over the greater trochanter (mean (SD) =

34.4 kN/m (SD 15.5)) and least stiff six cm posterior to the trochanter (averaging 14.1 kN/m (SD 7.2)). In the same study, using their measurements on the regional variations in soft tissue stiffness of the lateral pelvis, Laing and colleagues created a biofidelic hip impact simulator to measure peak femoral neck force and total impact force at the skin. They found hip protectors had a much greater influence on the femoral neck force compared to the total pelvic impact force. Where femoral neck force attenuation provided by hip protectors reached 34% compared to the unpadded trials, the hip protectors only reduced 9% of the total impact force. Furthermore, Laing and colleagues measured the effect that impact velocity, pelvic size and soft tissue stiffness had on the pelvic impact force and femoral neck force.

They reported that increasing impact velocity substantially increased the femoral neck force and the pelvic impact force. However, only the femoral neck force was substantially influence by the pelvic size and soft tissue stiffness. They found that increasing the size of the pelvis decreased the percent of total pelvic impact force delivered to the femoral neck (from 77% in the small pelvis condition, to 47% in the large condition) due to an increase in impact energy shunted anterior and posterior to the proximal femur. This interaction between contact area and pelvic stiffness in attenuating peak impact force, lends merit to studying, in more detail, how contact area relates to pelvic stiffness and deflection.

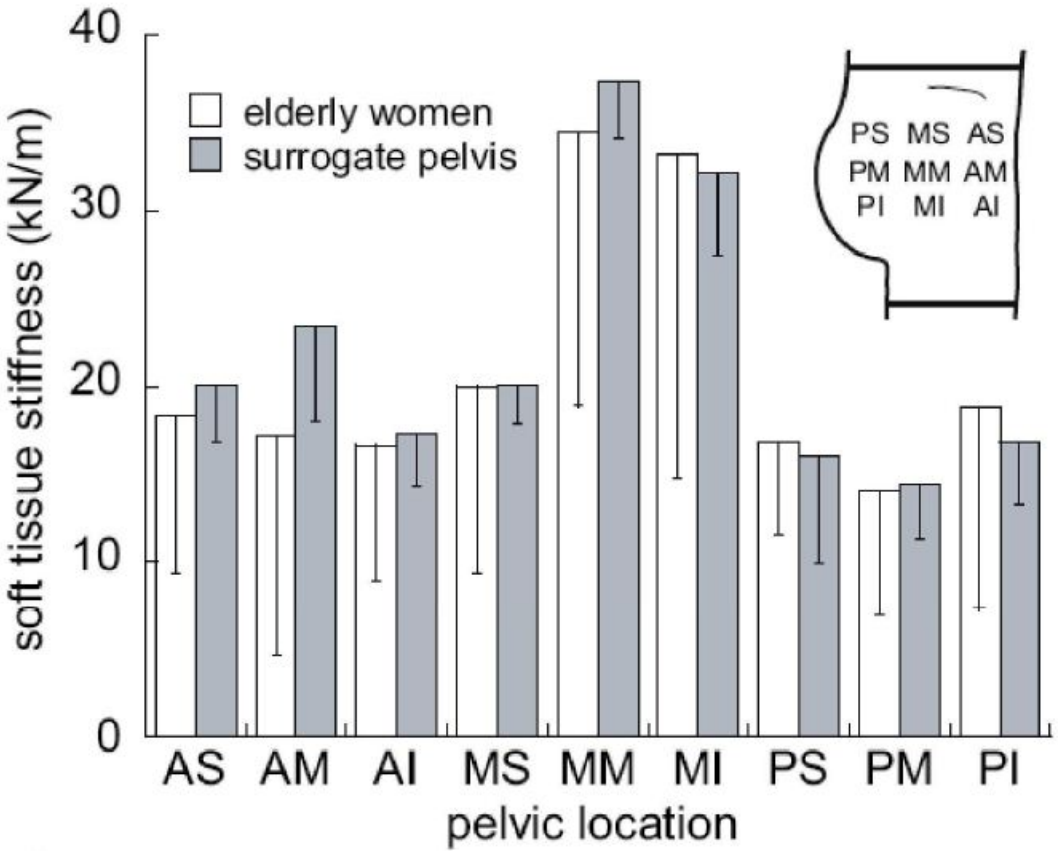

Figure 2.5: Regional variation in soft tissue stiffness of the lateral pelvis in an older adult woman. Stiffness was measured with a hand held device with rigid surface area, that measured the deflection (and load) as the device was loaded to areas of the lateral pelvis. Adapted from Laing and Robinovitch (2008c)

2.3.2 **Contact Pressure during Lateral Pelvic Impact**

In a study on the effect of soft shell hip protectors on pressure distribution, Laing et al. reported that approximately 17 % and 46% of the total force applied to the pelvis during lateral falls on average was applied directly to tissues within a radii of 1.25 and 2.50 cm from the greater trochanter, respectively (2008a). Choi and colleagues, using the biofidelic hip impact simulator previously mentioned (Laing and Robinovitch,2008b), reported that 83% of the total force was applied directly to the region over the greater trochanter and femoral diaphysis (2010b). The differences in force distribution between these studies can be explained by how they each measured pressure. Laing and colleagues used different sized circular load cells to attain average peak pressure for lateral release impacts on human participants. Choi et al. used a 2D pressure distribution plate, on top of a force plate, to sum pressures and get the percentage of total reaction force per defined area, for impacts from a mechanical surrogate pelvis. Interestingly, a subsequent study by Choi et al. (2010a) using the lateral release protocol with human participants, measured approximately 48.5 (SD=7) % of the total impact force was distributed to the greater trochanter. Even more intriguing, they found that only 23.8 (SD=7) % of the total impact force was distributed to this area in participants with high body mass index (BMI=kg/m^2, > 25 vs. < 18) (Figure 2.6). Although, it is assumed that the differences in impact force distribution for high BMI participants is due to their reduced pelvic stiffness (Figure 2.7), the possibility remains that this altered "stiffness" is partly contributable to the larger pelvic geometry. How pelvic linear stiffness and contact area modulate the measured effective stiffness of the pelvis is something not well understood.

2.4 **Characterizing Pelvic Deflection and Contact Area**

It is evident now, that in estimating the impact forces resulting from a fall from standing, the effective stiffness of the pelvis must be accurately characterized. The deformation the hip undergoes, as well as the changes in contact area, during a lateral impact are key determinants in estimating the effective stiffness of the pelvis. The concentration of this thesis will be on these two variables (deformation and contact area).

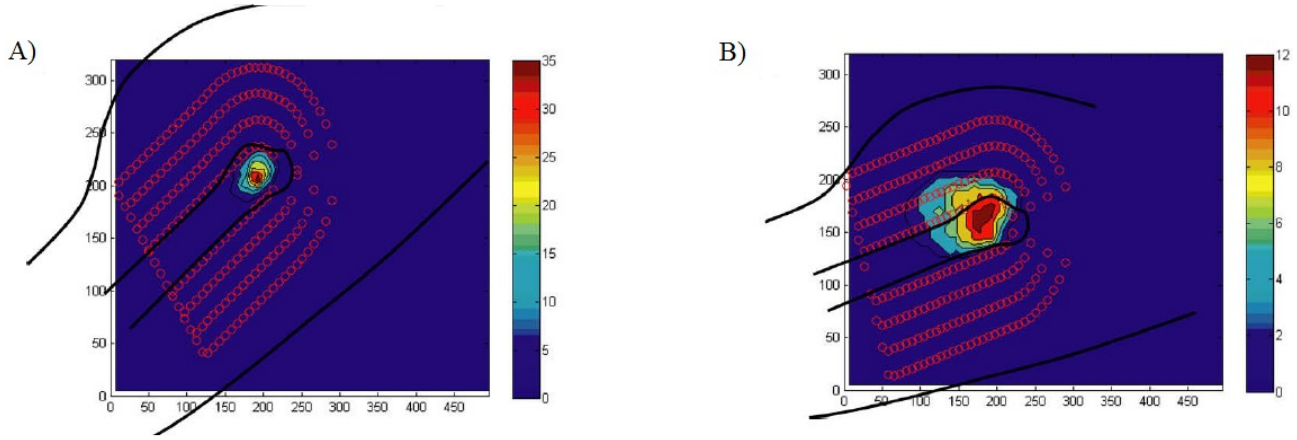

Figure 2.6: Example peak pressure profiles from trials in the unpadded condition between participants of low (A) and high (B) BMI. For a low BMI participant in the unpadded condition, pressure centered over the GT and the contact area was small. For a high BMI participant in the unpadded condition, peak pressure occurred over the GT and contact area was larger compared to the low BMI participant in the same condition. the magnitude of pressure is indicated by a color scale. Pressure unit on a color bar is N/cm2 (1 N/cm2 = 10 kPa). Note the different pressure ranges in the scales for parts A and B (Choi et al., 2010a).

2.4.1 **Quantifying Deflection during Impact**

Pelvis release experiments were originally used to predict the damping response of the pelvis in order to determine stiffness and damping properties for mathematical model predictions of impact force (Robinovitch et al., 1991). More recently, this protocol has been used to quantifying the force-deflection response of the pelvis to low velocity impacts (Laing and Robinovitch, 2010; Levine, 2011). Estimating pelvic stiffness via force-deflection methods assumes that during a lateral impact, the pelvis is primarily compressing in the frontal plane (or undergoing a central impact). The term *central impact*, or *normal impact*, is used when the velocity of the centre of gravity of the impacting body moves along the same line as the reaction force at the impacted surface. Using the force-deflection properties of the hip allowed for more direct measurement of effective stiffness (Laing and Robinovitch, 2010). Using this method, deflection was measured by tracking marker on the greater trochanter of the non-impacting hip during impact on a rigid force plate, measured with an eight-camera optical motion tracking system sampling at 240 Hz. Subsequent studies assessing pelvic stiffness have used similar methods, specifically with three-camera optical motion tracking systems sampling at a 400 Hz (Levine, 2011). Although, the frequency content for the majority of voluntary human movement is below 30 Hz (Winter, 2005), the high frequency nature of impacts on the human body underscores necessity of sampling deflection at appropriate rates.

Although not explicitly tested, previous studies (as well as my pilot data), using the lateral pelvic release protocol to measure pelvic compression, have shown time to peak deflection to range from 0.02 to 0.05 seconds for 5 cm drop heights. This means that at a sampling rate of 240 Hz and a sampling rate of 400 Hz, between about 4-12 and 8-20 data points would be recorded during the compressive phase of loading (i.e. until peak force) for each impact, respectively. While the acceptable number of points required to define a force-deflection curve depends largely on the behaviour that is exhibited by the object of interest, a rule of thumb in materials impact testing is at least 200 data points (Kessler and ASTM Committee D-20 on Plastics., 1987). Ideally then, in the instance of lateral pelvis release experiments, sampling pelvic deformation would occur between 4000 and 10000 Hz.

Contrastingly, sampling at 240 Hz and above might be more than sufficient for lateral pelvis release studies. Suppose the deflection of the pelvis during impact can be modelled by a fictitious contact spring between a rigid mass and the rigid impacted surface (force plate). Presume that contact spring is linear and has a stiffness k_1. Thus, the maximum deflection (x_m) is obtained with :

$$x_m = v_1\sqrt{\frac{m}{k_1}} \tag{3}$$

From which, assuming peak displacement results from integrating velocity (v_1 is the initial velocity at impact) over a quarter-period, the duration of loading phase (t) is:

$$t = \frac{\pi x_m}{2v_1} \tag{4}$$

Subsequently, using experimental values of *t* (0.02s to 0.05s) obtained from force plate data, a dominant signal frequency between 5 and 12.5 Hz is estimated (as the time at peak force in a spring is also the time at peak deflection). Thus, sampling at a rate of 240 Hz is more than 19 times the main signal frequency, and could possibly be sufficient to capture the majority of signal frequencies of interest in the signal, but still miss important discrete events like peak force and peak deflection.

Structural deformation studies in different fields of biomechanics have utilized high-speed camera technology successfully at sampling rates much higher than currently seen in pelvic release trials. Blunt lateral impacts studies by Viano and colleagues (Viano et al., 1989b; Viano and Lau, 1983) have used high-speed videography sampling at 500 to 1000Hz, to quantify the compression response of cadaver specimens (hip and thorax) to impact loads in car crashes. However, sampling rates this high have never been used to characterize pelvic deflection and pelvic stiffness in lateral release trials.

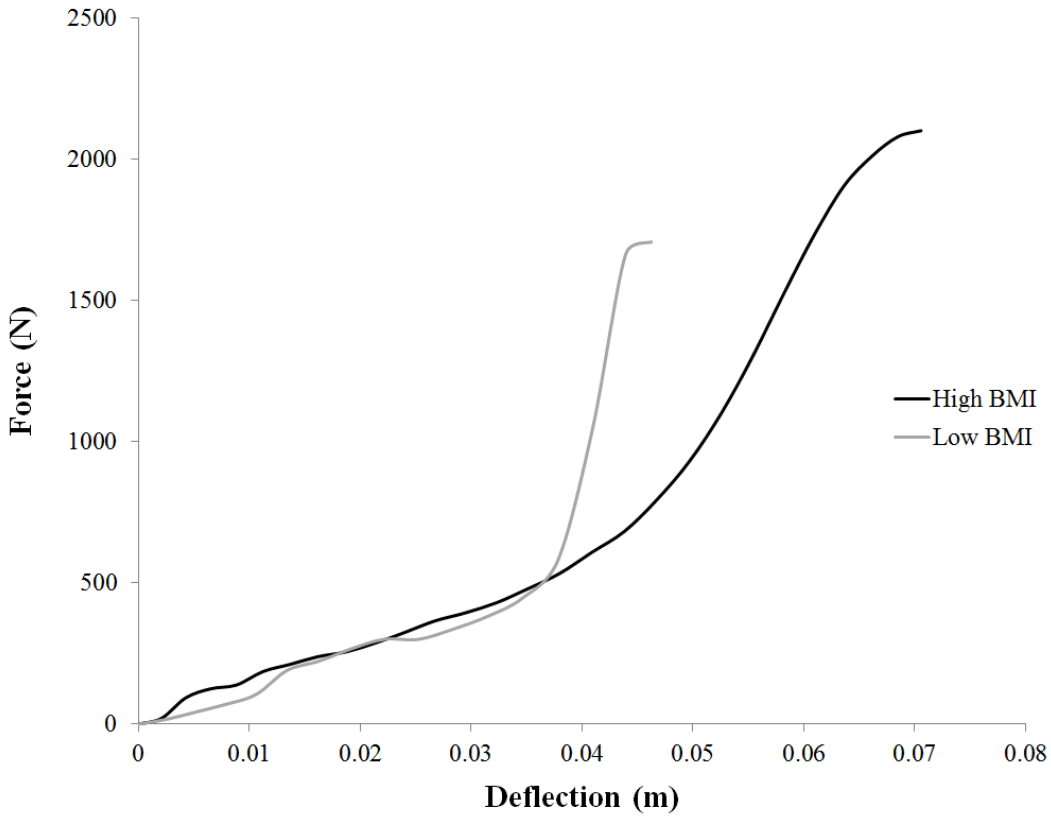

Figure 2.7: Example force vs. deflection traces from two individuals with varying BMI. Low BMI < 22.5 and high BMI > 28. Notice differences in the initial non-linear loading, followed by transition to linear and marked increase in stiffness, until a plateau near peak force.

2.4.2 **Contact Area**

Robinovitch et al. (1991, 1997a) utilized pelvis release experiments to characterize the stiffness of the pelvis from the natural frequency of oscillation recorded from the force plate. They observed effective stiffness to increase with increasing force (presumably due to increasing contact area and tissue compression as the impact progressed) at low levels (< 300 N) of force and remain constant for loads beyond 300 N. This non-linearity in pelvic stiffness is quite possibly a result of the contact area increasing during an impact, where it eventually maximizes and the force-deflection trace of a lateral impact becomes relatively linear (Figure 2.8).

Classical Hertz contact theory (Johnson, 1985) mathematically defines quasi-static contact, between rate-independent materials with small contact regions (relative to other dimensions of the object) and defines the relationship of linear elastic surfaces contacting with elliptical surface geometry (Figure 2.9).

During an impact, the rate of change of the normal component of relative velocity depends on the interaction force *F* and the displacement *x.* As the contact region is compressed during the impact, the approach of the center of mass of the pelvis to the impacting surface results in a reaction force *F* at the point of contact as defined by:

$$F = m\ddot{x} = k_* x^n \tag{5}$$

Where *n,* is the non-linearity coefficient (*n* =3/2 in Hertzian contact) and k_*, is the composite stiffness. Stiffness in this model is dependent on the material properties

(composite elastic modulus (E^*)) in the deforming contact region and the geometry of the two contacting surfaces (composite radius (R^*)) (Figure 2.9) where:

$$\frac{1}{E^*} = \frac{1}{E_1} + \frac{1}{E_2} \tag{6}$$

$$\frac{1}{R^*} = \frac{1}{R_1} + \frac{1}{R_2} \tag{7}$$

$$k_* = \frac{4}{3} E_* {R_*}^{1/2} \tag{8}$$

Where the maximum contact area radius a is given by

$$a = \left(\frac{F}{k_*}\right)^{1/3} {R_*}^{1/2} \tag{9}$$

Furthermore, the peak pressure, P_o

$$P_o \propto \left(\frac{E^*}{R^*}\right)^{\frac{2}{3}} \tag{10}$$

These equations imply that the effects of material elastic modulus (E^*) and geometry (R^*) on composite stiffness are equivalent. Thus, changes in elastic modulus have the same effect as proportional changes in curvature, and vice versa. In essence, the effects of material properties and contact geometry are inseparable, and in theory, it is impossible to determine from force-deflection responses alone whether the difference between two stiffness measurements is due to differences in material properties, surface geometry, or both.

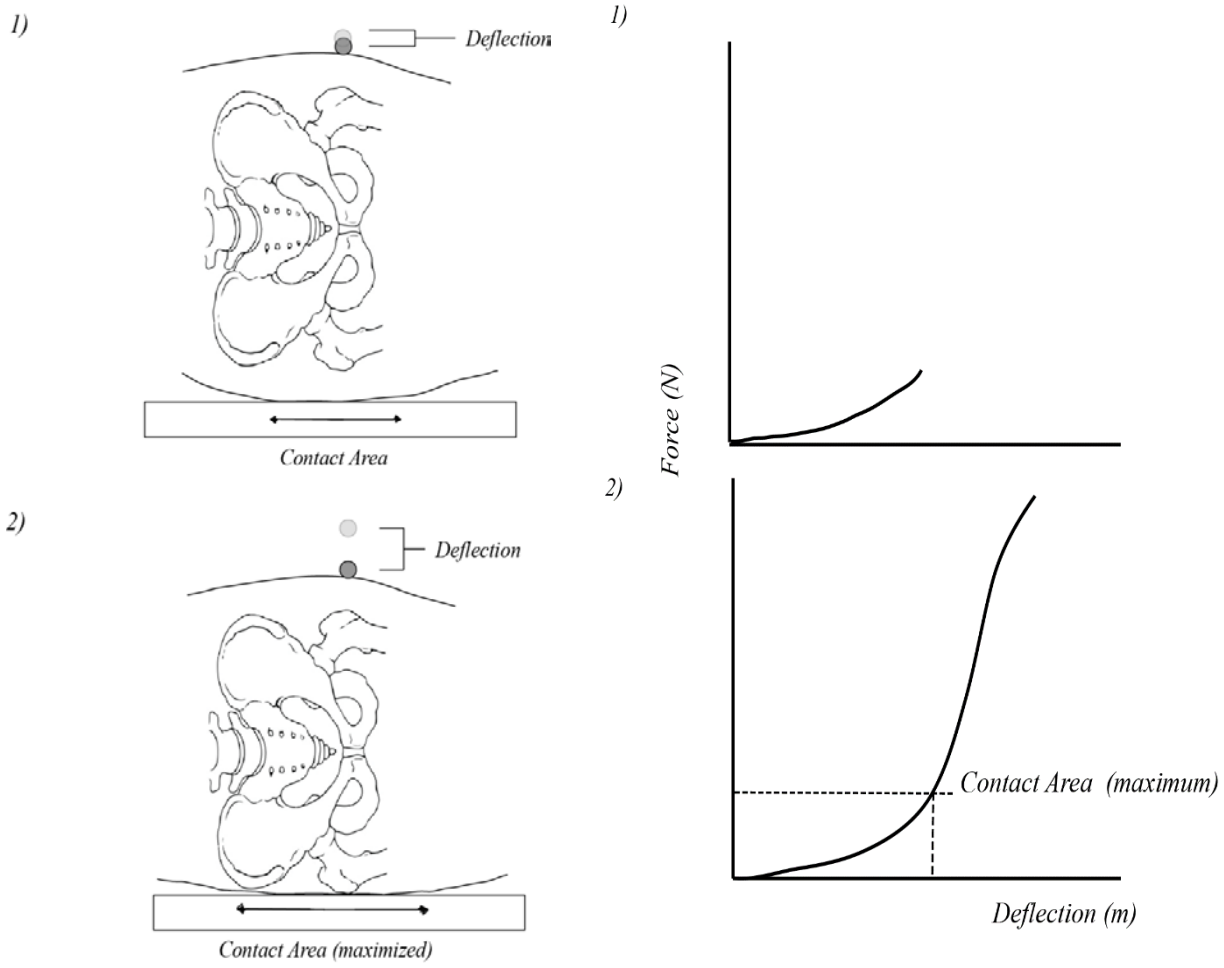

Figure 2.8: Theoretical force-deflection curve for lateral pelvis release. This illustrates how the change in contact area (from 1 to 2) might potentially modulate the non-linear effective stiffness of the pelvis.

Since Hertzian contact theory assumes elastic impact, it is unclear whether it can describe the interaction between the lateral pelvis and an impacting surface. Firstly, the lateral pelvis is viscoelastic in nature and hip impacts are highly dynamic, both of which are unaccounted for in Hertzian contact models. Secondly, the complex geometry of the pelvis does not comply with the assumptions of made in Hertzian contact, and furthermore the internal structure of the pelvis (i.e. the bony skeleton) is what is more important, and is not readily definable with surface geometry only. Although it has been suspected that damping and energy dissipation play a role in this non-Hertzian behaviour of the lateral pelvis (Laing and Robinovitch, 2010; Robinovitch et al., 1997b), elastic models (mass-spring) have been shown to best predict the impact forces in hip impacts (Laing and Robinovitch, 2010; Robinovitch et al., 1991). Furthermore, an elastic understanding of how contact area increases stiffness has been proposed by Robinovitch et al. (1991), where the soft tissue over lying the hip can be described by a rounded surface with an infinite number of springs and dampers in parallel. Where, assuming elasticity only (no dampers), as the impact initiates and contact area increases, more springs compress and create this non-linearity (Figure 2.10). Eventually, a stiffening of the soft tissue occurs at which point the stiffness of the underlying bone contributes to the linear portion of the force deflection profile of the hip. This scenario proposed by Robinovitch et al. (1991), along with the proportionalities' predicted by Hertz may provide some insight to the relationship between contact area and impact force, deflection and pelvic stiffness.

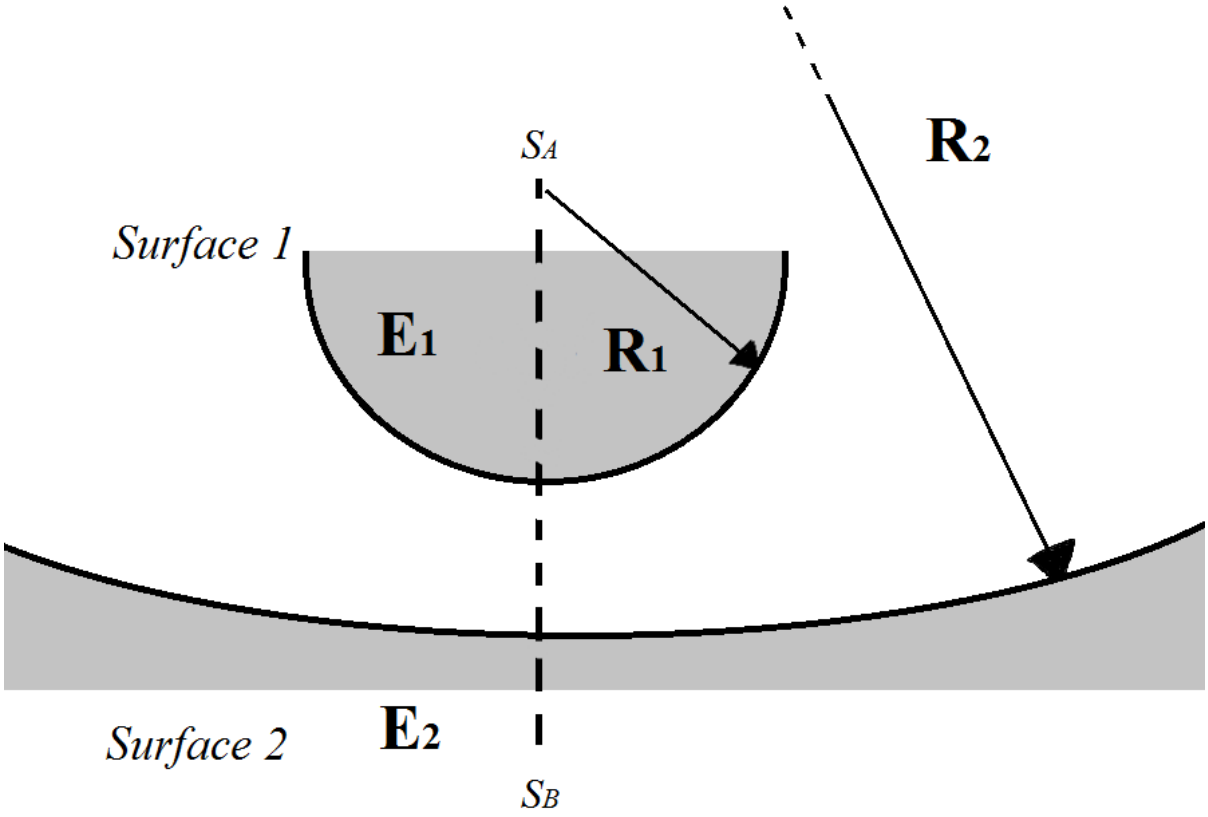

Figure 2.9: Hertz contact theory approximates the interaction of two elastic contact surfaces, whose curvature is defined by the inverse of the surface radius (R_1,R_2). The surfaces are depicted as axisymmetric about the axis S_A-S_B, with material properties defined by E_1 and E_2. Note for contact with a flat (planar) surface R = ∞.

2.4.3 **Conclusions**

From the review of literature, accurately predicting the risk of hip fracture is certainly non-trivial. Early research by Robinovitch et al. (1991, 1997b) utilized low velocity "pelvis release experiments" to measure the impact response the human pelvis using university-aged females. Consequently, the accurate characterization of impact response is highly dependent on the accuracy of experimental measurement techniques. Previous studies using the lateral pelvis release protocol, have not sampled pelvic deflection at rates over 400 Hz, and it is unknown whether this sampling rate is appropriate for the pelvis release experimental paradigm. However, to sample at higher rates requires the use of high speed videography; which has never been used with lateral pelvis release experiments. Additionally, little is known about the role that contact area plays in the distribution of load from lateral hip impact studies. Since most studies utilize net impact force from a force plate, very little is known about the relationship between load distribution and body size. This proposed thesis project aims to fill the gap in the current literature concerning these two areas in hip impact research. The specific hypotheses for these studies can be found in chapter one, and chapters three and four.

Chapter 3
The Effect of Motion Capture Technique and Sampling Rate on Biomechanical Measures of Lateral Hip Impact Response

3.1 Introduction

Impact related injuries are devastating and can affect any part of the body susceptible. Fortunately, a considerable amount of literature exists on the biomechanics of impact injury to the human thorax (Cooper et al., 1982; Nahum et al., 1971; Song et al., 2009), abdomen (Beillas et al., 2013; Cooper and Taylor, 1989; Viano et al., 1989b) and hip (Cesari et al., 1980; Etheridge et al., 2005; Robinovitch et al., 1991a), to impact loads. In-situ, these impact loads can occur in a variety of ways (high energy vs. low energy) and environments (traffic collisions, contact sports, in the home etc.), and all can cause a significant level of injury to a person.

Hip fractures, for example, can occur from fall related impacts (relatively low velocity) in older adults (Grisso et al., 1991; Nevitt and Cummings, 1993; Zuckerman, 1996), or through high velocity side-impact vehicle collisions (Viano, 1988); both resulting in debilitating injuries. Naturally, many studies have focused on the biomechanical response of the human hip and pelvis to both high (Cesari et al., 1980; Viano et al., 1989b) and low velocity impacts (Beason et al., 2003; Etheridge et al., 2005), to understand the nature of these injuries and explore the possibilities of predicting or preventing them.

In the study of hip fracture biomechanics, various experimental methods have been used to measure the loads, strains and energies applied to the lateral hip (proximal femur) during impact and the respective tolerances of the hip and pelvis to fracture or injury. Blunt

lateral impact studies by Viano and colleagues (1989a; 1989b; 1983) used load cells, accelerometry and high-speed videography, sampling at 500 to 2000Hz, to quantify the load, compression and force-deflection response of cadaver specimens (hip and thorax) to impact loads in simulated automobile collisions. Similar studies of side-impact vehicle collisions, have measured pelvic deflection at 500 or 1000 Hz sampling rates. In-vivo studies of fall related hip impacts by Laing and Robinovitch (2010) directly measured the force-deflection behaviour of the pelvis during low velocity "pelvis release experiments" (Robinovitch et al., 1991). This method involved tracking a marker on the opposite greater trochanter of the impacting hip, during the compressive phase of impact. In their study, pelvic deflection was measured with an eight-camera optical motion tracking system, sampling at 240Hz, whereas subsequent studies using this method have sampled pelvic deflection at 400Hz (Bhan et al., 2013; Levine et al., 2013; Levine, 2011).

At a minimum, to digitally sample any analog signal and preserve its frequency content, the sampling rate must be more than twice the highest frequency present in the signal. Incorrectly sampling a signal, or violating the Nyquist-Shannon sampling theorem, can cause frequency aliasing and alter the content of the signal of interest (Cho et al., 2011; Shannon, 1949). Furthermore it is often suggested that, to adequately capture time-varying peaks or minimums, a sampling rate of at least ten times the highest frequency present in the signal is used. Therefore, in any impact testing, inappropriate sampling rates can introduce inaccuracies in the collected data and measures of impact severity (ex. peak force, peak deflection etc.). Unfortunately, the effects of sampling rate on biomechanical measures of interest, during impact testing, have never been studied and it remains unknown if the

sampling rates previously used during lateral release experiments were appropriate. Although the importance of sampling rate on an array of biomechanical signals has previously been highlighted (Andrews and Callaghan, 2003; Durkin and Callaghan, 2005; Jayne et al., 1990), it is of particular interest in impact studies due to the small time duration over which impacts are applied to the body (i.e. high impulse).

Additionally, it is also of interest to maximize the number of data points that are collected during impact experimentation. Since the force-deflection response is often of interest, either to characterize the energy absorbed, or to estimate the stiffness of the system being studied; a greater number of data points collected during the impact event reduces errors in numerical integration (calculating energy absorbed) and curve fitting (modeling stiffness). Previous studies using the "pelvis release" paradigm have reported the time to peak force for the majority of impacts to range between 0.02 to 0.05 seconds. At the highest sampling rate used previously for in-vivo "pelvis release " studies (400Hz), this would imply anywhere between 8 and 20 data points were captured for any one impact. Higher velocity impact studies (~3-4 m/s) have shown peak force to occur below this range (< 20 ms) (Beason et al., 2003; Viano et al., 1989b), and studies using impact velocities of about 8.5 m/s reporting time to peak force below 10 ms (Matsui et al., 2003). Clearly, this short duration, high impulse event requires a maximization of sampling rate in order to collect a sufficient amount of data points, in addition to not aliasing the underlying signal of interest.

In the field of materials impact testing, 200 data points has been suggested as a "rule of thumb" to accurately characterize the force-deflection response of a material to impact loads (Kessler and ASTM Committee D-20 on Plastics., 1987). Using the time to peak force

with impacts seen in previous lateral impact studies (7-50 ms), complying with this suggestion of 200 data points requires sampling between 4000 to 10000+ Hz, depending on the condition of the experiment (i.e. higher or lower impact velocities) (Figure 3.1). At present, to achieve these greater sampling rates requires the use of high-speed videography. As previous lateral impact studies with human volunteers have used 3D optical motion tracking systems, it remains unknown how high-speed videography compares with 3D optical motion tracking for lateral pelvis release studies.

Accordingly, the purpose of this study was two-fold: 1) To determine the *effects of motion capture system* (3D optical motion tracking vs. 2D high speed videography) on five commonly reported measures of impact severity (peak force, time to peak force, peak deflection, time to peak deflection and energy absorbed); 2) to determine *the effects of sampling rate* on the five aforementioned discrete measures of impact severity. Thirteen participants were recruited for lateral pelvis release experiments, where pelvic impact force and deflection were measured simultaneously with the two different motion tracking systems, at two drop heights (1.5cm and 5cm). Data collected with high speed videography system was then used to determine the effect of sampling rate (9000 Hz compared to 4500, 1500, 500 and 300 Hz) on measures of impact severity.

It was hypothesized that there would be no significant difference in any of the dependent measures of impact severity (peak force, time to peak force, peak deflection, time to peak deflection and energy absorbed) between the two motion capture systems (3D optical motion tracking and high-speed videography) sampling at 1500 Hz, for either drop height (1.5cm and 5cm). Furthermore, it was hypothesized that sampling at lower rates would

reduce the measured peak force, peak deflection and energy absorbed, while increasing the time to peak force and time to peak deflection when compared to the "gold-standard" at 9000 Hz.

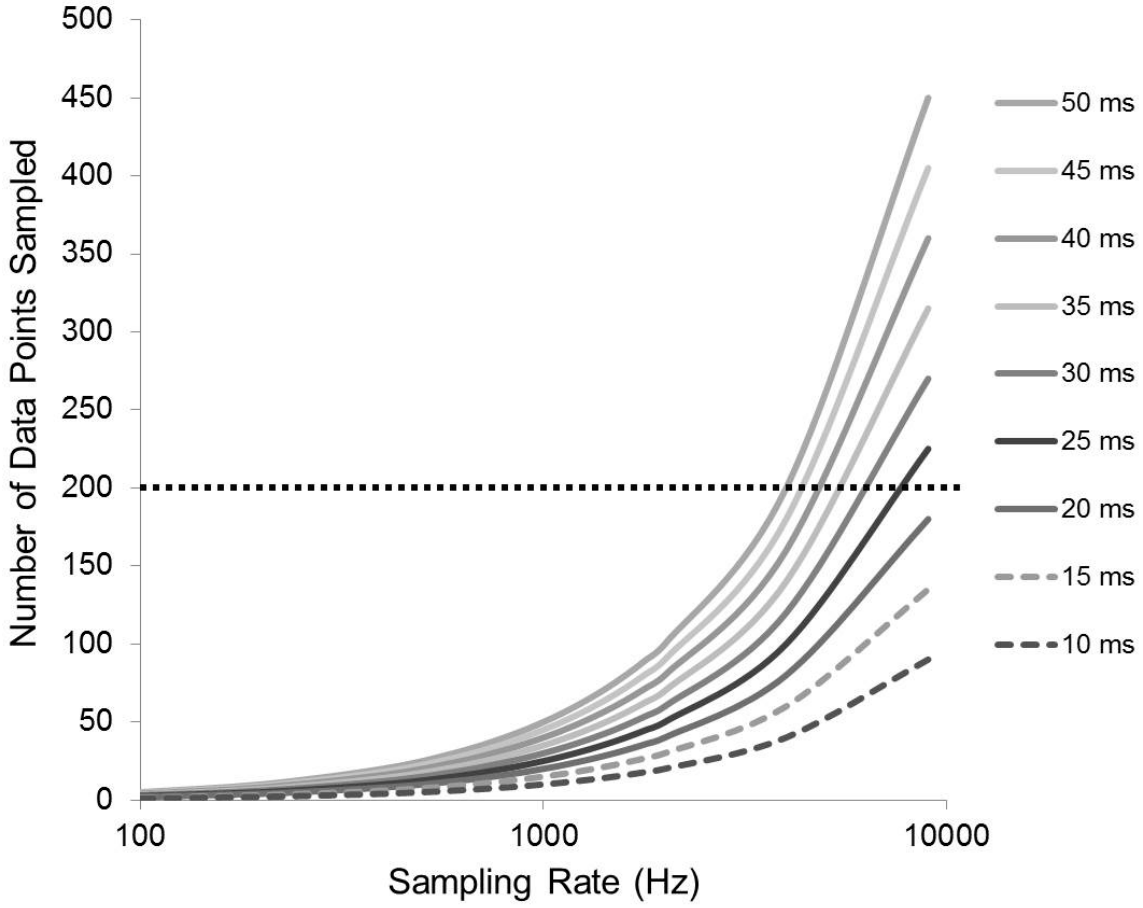

Figure 3.1 The effect of sampling rate on the number of data points theoretically collected during various time to peak force durations seen in lateral hip impact studies. Solid traces indicate impact durations commonly seen during in-vivo "lateral pelvis release experiments. The dashed traces indicate impact durations seen commonly during lateral impact studies conducted at higher impact velocities, with stiffer, cadaver specimens (3-4 m/s). The horizontal dashed line at 200 data points signifies the suggested number of data points for impact testing of materials (America Kessler and ASTM Committee D-20 on Plastics. 1987)

3.2 **Methods**

3.2.1 **Participants**

Thirteen healthy, university-aged female participants were recruited from the general university population. Participants completed a short health questionnaire regarding medical history and current health status, confirming the information provided to the researcher during the recruiting stage of the study. Participants were excluded if they: 1) had a history of fracture to the femur, pelvis or spine, or fractures to any bone within the past year; 2) had experienced any other musculoskeletal injury or physiological disorder within the past year; or 3) they had been diagnosed with osteopenia or osteoporosis. All participants provided informed written consent and the study was approved by the Office of Research Ethics at the University of Waterloo.

Table 3-1 Anthropometrics for thirteen participants recruited in study.

	Age (years)	*Height (cm)*	*Mass (kg)*	*BMI (kg/m²)*
Mean	24.5	166.7	66.0	23.7
SD	3.2	6.9	11.5	3.8

3.2.2 **Experimental Protocol**

The experimental protocol required the participant, dressed in tight-fitting spandex shorts or tights, to lie on their left side with their pelvis supported by a sling above the impact surface (force plate). The participant's arms were flexed above the shoulder and under the head to ensure that they would not contact the impact surface or provide any bracing during the pelvis release. The hips were flexed to 70 º, and knees flexed to 90 º. This position approximated the position assumed following a fall from standing height used in previous impact studies (Laing and Robinovitch, 2010; Robinovitch et al., 1991). The sling was attached to a height-adjustable set of strong nylon ropes and a turnbuckle; this unit was then connected to the electromagnet (Figure 3.2). With the magnet engaged, the participant's pelvis was raised to a height of 1.5 cm or 5 cm. These heights were selected to provide an impact velocity of approximately 0.5 and 1.0 m/s, respectively. Once suspended above the force plate, the participant was instructed to relax their core and extremity muscles. Upon the participant confirming that they were 'ready' to begin the trial, the magnet was subsequently disengaged at random times (between one and three seconds) and the subject's pelvis was impacted on the force plate.

The time-varying loads applied to the pelvis were measured by the force plate (model OR6-3, Advanced Medical Technology, Inc., Watertown, Massachusetts, USA), sampling at 36000 Hz. Concurrently, two motion capture systems were used to track the position of one Optotrak smart marker (Northern Digital, Waterloo, Ontario, Canada) affixed to the area overlying the participant's right greater trochanter (Figure 3.3). The motion of that one marker was collected simultaneously by both the 3D motion capture system (OPT, Optotrak,

Northern Digital, Waterloo, Ontario, Canada) sampling at 1500 Hz, and a 2D high speed videography system (HSV, AOS Technologies, Cheshire, CT) sampling at a rate of 9000 Hz, for two seconds. Each participant underwent four consecutive trials per height condition, for a total of eight trials. Order of height conditions were randomized before initiation of the experiment.

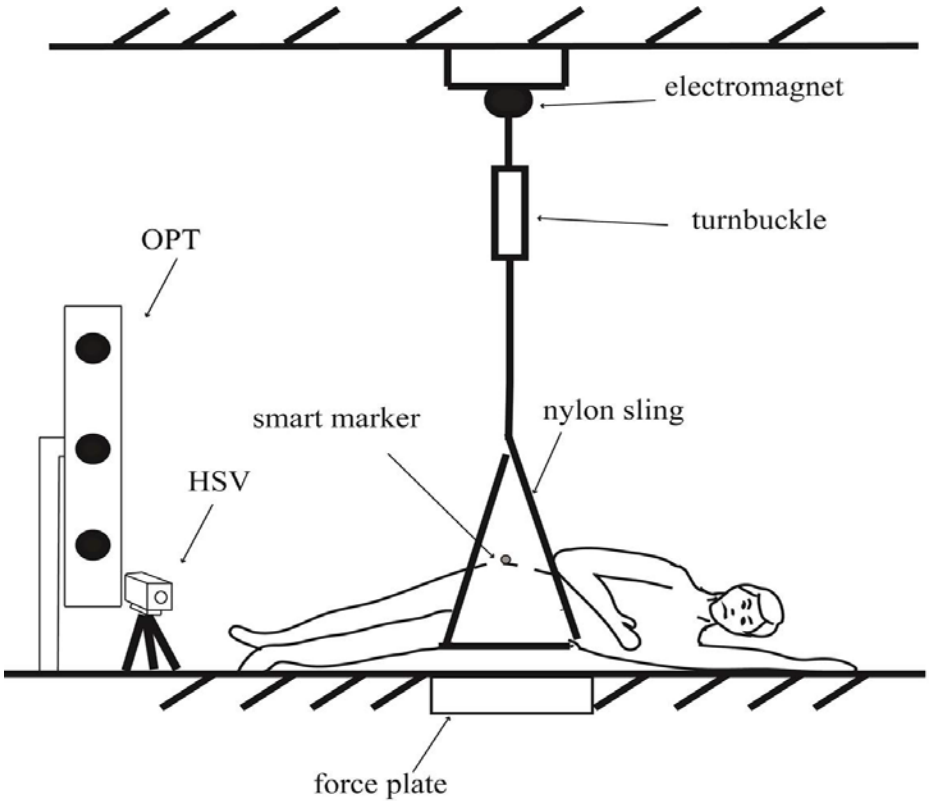

Figure 3.2: The participant was positioned on their left side with their pelvis supported by the nylon sling. The upper torso and shoulder, as well as the lower legs were contacting the ground, but not the force plate.

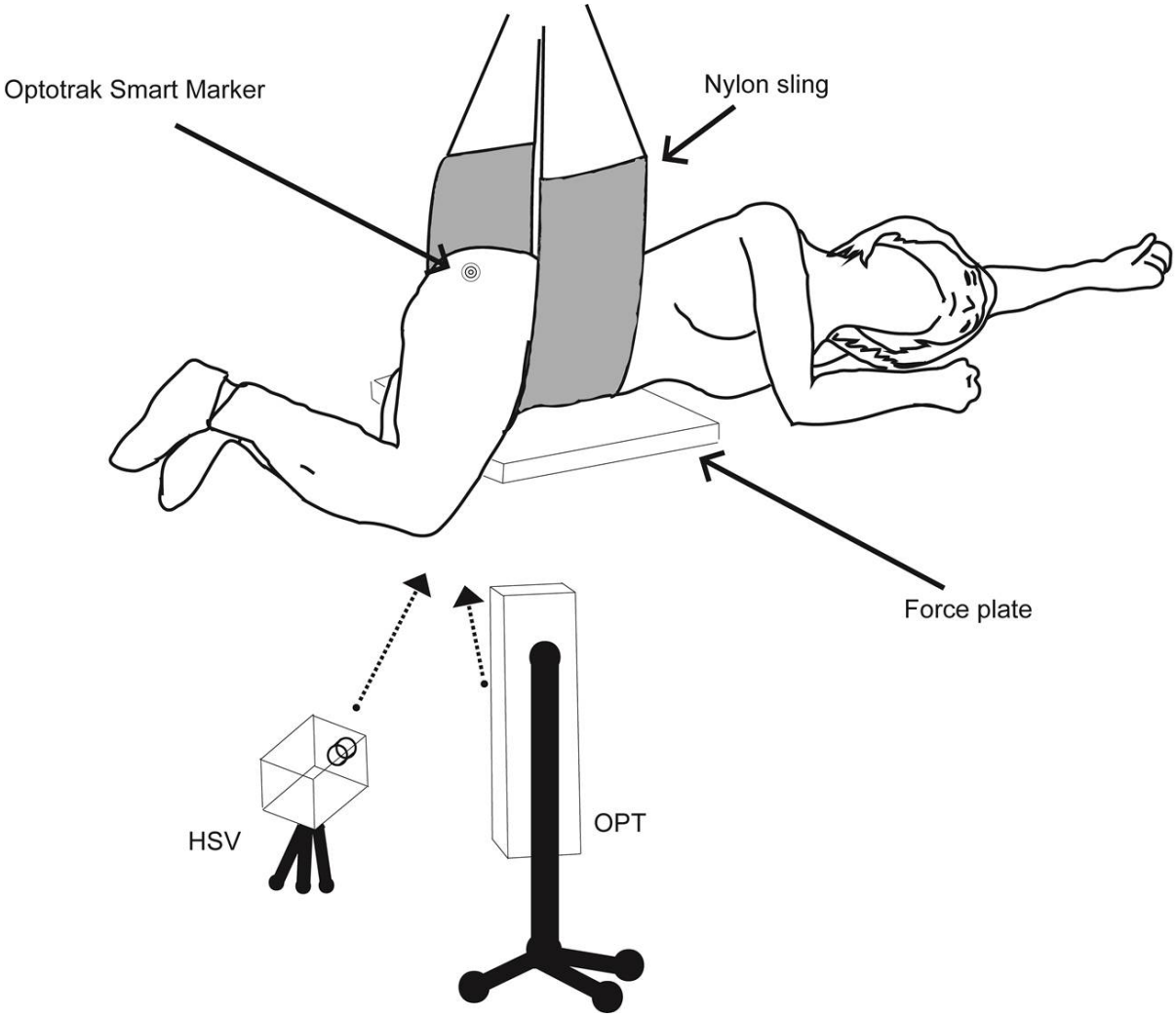

Figure 3.3: Visibility of the greater trochanter optical marker from the perspective of the HSV and OPT camera. The placement was determined to ensure the complete visibility of the marker throughout the entire impact trial by both motion capture systems.

3.2.3 **Camera Calibration**

To ensure that the HSV system was measuring the same marker motion as the OPT system, a rigid body was created for the HSV camera, and used to align to the global co-ordinate system of the OPT system. The rigid body was affixed to the HSV so that the y-axis of the rigid body local co-ordinate system was parallel with the back of the HSV camera; this was assumed to be parallel with the image plane of the CCD sensor in the camera (Figure 3.4). The x-axis of the rigid body was defined as being parallel with the long axis of the HSV camera (from back of camera to the lens), and orthogonal to the image plane of the camera sensor. The z-axis of the HSV rigid body was orthogonal to both the x and y-axis, and defined to be parallel with the vertical axis of the global z-axis of the OPT system.

The process of calibration was completed in multiple steps. The first step was the unique placement of four OPT camera banks to ensure a large capture volume that included the space directly above and around the force plate (where the impact trials were to take place), and also the space where the HSV camera was to view the impact trial from (Figure 3.5). Once arranged, the OPT was calibrated using its manufacturer provided calibration cube, and a global co-ordinate system was established using the four marker digitizing probe to establish the origin, positive x-axis, and positive y-axis (a cross product of the x and y produced the orthogonal z-axis). These three established points were labeled with a permanent marker on the force plate so that there would be a consistent global reference frame, both within an experiment, as well as between them.

The second step required setting up the HSV camera to view the impacts. To ensure that the HSV camera could view the impact, the participant was placed in the sling with the hip marker affixed to their right trochanter, assuming the impact configuration described above (section 3.3.2). The HSV camera was then manually adjusted to ensure it was aligned to the OPT as well as capture the impact event. The live rigid body view of First Principles software was used as a guide for aligning the HSV with OPT. The HSV camera was considered to be aligned to the OPT when the angles between the three axis of the global coordinate system of the OPT and the transformation of the HSV camera rigid body in the global coordinate system were below 0.5 degrees. Once the HSV and OPT were aligned, the next step was to calibrate the HSV (Figure 3.6).

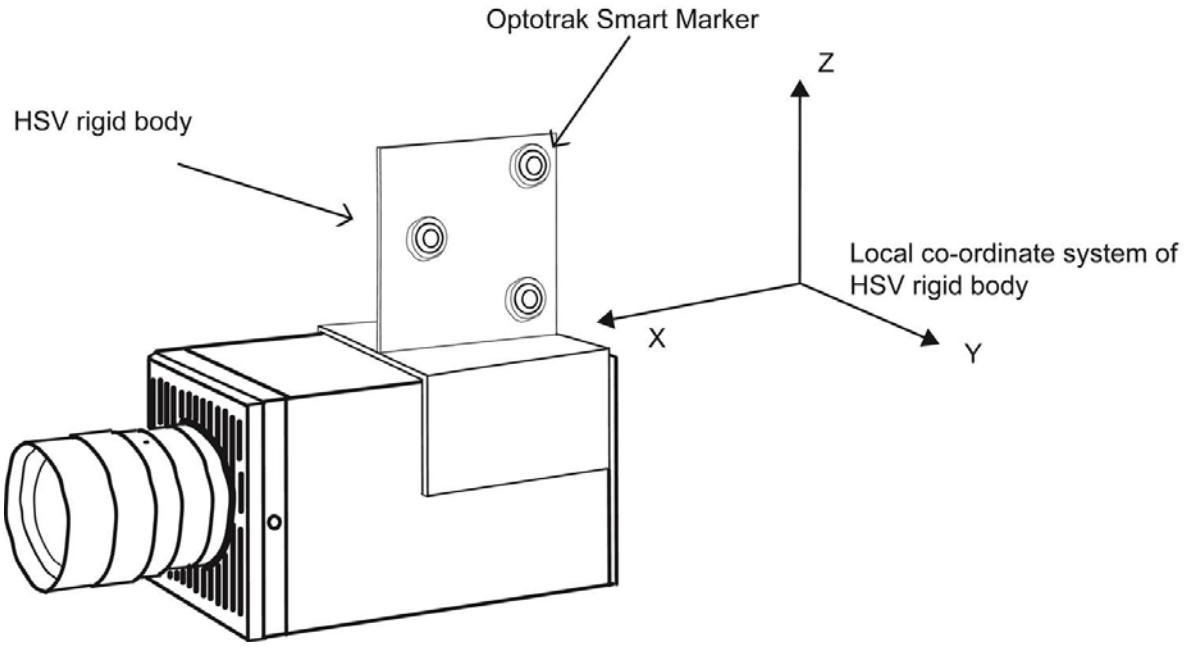

Figure 3.4: Design of rigid body for HSV camera. To ensure that the OPT and HSV systems were tracking the same marker motion, this rigid body was used to align the HSV to the OPT system's global co-ordinate system. The difference in angle between the corresponding axes of the HSV rigid body and the global co-ordinate system of the OPT were minimized to below 0.5 degrees.

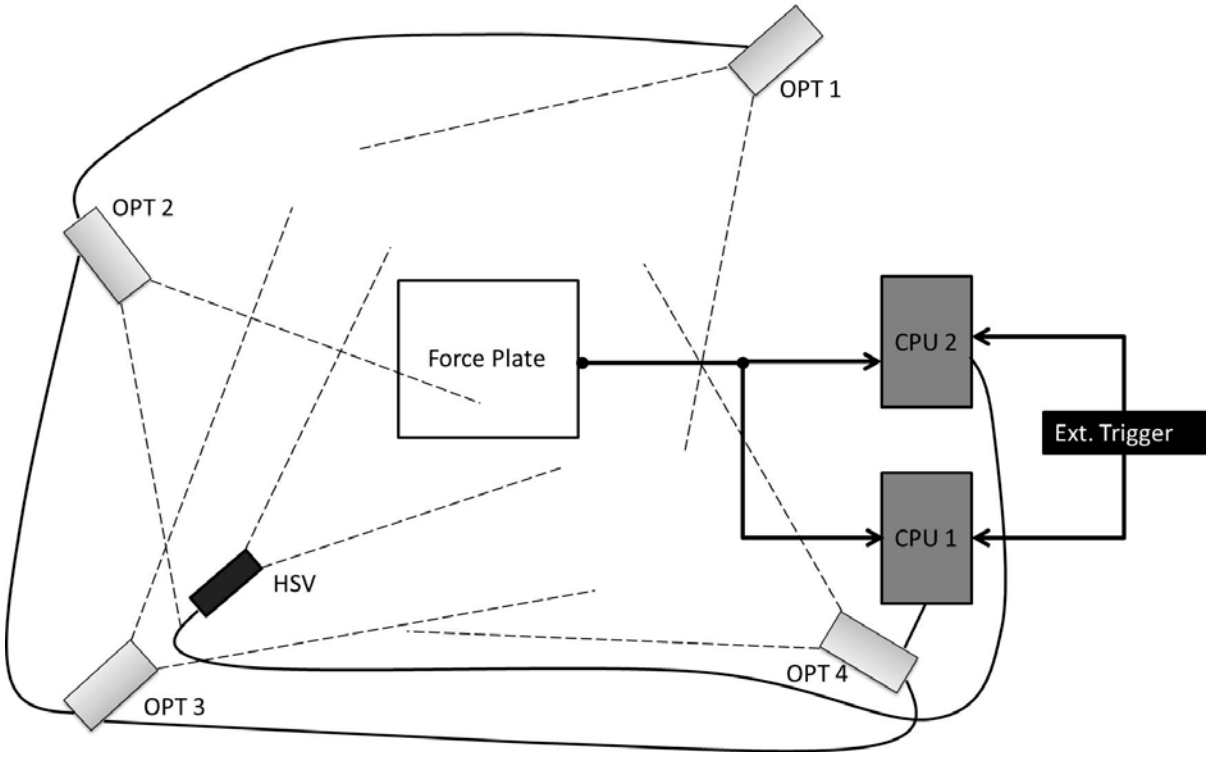

Figure 3.5: Birds eye view of the experimental set up. Labeled are four OPT camera banks (1-4), the HSV camera, the force plate, and the two computer systems needed to collect both systems (CPU). Dotted lines show the theoretical field of view of each camera. With the force plate centered in the middle of the capture volume, four OPT camera banks were used to allow for proper alignment of OPT and HSV. The second OPT camera bank (OPT 2) was aligned to view the HSV camera rigid body. This allowed for proper calibration of the HSV with respect to the OPT system, and subsequently, the impact event.

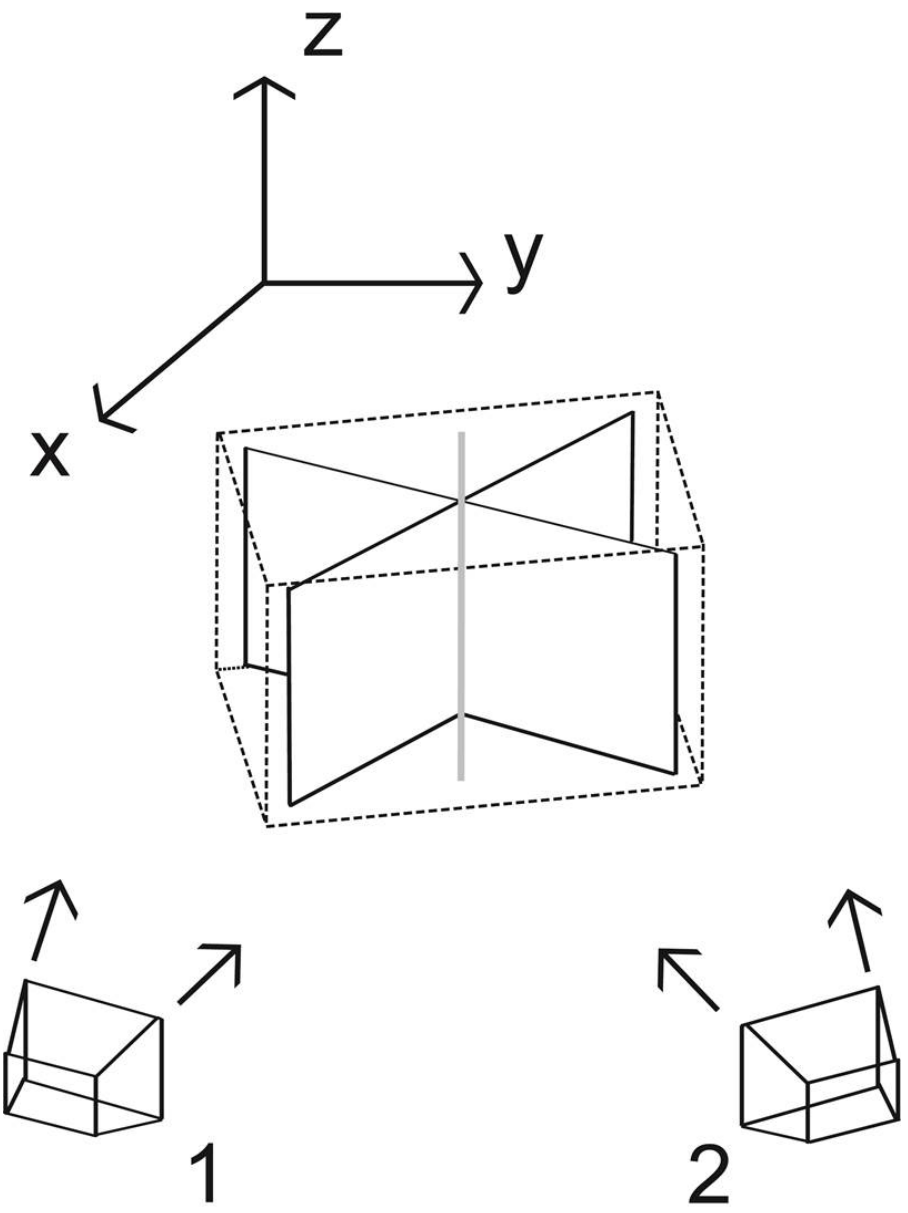

Figure 3.6: This figure illustrates the theoretical alignment of two cameras tracking a vertical displacement vector (light grey line). Since the intersection of two planes is a line, minimizing rotations about the x and y axis would assure the best alignment between the two camera systems. The OPT and HSV camera system were aligned to reduce rotations between the x and y-axes of the HSV rigid body and the OPT global co-ordinate system.

Since 2D videography is in essence a planar view of space, its accuracy is dependent on being focused to the plane of motion of the object it is tracking. This is challenging during repeated impact trials where the participant is removed and placed back in the sling after each impact. In attempts to mitigate this source of error, two single plane laser levels were used to identify the location of the hip marker during calibration, and the location of that calibrating plane during impact trials. Therefore, with the participant still in the sling, and the HSV aligned to view the hip marker, two single plane laser levels were positioned (originating from either side of the HSV camera) to intersect at the hip marker. Since the intersection of two planes is a line, this allowed an estimate of the plane in space that the camera was to be focused to. It also allowed for repeatable positioning of the participant throughout the experiment. Once the two lasers were intersecting on the hip marker, the participant was removed from the sling, and a planar calibration object was positioned at the intersection of the two laser planes. The intersection point was easily identifiable with a planar calibration object as the correct position was when the two lasers made a line in a plane. Once the intersection point was identified, a still image was obtained and used as the calibrating frame for the HSV. This intersection point from the two lasers was then used to realign the participant to the calibrated image plane during each impact (Figure 3.7).

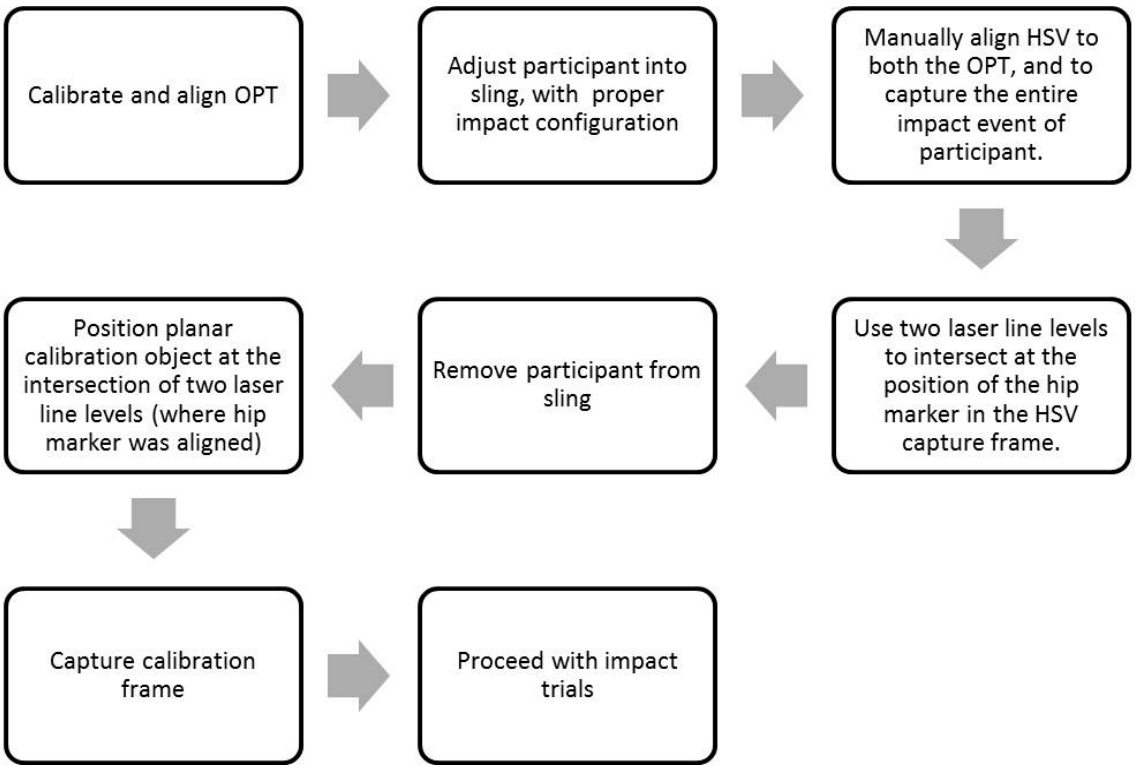

Figure 3.7: Steps to calibrating the HSV system with the OPT system, and also the image plane.

3.2.4 **Data Analysis**

Since the deflection measured by both systems was temporally synced by external trigger, the HSV force data was down sampled to 1500 Hz to match the OPT force data. From this trace the frame of impact initiation was selected from the HSV force plate data. This time of initial impact (T_{imp}) was determined by calculating the mean force and standard deviation during the first 500 samples of the unloaded period at the beginning of the trial (prior to impact), and calculating the time at which force exceeded three times the standard

deviation of the unloaded phase. This frame of impact initiation was used for both the HSV and OPT force data.

3.2.4.1 OPT Force and Deflection Data

To calculate the peak force and peak deflection undergone by the pelvis during impact, the force of initial impact (F_{imp}) and vertical position (D_{imp}) of the right trochanter marker were measured at the frame of impact initiation (T_{imp}). As the OPT measured deflection in reference to a global point of origin (corner of force plate), the deflection of the pelvis was calculated as the time-varying vertical position of the pelvic marker subtracted from this initial pelvic width (D_{imp}) (vertical position of marker at T_{imp}). The time point at which peak pelvic deflection occurred was measured by subtracting every subsequent vertical position of the hip marker from D_{imp}. This gave a positive value for the deflection of the pelvis from the initiation of impact to peak deflection (D_{max}). The peak force (F_{max}) was calculated as the maximum force measured during the entire impact. The time at which peak force and peak deflection occurred were then subtracted by T_{imp}, to give the time to peak force (T_{Fmax}) and time to peak deflection (T_{Dmax}), respectively. To calculate the energy absorbed at peak force (E_{max}), the force-deflection data from T_{imp} to T_{Fmax} was integrated by trapezoidal integration, calculated with the trapezoidal integration function native to MATLAB software (The MathWorks, Inc., Natick, Massachusetts) .

3.2.4.2 HSV Force and Deflection Data

The HSV system captured deflection by filming the same marker (Optotrak smart marker) on the right trochanter of the subject, as the OPT system. This video data was then post processed using the particle tracking feature of the ProAnalyst software (Xcitex, Cambridge, Massachusetts). ProAnalyst is a full-featured auto-tracking software which can measure position of unique objects in the image window. The theory behind analysis of 2D kinematics of an object can fundamentally be thought of as mapping of an object in space to the unique two-dimensional space represented by the photographic image (Figure 3.8). This technique requires calibration of the image plane to object space with a two dimensional calibration frame with known, identifiable landmarks. Thus, a planar calibration object was used to determine calibrated distance per pixel. Deflection was calculated as the vertical distance the right trochanter marker travelled, subtracted from its position at the time of impact initiation (T_{imp}). The peak deflection of the pelvis was calculated as the maximum positive value for the deflection of the pelvis from the initiation of impact to peak deflection (D_{max}). The peak force (F_{max}) was calculated from the maximum force measured during the entire impact. The time at which peak force and peak deflection occurred were then subtracted by T_{imp}, to give the time to peak force (T_{Fmax}) and time to peak deflection (T_{Dmax}). To calculate the energy absorbed at peak force (E_{max}), the force-deflection data from T_{imp} to T_{Fmax} was integrated by trapezoidal integration (MATLAB, The MathWorks, Inc., Natick, Massachusetts).

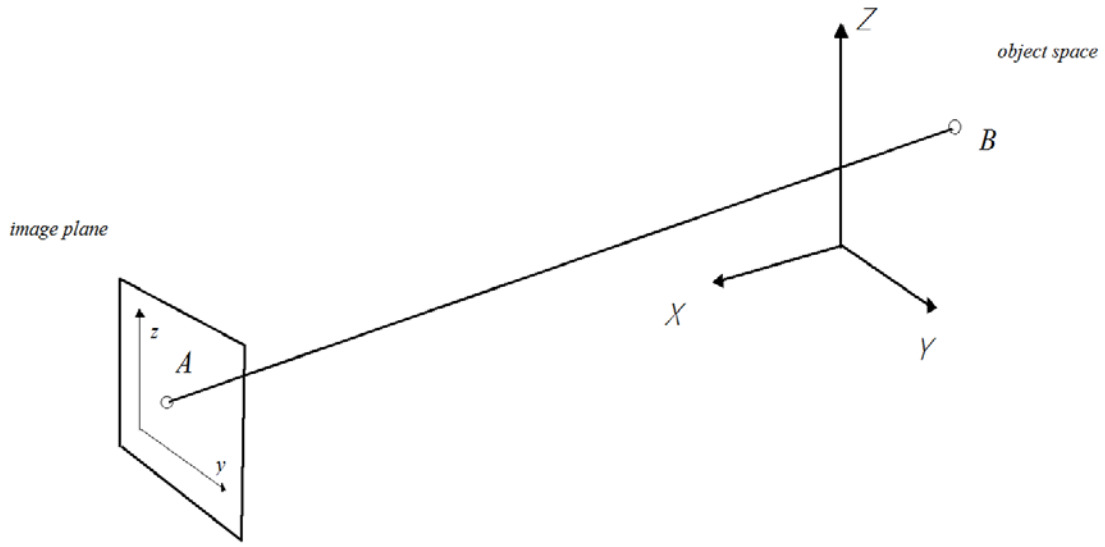

Figure 3.8: Example of spatial representation of object B in the object space, and its corresponding representation (A) in the image plane of the high speed camera.

3.2.5 **Statistics**

From thirteen participants, a total of 46 trials at 1.5cm, and 43 trials at 5cm, had sufficient data (no marker occlusion) to compare between both systems. Subsequently, those 43 trials at the 5cm drop height were used to test the effects of sampling rate. To test for significant differences between the two systems sampling at 1500 Hz, the dependent variable of interest (F_{max}, T_{Fmax}, D_{max}, T_{Dmax}, E_{max}) measured by the OPT system was subtracted from the measurement by the HSV for every single impact trial. The mean difference was then bootstrapped (5000 iterations, with replacement) and the bias corrected and accelerated (BCa) 99% confidence intervals were calculated for each dependent variable (Efron, 1987).

If the BCa confidence interval for the dependent variable did not include zero, the dependent variable was deemed significantly different between systems (this was done for each drop height separately). Additionally, since subjects in "lateral release experiments" generally are considered independent units of study, dependent measures of interest were averaged within subjects and a two-way repeated measures General Linear Model (GLM) was used to test significant differences between measurements systems and whether there was a significant interaction between measurement system (HSV and OPT) and drop height (1.5 and 5 cm).

For the second purpose of the study, the difference between dependent variables measured at 9000 Hz (considered the 'gold standard' measurement in this study) and those measured at subsequent sampling rates (4500, 1500, 500 or 300 Hz) was calculated for each trial. The mean difference was then bootstrapped (5000 iterations, with replacement) and the BCa 99% confidence interval was calculated for each dependent variable, at each subsequent sampling rate. If the BCa confidence interval for the mean difference between the 'gold standard' 9000 Hz rate and subsequent sampling rate did not include zero, the dependent variable was deemed to be significantly different. A subject level analysis was also conducted for sampling rate effects, as dependent measures of interest were averaged within subjects and a one-way repeated measures General Linear Model (GLM) was used to test for significant differences between five levels of sampling rate (9000, 4500, 1500, 500, 300 Hz) for each dependent variable. Post-hoc pairwise comparisons were used to determine which sampling rates were significantly different from the 9000 Hz sampling rate level. Hyun-feldt corrections were used where violations of sphericity were detected. All confidence interval

inferences were used with 99% confidence intervals, and all subject level statistical analyses (GLM) were performed with using an α of 0.05 for uncorrected tests. All bootstrapping and subject level analyses were conducted with SPSS statistical software (SPSS Version 20, SPSS Inc., Chicago, IL, USA).

3.3 **Results**

3.3.1 **Effects of Motion Capture System**

The only statistically significant differences between the HSV and OPT system were for T_{Fmax} and E_{max}, for both drop heights (Table 3-2). At the 1.5 cm drop height, the OPT system measured higher values for T_{Fmax} and E_{max} by 0.6 ± 1.2 (SD) ms and 0.2 ± 0.8 (SD) J, respectively. At the 5 cm drop height, the OPT system measured significantly higher values for T_{Fmax} by 0.7 ± 1.1 (SD) ms and E_{max} by 0.8 ± 1.4 (SD) J. There were no significant differences between camera system for F_{max}, D_{max} and T_{Dmax} at either height. At the subject level analysis (repeated measures GLM), only T_{Fmax} was significantly different between the two systems ($F_{1, 12} = 19.370$, $p = 0.01$), where OPT measured a greater time to peak force (51.3 ± 15.4 (SD) vs 50.6 ± 15.5 (SD)) compared to HSV (Table 3-3). Furthermore, no significant camera by height interaction was observed. Appendix B shows empirical cumulative distributions for each system, calculated for every dependent measure, across all trials, for all subjects.

Table 3-2: Mean and bootstrapped bias-corrected and accelerated 99% confidence intervals (BCa) for the difference in the measurement of the dependent variable of interest between the HSV and OPT systems (HSV value minus the OPT value). BCa intervals were calculated over 5000 iterations. A significant difference between systems was concluded if the confidence interval did not include zero mean difference. Significantly different variables, by this definition, are denoted by *.

		Mean Difference	*BCa 99% Confidence Interval*	
			Lower	*Upper*
	1.5 cm			
	F_{max} ***(N)***	-0.290	-0.881	0.231
*	T_{Fmax} ***(ms)***	-0.609	-0.928	-0.275
	D_{max} ***(mm)***	-0.365	-0.939	0.218
	T_{Dmax} ***(ms)***	-0.304	-0.913	0.362
*	E_{max} ***(J)***	-0.235	-0.467	-0.010
	5 cm			
	F_{max} ***(N)***	2.579	-1.572	6.967
*	T_{Fmax} ***(ms)***	-0.744	-1.070	-0.419
	D_{max} ***(mm)***	-0.727	-1.674	0.224
	T_{Dmax} ***(ms)***	-0.124	-0.682	0.558
*	E_{max} ***(J)***	-0.811	-1.240	-0.384

Table 3-3: Subject level dependent variables measured for the HSV and OPT systems, at two drop heights tested. Main effect of height was ignored, but significant effects of system and a height by system interaction was evaluated. Data presented in parentheses are standard deviations. Variables that were deemed significantly different ($p < 0.05$) are denoted by *.

		Height	*HSV mean*	*OPT mean*	*System p-value*	*System x Height p-value*
	F_{max} *(N)*	***1.5 cm***	888.3 (134.5)	888.5 (134.4)	0.283	0.194
		5 cm	1313.6 (211.6)	1310.7 (210.8)		
*	T_{Fmax} *(ms)*	***1.5 cm***	57.0 (18.6)	57.6 (18.4)	0.001	0.769
		5 cm	44.3 (8.4)	45.0 (8.4)		
	D_{max} *(mm)*	***1.5 cm***	30.2 (7.7)	30.5 (7.1)	0.392	0.549
		5 cm	44.2 (8.6)	45.2 (6.8)		
	T_{Dmax} *(ms)*	***1.5 cm***	62.6 (16.8)	62.8 (16.4)	0.469	0.777
		5 cm	55.3 (7.9)	55.4 (7.6)		
	E_{max} *(J)*	***1.5 cm***	11.2 (6.6)	11.0 (5.8)	0.221	0.164
		5 cm	18.1 (7.3)	20.4 (9.0)		

3.3.2 **Effects of Sampling Rate**

In general, decreasing the sampling rate to levels below 4500 Hz decreased the measured F_{max} and D_{max} and increased T_{Fmax} and T_{Dmax} (Table 3-4). The greatest significant differences were seen on temporal measures T_{Fmax} and T_{Dmax}, where decreasing sampling rate to 300 Hz resulted in, on average, a 3.7 ± 1.1 (SD) ms and 3.5 ± 2.2 (SD) ms increase in the time at which peak force and peak deflection was measured, respectively. Conversely, decreasing sampling rate from 9000 Hz to 300Hz, significantly reduced F_{max} and D_{max} by 8.8 ± 10.1 (SD) N and 0.2 ± 2.5 (SD) mm, respectively. Measurements of energy absorption significantly increased as sampling rate was reduced to 500 and 300 Hz, where E_{max} increased by 0.3 ± 0.7 (SD) J and 0.4 ± 1.1(SD) J, respectively. Across all dependent variables, 4500 Hz was the only sampling rate that was not significantly different when compared to data sampled at 9000 Hz. At the subject level analysis (repeated measures GLM), sampling rate had a significant effect on every dependent variable measured (Table 3-5). Post-hoc pairwise analysis revealed that sampling F_{max} ($F_{4, 48} = 32.367$, $p < 0.001$) at 1500 Hz or below resulted in a mean 4.3 ±7.0 (SD) N reduction in peak force estimates (all $p < 0.05$ for rates at or below 1500 Hz). Sampling T_{Fmax} ($F_{4, 48} = 421.174$, $p < 0.001$) at 1500 Hz or below resulted in a mean 2.2 ± 1.5 (SD) ms increase in the measured time to peak force (all $p < 0.001$ for rates at or below 1500 Hz). Similarly, sampling D_{max} ($F_{4, 48} = 25.200$, $p < 0.001$) and T_{Dmax} ($F_{4, 48} = 50.188$, $p < 0.001$) at 500 and 300 Hz resulted in a mean 0.2 ± 0.2 (SD) mm decrease and 2.8 ± 2.2 (SD) ms increase in the measured peak deflection and time to peak deflection, respectively (all $p < 0.001$). However, only sampling E_{max} ($F_{4, 48} = 5.176$, $p = 0.011$) at 300 Hz significantly increased by on average 0.4 ± 1.1 (SD) J when compared to data at 9000 Hz.

Table 3-4: Average and bootstrapped bias-corrected and accelerated 99% confidence intervals (BCa) for the mean difference in the measurement of the dependent variable of interest between 9000 Hz and the subsequent sampling rate in question. Positive values indicate the measured value increased compared to that measured at 9000 Hz. BCa intervals were calculated over 5000 iterations. Significant difference between systems were determined likely if the confidence interval did not include zero mean difference. Significantly different variables are denoted by *.

			Sampling Rate (Hz)			
			4500	***1500***	***500***	***300***
F_{max} ***(N)***	***mean***		-0.188	-0.754*	-3.391*	-8.791*
	CI	***Lower***	-0.502	-1.319	-5.167	-13.373
		Upper	0.000	-0.251	-1.946	-4.961
T_{Fmax} ***(ms)***	***mean***		0.119	0.664*	2.164*	3.740*
	CI	***Lower***	-0.002	0.535	1.937	3.313
		Upper	0.202	0.788	2.384	4.159
D_{max} ***(mm)***	***mean***		-0.247	-0.332*	-0.487*	-0.503*
	CI	***Lower***	-1.221	-1.308	-1.787	-1.679
		Upper	0.040	-0.029	-0.099	-0.133
T_{Dmax} ***(ms)***	***mean***		0.298	0.717*	2.111*	3.520*
	CI	***Lower***	-0.194	0.162	1.419	2.758
		Upper	0.866	1.403	2.859	4.332
E_{max} ***(J)***	***mean***		0.051	0.156	0.298*	0.418*
	CI	***Lower***	-0.047	-0.015	0.008	0.020
		Upper	0.136	0.326	0.573	0.802

Table 3-5: Subject level dependent variables measured across five sampling rates. Numbers in parentheses are standard deviations of the means above them. P-values denoted are for overall main effect of sampling rate tested for that variable. Sampling rate had a significant main effect on every variable measured, and variables measured that were significantly different compared to the 9000 Hz condition (pairwise post-hoc analyses) are denoted by *. All significance levels were evaluated at $\alpha < 0.05$.

	Sampling Rate					*Sampling rate*
	9000	***4500***	***1500***	***500***	***300***	***p-value***
F_{max} *(N)*						
mean	1314.3	1314.1	1313.6 *	1310.9 *	1305.6 *	$p < 0.001$
	(212.0)	(211.8)	(211.7)	(212.3)	(210.3)	
T_{Fmax} *(ms)*						
mean	43.4	43.5	44.1 *	45.5 *	47.1 *	$p < 0.001$
	(8.4)	(8.5)	(8.4)	(8.2)	(8.3)	
D_{max} *(mm)*						
mean	44.7	44.7	44.6	44.6 *	44.5 *	$p < 0.001$
	(9.3)	(9.4)	(9.4)	(9.4)	(9.4)	
T_{Dmax} *(ms)*						
mean	55.0	55.3	55.7	57.1 *	58.5 *	$p < 0.001$
	(8.5)	(8.7)	(8.6)	(8.8)	(8.7)	
E_{max} *(J)*						
mean	19.3	19.3	19.4	19.5	19.7 *	$p = 0.021$
	(8.9)	(9.0)	(8.9)	(8.8)	(8.8)	

3.4 **Discussion**

This study tested the differences between two motion tracking systems (3D optical motion tracking vs. 2D high speed videography) as they simultaneously measured the linear force-deflection response of the pelvis during lateral pelvis release experiments (Figure 3.9 and Figure 3.10). Although it was hypothesized that there would be no significant difference between the two systems, tests revealed that both systems were similar in estimating all but two measures of impact severity, time to peak force (T_{Fmax}) and energy absorbed (E_{max}), which were significantly different between systems at both drop heights tested (Table 3-2). Alternatively, at the subject level, only T_{Fmax} was significantly different between the two systems ($p < 0.001$) with no significant interaction between system and height (Table 3-3). The second purpose of this study was to determine the effects of reduced sampling rates on measures of impact severity. As hypothesized, this study demonstrated that measurements of peak force and peak deflection significantly decreased when sampled at lower rates (1500, 500, 300 Hz), while temporal measures (time to peak force and time to peak deflection) increased (Figure 3.10). Specifically, sampling at or below 1500 Hz significantly increased measures of time to peak force by on average 9.5 ± 0.6 (SE) % and increased time to peak deflection by on average 6.8 ± 0.1 (SE) %. Similarly, decreasing sampling rate from 9000 Hz to 300Hz significantly reduced F_{max} and D_{max} by 0.7 ± 0.1 (SE) % and 0.5 ± 0.1 (SE) %, respectively. Contrary to expectation, measurements of energy absorption (E_{max}) showed significant increases (as opposed to hypothesized decreases) as sampling rate was reduced to 500 and 300 Hz, where E_{max} increased by 2.2 ± 0.8 (SE) % and 2.8 ± 1.2 (SE) %. Alternatively, no significant differences were found at 4500 or 1500 Hz for E_{max} when

compared to data sampled at 9000 Hz. At the subject level, sampling at or below 1500 Hz significantly reduced estimates of peak force, and time to peak force. Whereas, significant differences were seen in peak deflection (decreased) and time to peak deflection (increased) when sampled at or below 500 Hz, and at 300 Hz for energy absorbed.

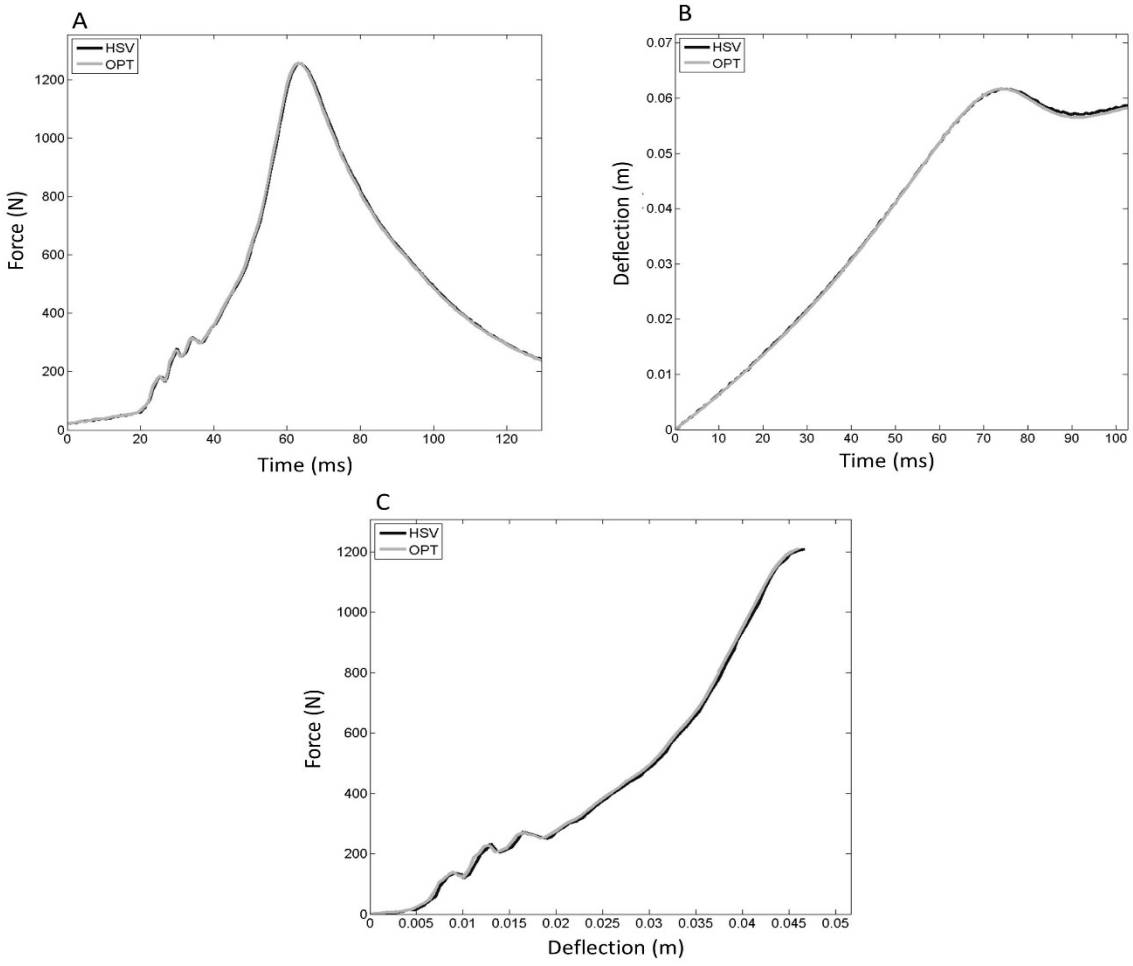

Figure 3.9: Time varying data showing trials which had the lowest differences between systems. A) Time-varying force for the same impact trial. B) Time-varying deflection for one impact trial. C) Force deflection trace for one impact. Black data traces are measured by the high speed videography system (HSV), while grey traces are data measured by the Optotrak system (OPT).

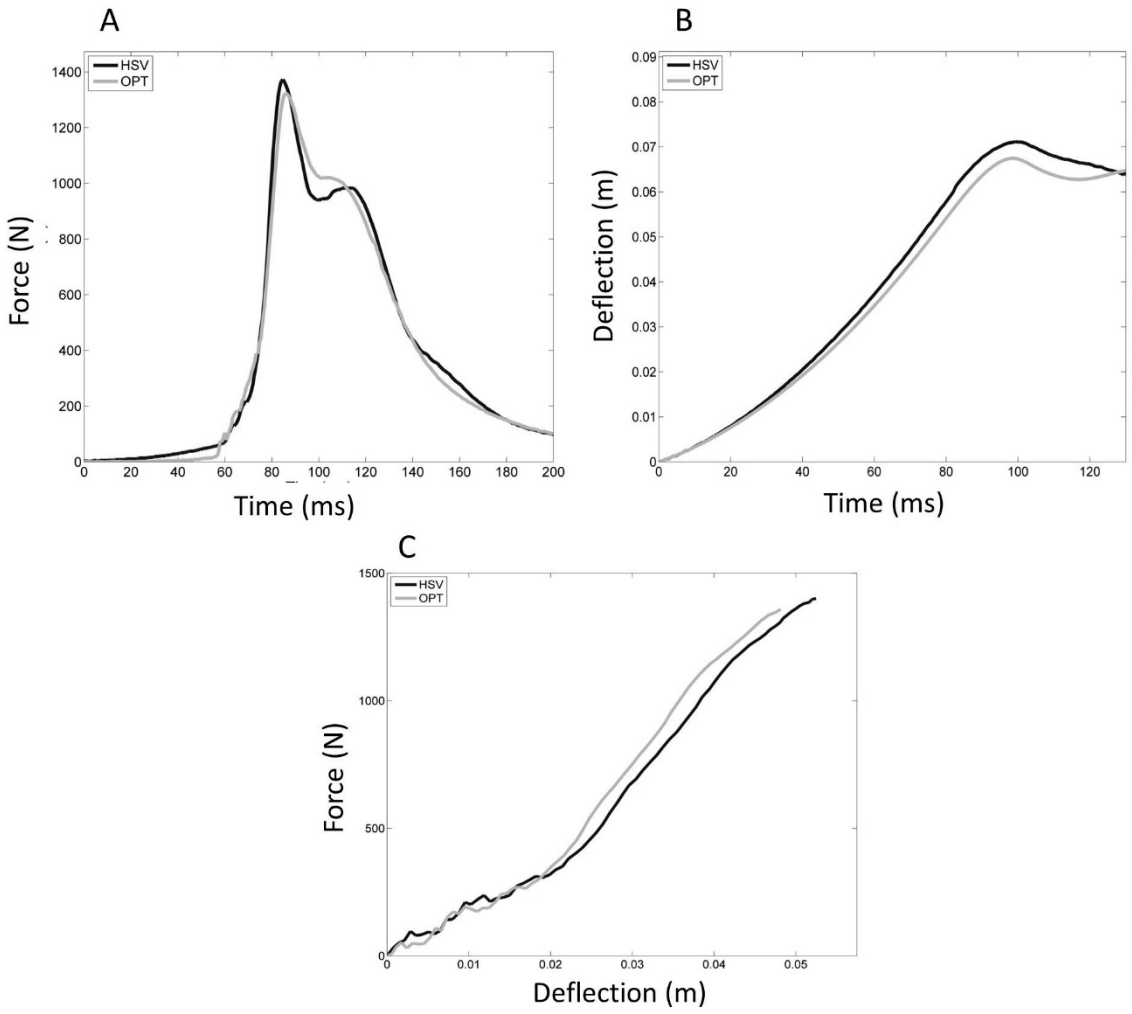

Figure 3.10: Time varying data showing trials which had the greatest differences seen between systems in this study. A) Time-varying force for the same impact trial. B) Time-varying deflection for one impact trial. C) Force deflection trace for one impact. Black traces are data measured by the high speed videography system (HSV), while grey traces are data measured by the Optotrak system (OPT).

3.4.1 **Effects of Motion Capture System**

The reason for the observed differences between systems for T_{Fmax} is uncertain, and considering its magnitude, of minimal consequence. In this study, both systems were synced with a common external trigger, but a significant mean difference was still measured. Furthermore, even after averaging together trials within a participant (subject level analysis), a significant difference remained between systems for time to peak force. One possibility for this difference could be the presence of slight drift between systems as they sample over time. Temporal drift describes the gradual asynchrony between two digitally sampled signals, when collected by two separate data acquisition systems (DAQ). If two systems, sampling at the same frequency, are initiated at the same time— they can become asynchronous due to inherent differences in maintaining correlation with real time. Pilot testing on the synchronization between systems showed the presence of a slight drift between systems as they sampled square waves from a signal generator (Appendix A). These pilot tests showed a maximum possible drift between systems of three frames over two seconds of collection. However, the drift was not necessarily the same for each trial, and was random in nature. Regardless of the root cause of the temporal discrepancy, it is important to consider the magnitude of the difference between systems. For two systems sampling at 1500 Hz, a discrepancy of one frame (1/1500) is approximately 0.667 ms (if the systems are off by two frames, the difference is 1.334 ms etc.). In this study, the mean difference between systems was -0.609, 99% CI [-0.928, -0.275] ms at the 1.5 cm drop height and -0.744, 99% CI [-1.070, -0.419] ms at the 5 cm drop height. Meaning, on average, the Optotrak system measured a longer time to peak force than the high speed camera system, by about one frame,

which is relatively small in the context of pelvis release studies. In this study T_{Fmax} ranged around 44 to 58 ms (As measured by HSV—Table 3-3), making one frame approximately 1.5% ((0.667 ms / 44 ms) x 100%) of total time to peak force at the most. Therefore, the differences in time to peak force, although statistically significant, are of minimal in the context of lateral pelvis release studies.

Of greater interest are the observed differences between systems with regard to the measured absorbed energy (E_{max}). It is possible that the differences between systems in energy absorption are due to the differences in time to peak force, since OPT measured both a greater energy absorption and time to peak force compared to HSV. Hypothetically, if the OPT measured approximately one extra frame of data force, a significant amount of extra energy could be measured if the pelvis deflection during that extra frame was considerable. For example, if the pelvis was loaded at a constant 1m/s (initial velocity) during the time of peak force, it would deflect 0.00067 m over one frame (1/1500 x 1 m/s). If we use the average peak force measured by the OPT system at 5cm (~ 1311 N), this would result in an additional 0.87 J of energy measured by the OPT system (around the observed energy difference of 0.235 to 0.811 J, for the 1.5 and 5cm drop height respectively). However, upon observing the relationship between the difference in E_{max} and T_{Fmax} for both heights, this possibility accounted for some —but not all— of the differences between the systems (Figure 3.11). If a longer time to peak force measured by the OPT system was responsible for all of the overestimation of energy absorption by OPT, all of the data points in Figure 3.11 would reside in the lower left quadrant (further analysis using contingency tables available in

Appendix C). However, this was not the case, and does not explain all of the discrepancy between OPT and HSV for E_{max}.

Another reason for the differences between systems for E_{max} could be due to differences in tracking the deflection of the pelvic marker throughout the impact. Although the two systems were not significantly different in peak deflection measurements, any differences between systems during the course of the deflection interval can accumulate as significant differences in E_{max}. Trapezoidal integration, and numerical integration in general, is an additive process that amplifies low frequency spectral components of a signal (Winter and Patla, 1997). Therefore, slight non-constant errors (low frequency spectra) that might not appear significant in the maximum deflection of the pelvis can become amplified when E_{max} is calculated. A look at the differences between OPT and HSV during the entire interval of pelvic deflection shows this type of low frequency, non-constant, difference between systems (Figure 3.12). Since both systems track the marker using an inherent centroid estimation algorithm, there are bound to be systematic differences between both systems as the tracked the center of the marker over time. However, since this was not explicitly tested in this study, it is not clear which system is prone to which behavior. Moreover, how much this can alter measures of energy absorption is speculative, but still of possible concern (Appendix D).

Here again, it is important to consider the differences between systems in the context of the magnitude of E_{max}. At the 1.5 cm drop height the HSV system measured an average E_{max} of 11.2 J with an average difference of 0.2 J. This equates to about 1.8% of the total energy measured ((0.2 J/11.2 J) x100%). Likewise, at the 5 cm height, an average E_{max} of 18.1 J was measured, with an average difference of 0.8 J, equating to 4.4% of the total energy

measured. Intriguingly, averaging data within a participant for subject level analysis removed the significant difference between systems in terms of E_{max}. Subjects in "lateral release experiments" generally are considered independent units of study and averaging data across impact trials for statistical testing is common (Bhan et al., 2013; Levine et al., 2013a). This suggests that concerns of differences between studies due to different measurement technology might be lessened if data are analyzed at the subject level (since averaging will reduce variability). Although, this was not explicitly tested in this study, the results are encouraging for when comparing data between studies which used either 3D optical motion capture or 2D videography.

It is worth mentioning that although both systems were statistically similar for force measurement, the least agreeable trial (shown in Figure 3.10) does raise concerns. Since the force voltage signal was split after it was outputted from the force plate, ideally both computers should have the same measurement of force. Admittedly, there is a possibility that differences might exist between computer A/D cards in sampling this analog voltage signal, but the nature of the differences in force data shown in Figure 3.10, suggest the possibility for differences beyond just random errors in digital sampling (there seem to be shifts in both phase and amplitude). This necessitates further diagnostic testing to determine the root cause of these differences between systems in measuring force.

Finally, it is also worth emphasizing that the results obtained from this study are highly dependent on the methods utilized. The OPT system actively tracks its markers as they move through a pre-calibrated volume. HSV is largely post-processed and is highly dependent on the accuracy of manual calibration and the auto tracking software, which in

itself is highly dependent on the quality of the videography. As such, considerable efforts were taken to ensure that the HSV system was aligned with the OPT system, and that the HSV system was accurately calibrated, to minimize differences in measuring force and deflection. Without these efforts, even greater differences between 2D videography and 3D motion tracking may have arisen. Furthermore, this study only set out to characterize the differences between the two systems, and determine if they agree. Whether the values measured are truly indicative of the underlying biological system remains unknown and of concern for future studies.

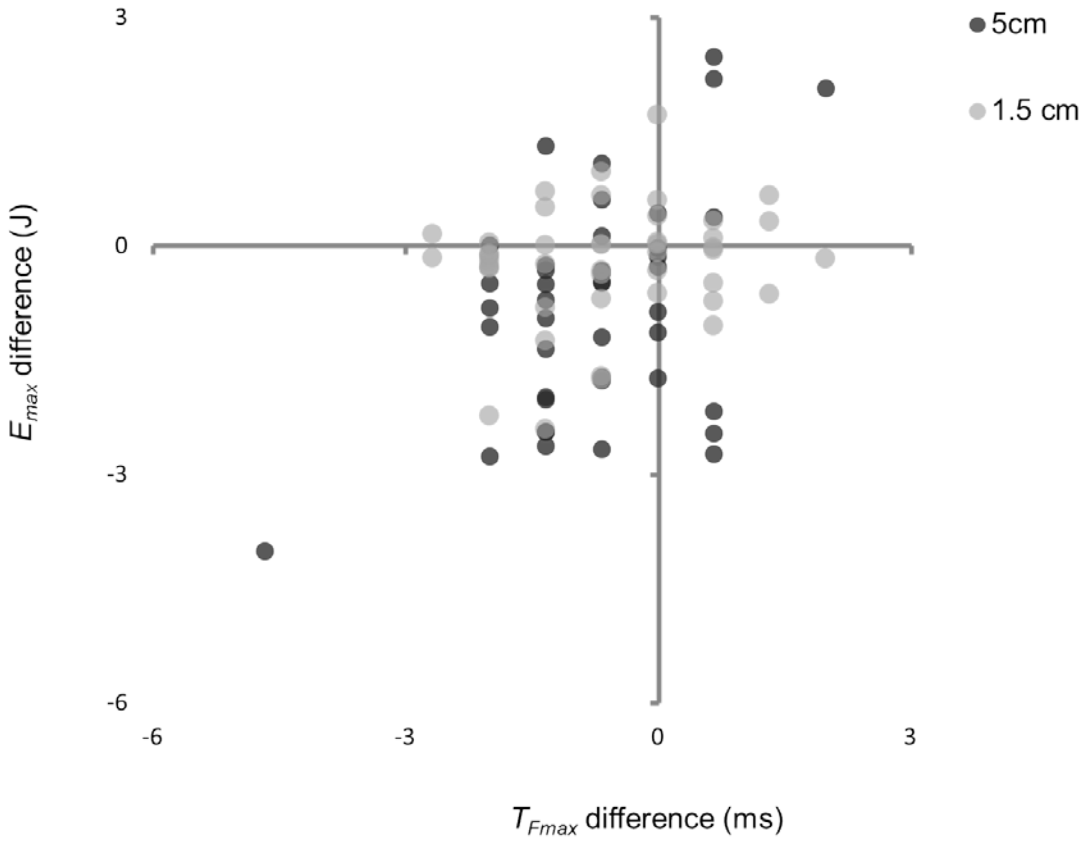

Figure 3.11: Relationship between difference in time to peak force and the difference in energy absorption measured by each system. Difference was calculated by subtracting the respective value measured by the Optotrak system (OPT) from that measured by the high speed video system (HSV). If the longer time to peak force measured by the OPT system was responsible for all of the overestimation of energy absorption by OPT, all of the data points would reside in the lower left quadrant (further analysis in Appendix C). However, this was not the case, and does not explain all of the discrepancy between OPT and HSV for E_{max}.

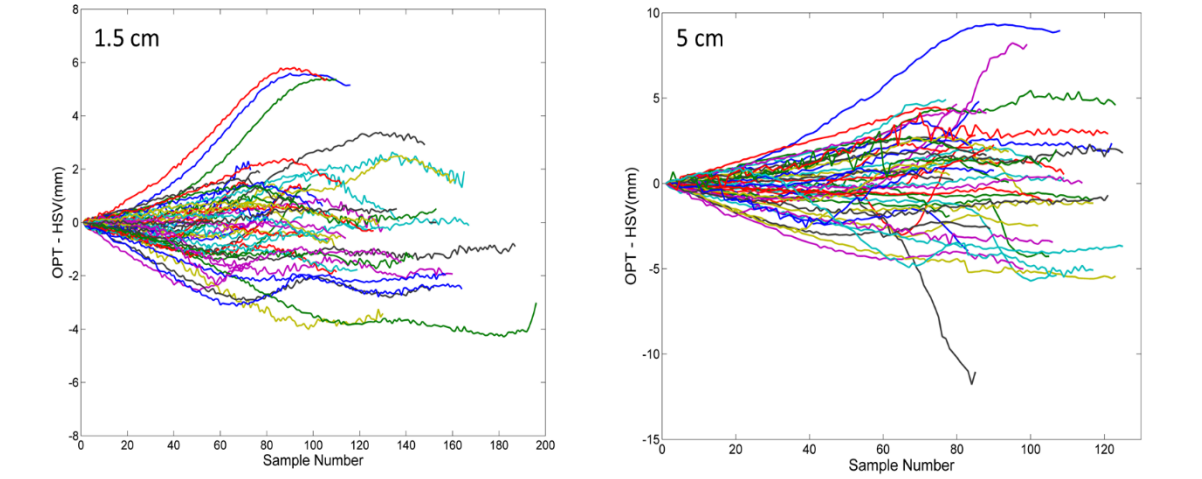

Figure 3.12: Time-varying difference traces calculated for the deflection signals measured by both systems from impact initiation until peak force. These traces were calculated by subtracting the deflection measured by the high speed video system (HSV) from the deflection measured by the Optotrak system (OPT) or every time point, for every impact. Different colours represent different impact trials. Of interest is the time varying bias that occurs as the impact trial propagates between the two systems. This can lead to significant differences between systems upon integration to calculate energy.

3.4.2 **Effects of Sampling Rate**

In regards to sampling rate, this study provides important insight for both previous and future biomechanical impact studies using the lateral pelvis technique. It appears that previous studies (and future studies for that matter) using sampling rates below 1500 Hz might not completely capture certain measures of impact severity (F_{max}, T_{Fmax}, D_{max}, T_{Dmax}, E_{max}). However, the magnitude of the differences are minimal for F_{max} and D_{max} which all averaged to less than a 1% change from data sampled at 9000 Hz (Figure 3.13). Contrastingly, temporal measures of impact severity were more susceptible to the effects of sampling rate, where sampling as low as 300 Hz resulted in an increase in time to peak force and time to peak deflection of 9.5 ± 0.6 (SE) and 6.8 ± 0.7 (SE) % respectively. Likewise, E_{max} increased by 2.8 ± 1.2 (SE) % when data was sampled at 300 Hz. All in all, sampling data at 4500 Hz was the lowest frequency that did not result in any significant differences for any dependent variable, and seems like a suitable sampling rate for future studies interested in measuring all of the dependent variables tested in this study. In terms of number of data points, sampling at 4500 Hz would result in 90 to 225 data points for impacts occurring between 20 and 50 ms (from initiation till peak force), which is a marked improvement from data sampled at 400 Hz (8 to 20 points) or 1000 Hz (20 to 50).

Particularly interesting is the variability in measurements of energy absorption as a result of lower sampling rate. Since energy absorbed is calculated by numerical integration, it is highly sensitive to the errors occurring during the entire force-deflection curve as a result of reduced sampling (Figure 3.14). Specifically, numerical integration is sensitive to the number of partitions over which the finite integral is estimated. The greater the number of

discrete partitions over an interval, the smaller the estimation distance between adjacent points for integration, and subsequently the lower the error in estimating the integral of a curve between those points (Chapra and Canale, 2005). Thus, the higher the sampling rate, the smaller the interval between adjacent points. Resultantly, not only did sampling at 300 Hz produce a significant increase in E_{max}, its effect on each trial was highly variable (Figure 3.15), where sampling the force-deflection curve at 300 Hz in some trials lead to an increase in energy and other to a large decrease. Comparatively, the effect of reduced sampling was more predictable for time to peak force, as all trials resulted in an increase when sampled at 300 Hz.

Averaging data within a participant at the subject level appears to reduce some of the variability in sampling E_{max} at lower sampling rates. In this study, analyzing data at the subject level reduced the lowest non-significant sampling rate to 500 Hz for E_{max}. Additionally, subject level analysis reduced the lowest non-significant sampling rate to 1500 Hz for D_{max} and T_{Dmax}. This suggests that the effects of sampling rate are reduced when averaging data across multiple impacts from a subject. Admittedly this is not a substitute for undersampling biomechanical data, but it does allow for a better understanding of the differences between previously conducting studies at differing sampling rates that employed subject level analyses.

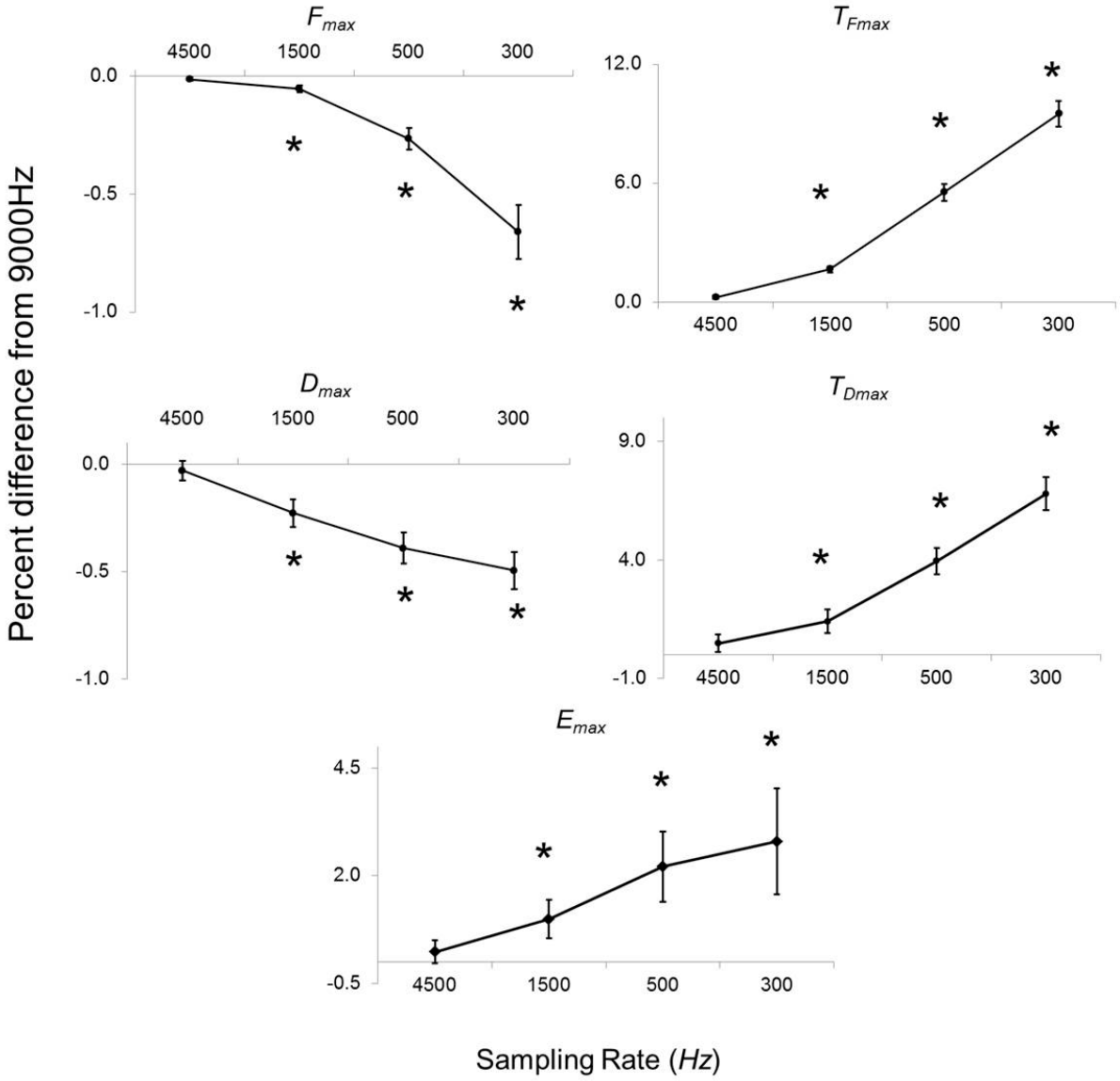

Figure 3.13: Mean percent difference in calculated dependent variable of interest at various sampling rates. Positive percent difference means the value increased compared to the value at 9000 Hz. A negative percent difference means the value decreased. Values are labelled with the standard errors for the percent difference. Not confidence intervals, which are shown in Table 3-4. * denotes sampling rates that were significantly different from the control 9000Hz level, as determined from the confidence intervals (Table 3-4).

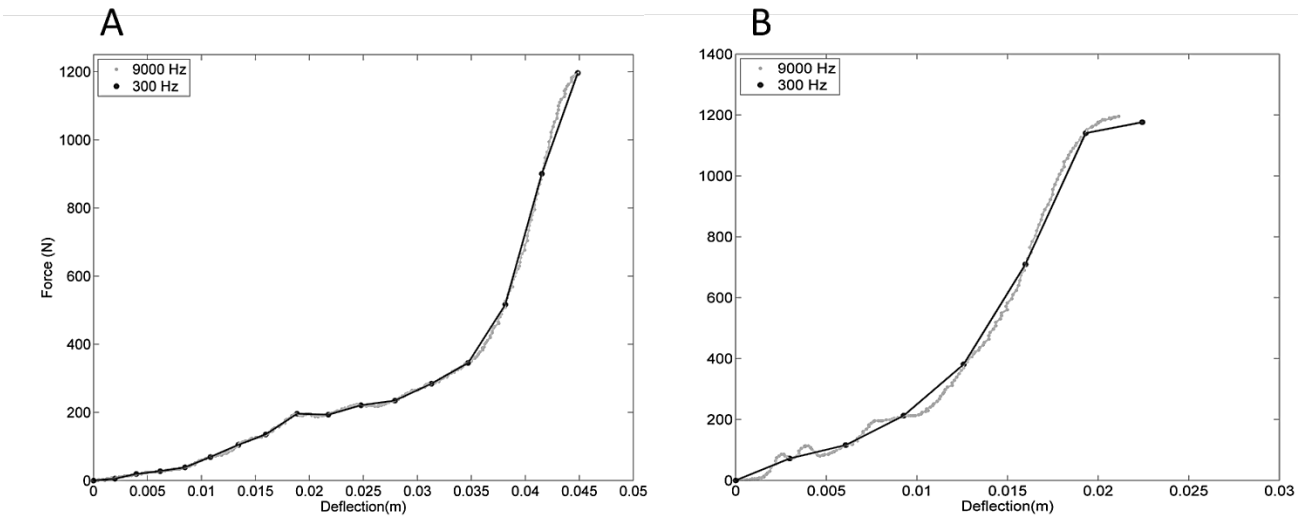

Figure 3.14: The effect of sampling force deflection response of the pelvis at 300 Hz (black), compared to sampling it at 9000 Hz (grey) for two separate impact trials (separate participants). Panel A shows very little change in the force-deflection curve measured at 300 Hz, whereas data in in panel B is markedly different. The shape of the loading history has a large effect on how well reduced sampling can represent the underlying biological signal.

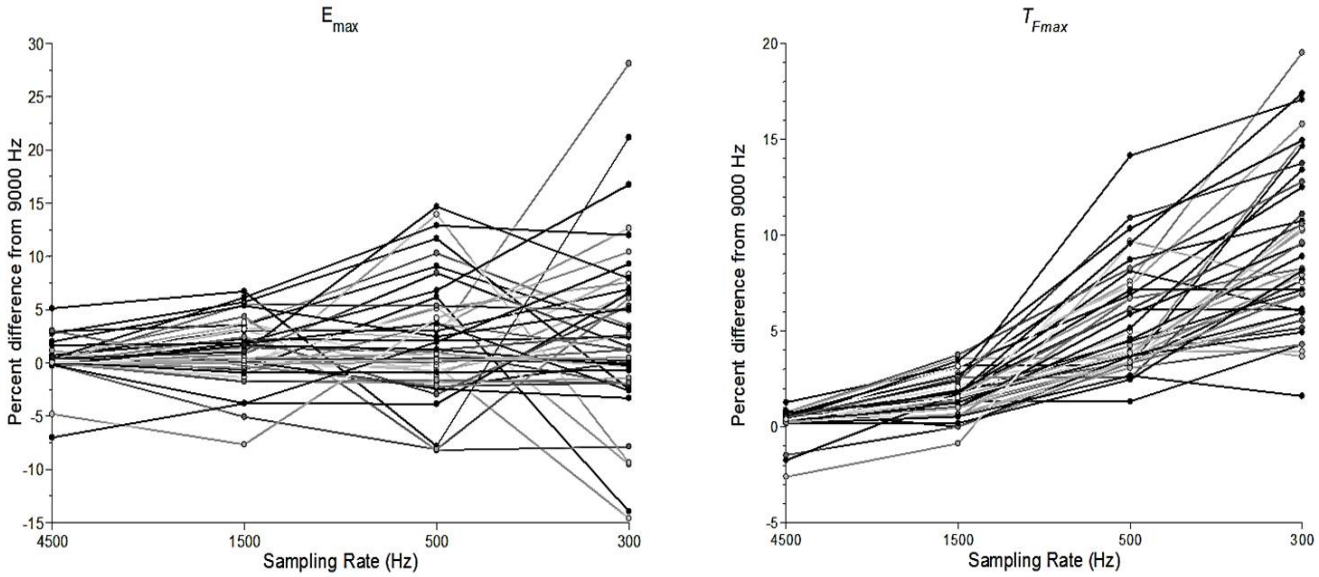

Figure 3.15: Percent difference from data measured at 9000 Hz to those measured at 4500, 1500, 500 and 300 Hz. Data for every trial analyzed is shown. Panel on the left is energy absorbed (E_{max}) and on the right is time to peak force (T_{Fmax}). Of interest is the variability that reduced sampling rates can have on estimates of energy absorbance, compared to time to peak force. Both variables increase in variability as data sampling is reduced to 300 Hz, but the trend is more apparent for time to peak force.

3.4.3 **Limitations**

This study had several limitations. Firstly, considering that previous studies of impact dynamics during falls on the hip have not filtered force or deflection data (Bhan et al., 2013; Laing and Robinovitch, 2008a; Laing and Robinovitch, 2010; Laing et al., 2006), force and deflection data were not filtered. The process of a filter design and filter cut-off is a confounding factor, and not clearly agreed upon in the impact biomechanics literature and was left out of this study. Therefore, this study provides assessment of the differences in the measurement of raw data signals between systems. Second, this study used human participants impacted at 0.5 and 1.0 m/s, and the results presented here should only be extrapolated with caution. It was assumed in this study that the individual mechanical characteristics of each subject would not affect the observed difference/variance in dependent variables of interest. However, this assumption was not critically assessed and it is possible that at extreme ends of the spectrum of biological tissue it becomes inappropriate. To verify these results for varying ranges of materials and configurations further testing is needed. Lastly, if the only question is whether there is a difference between these systems, then the answer is inevitably yes; there will always be a difference. If enough data is collected, then there is a high likelihood of seeing a "significant" difference. If there is not enough data, the likelihood is lower. What is more important to focus on is whether there is a difference between these systems that matters, and the definition of "matters" depends on the specific research questions being explored. For the purposes of lateral pelvis release experiments the differences between these systems are minimal and within acceptable limits. However, care must be taken in appropriating the acceptable level of difference when choosing a motion

capture technique or sampling rate for other impact related studies with vastly different subjects and methods, than that were used here.

3.4.4 **Conclusions**

In summary, this study shows that 3D optical motion capture and 2D high-speed videography perform similarly in measuring the impact response of the human pelvis during lateral pelvis release impact trials, at 1.5 and 5 cm drop height. Although significant differences were seen between systems in measuring T_{Fmax} and E_{max}, the magnitude of differences were at or below 5% of the total magnitude of each measured variable. Furthermore, averaging impacts within a subject reduced the differences between systems for E_{max}. Tests on the effect of sampling rate found differential effects contingent on the dependent variable measured. Sampling as low at 300 Hz, significantly reduced measures of F_{max} and D_{max}, but only by on average 0.7 and 0.5 %, respectively. Whereas measures of T_{Fmax} and T_{Dmax} increased by on average 9.5 and 6.8 %. Sampling E_{max} at 500 Hz and 300 Hz increased measures of impact absorption by 2.2 and 2.8 % respectively. Sampling at 4500 Hz was the lowest sampling rate that was not significantly different from 9000 Hz across all dependent variables. These results show that 3D optical motion capture and 2D high-speed videography are comparable in measuring hip impact dynamics in human participants during lateral pelvis release trials. Additionally, they suggest that careful attention should be paid to sampling rate during lateral impact trials, with specific concern for the effect that sampling rate has on the dependent variable of interest.

Chapter 4
Contact Area in Lateral Hip Impact Mechanics

4.1 Introduction

Previous studies have suggested that more than 90 % of hip fractures result from falls (Aharonoff et al., 1998; Grisso et al., 1991). However, only about 1-2 % of falls actually result in a hip fracture (Sattin, 1992; Tinetti et al., 1988). Evidence suggests that the mechanics of the actual fall (i.e. direction of fall and location of impact) is a better predictor of hip fracture compared to indices of bone fragility (i.e. osteoporosis) (Ford et al., 1996; Greenspan et al., 1994; Hayes and Myers, 1997; Nevitt and Cummings, 1993). Direct impact on the trochanteric area of the hip during a sideways fall is particularly detrimental in the event of a fall (Hayes et al., 1996). As a result, many biomechanical interventions have been engineered to mitigate the force directed to the greater trochanter (GT) during an impact.

Hip protectors (Koike et al., 2009; Laing et al., 2011; Laing and Robinovitch,2008b), compliant floors (Laing et al., 2004; Laing and Robinovitch, 2009; Laing et al., 2006), and even increased soft tissue thickness overlying the greater trochanter (Maitland et al., 1993; Majumder et al., 2008; Robinovitch et al., 1995b) have all been shown to reduce the impact force on the lateral hip. If a simple springs-in-series approach is used to model impacts between the pelvis (of stiffness k_p) and a surface (of stiffness k_f), total system stiffness is calculated as: $(k_p \times k_f)/(k_p + k_f)$. By adding various materials of lesser stiffness between the bony pelvis/greater trochanter and impacting surface (ex. hip protector, compliant flooring, soft tissues) total system stiffness decreases. In effect, this reduces the frontal plane

compressive stiffness of the pelvis, and helps to reduce the peak impact force transmitted to the lateral hip.

This reduced system stiffness is of particular interest when considering epidemiological research that suggests increased body mass index (BMI) is associated with a lower risk for hip fracture in the elderly (Armstrong et al., 2011; De Laet et al., 2005; Meyer et al., 1995a; Meyer et al., 1995b; Pruzansky et al., 1989; Stolee et al., 2009). Previous research has shown a positive correlation ($r = 0.86$) between BMI and soft tissue depth above the greater trochanter (Maitland et al., 1993), and it has been suggested that the additional soft tissue helps to reduce total pelvic stiffness and subsequently reduces the force transmitted to the greater trochanter (Laing and Robinovitch, 2008b; Robinovitch et al., 1995b). However, confounded within BMI (calculated as the mass in kg divided by the square of height in meters) is mass, which is directly related the impact energy (kinetic energy = $1/2mv^2$,m= mass,v=linear velocity). Therefore, the increased mass that might come along with higher BMI would be expected to increase the force of impact. Appropriately, previous research has used mass or effective mass as significant predictors of impact load (Bouxsein et al., 2007; Dufour et al., 2012; Robinovitch et al., 1991; van den Kroonenberg et al., 1995). Despite these model predictions of increased load with increased mass, epidemiological literature continues to affirm a reduced risk of hip fracture for older adults with higher BMI (Armstrong et al., 2011; Morin et al., 2009).

Although, a single-degree-of-freedom system approach has been beneficial in furthering our understanding of the mechanics of hip impacts, and predicting impact forces (Laing and Robinovitch, 2010; Robinovitch et al., 1991, 1997b), no literature exists on the

spatial distribution (i.e. contact area) of loads on lateral pelvis during hip impact. Although mass-spring models might be good estimates using rigid body assumptions, the pelvis is a deformable and complex structure, and little is known about how this load distribution (loading specific to the greater trochanter) changes as a function of individual anthropometries (ex. mass, effective mass, BMI etc.), and how it relates back to hip fracture risk.

A theoretical understanding of load distribution for simple elastic structures stems from the Hertzian contact theory of elastic deformation, which is a model that has been applied to a wide spectrum of biomechanical studies concerned with load distribution (Fregly et al., 2003; Gefen, 2007; Hirokawa, 1991). This theory describes the contact between an elastic sphere and a rigid half-space. The equations from the model describe the relationship between contact area (*a*) and the specific variables of interest in hip impact research (*F = force*, *x = deflection*), where the functional dependence with contact area is:

$$a \propto x \tag{11}$$

$$a \propto F^{2/3} \tag{12}$$

Although the lateral hip is not a sphere, it has been geometrically modelled as one before (Laing and Robinovitch,2008b), and these equations provide a mechanical basis for investigating the relationship between force, deflection, contact area and load distribution lateral hip impacts.

Although a closer look at load distribution would offer a better understanding of hip fracture risk between individuals, it has been scarcely studied in-vivo, with human participants. Early studies used the size of hematoma's in hip fracture patients to estimate the total contact area between the lateral hip region skin surface and ground during impact at 110 cm^2 (Askegaard and Lauritzen, 1995), with other work suggesting the contact area of the actual greater trochanter might be only 2 - 6 cm^2 (Lauritzen, 1997). A study by Laing et al. (2008c) on a mechanical test system, found that increasing the size of a surrogate lateral hip (anterior to posterior radius of curvature) decreased the percentage of total impact force transmitted to the femoral neck. Another study by Laing and Robinovitch (2008b), used various diameter load cells to determine the effect of soft shell hip protectors on the magnitude and distribution of impact force during lateral pelvis release experiments. They found that in the unpadded condition, only about 17 % of the total impact force was directed within a 1.25 cm radius around the greater trochanter. However, in their study they used separate trials with finite sized load cells to approximate this percentage, and were not able to estimate force distribution within a particular trial. A more recent study by Choi et al. (2010a) used a pressure plate of 4096 sensors to determine the pressure distribution over the hip during lateral pelvis release experiments. In their study, they found significant differences in the effectiveness of hip protectors in reducing pressure to the lateral hip between a low (n=7) and high (n=7) BMI group of participants. In addition, they found low BMI participants had significantly higher peak pressure, with no difference in peak force between the groups. Contrastingly, a separate study by Levine et al. (2013) found significantly higher peak impact forces for high compared to low BMI participants, but this

relationship reversed when impact force was normalized by mass. The discrepancies between the two studies might lie in methodology, where in the Choi study, participants were bracing their upper body with their arm in attempts to mimic a more "realistic" falling configuration, with a slightly elevated torso. The study by Levine et al. had participants lie completely lateral, without engagement of the participants' arm, in attempts to better study the dynamics of the impacted pelvis.

Accordingly, there were three primary objectives to this current study, with the overall purpose to investigate the relationships between contact area and load distribution: First, to determine the relationship between time-varying impact variables. Particularly, whether time-varying force (F_t) and deflection (D_t) were significantly correlated (Pearson product-moment correlation) with time-varying contact area (C_t) during the compressive phase of a lateral hip impact (from impact initiation to peak force), and if transformation of the impact force (power law transformation, FT_t) was more highly correlated with contact area; as suggested by Hertzian contact theory (equation 11 and 12). It was hypothesized that time varying contact area would be positively correlated with time-varying impact force and deflection, with power-law transformation of impact force being correlated to a greater degree with time varying contact area. Second, to investigate how contact area at peak force was associated with total peak force and force within a 5cm radius circle surrounding the greater trochanter (*GT relevant force*). In particular, how peak impact force (F_{max}), normalized peak impact force (F_{max}/m_{eff}), GT relevant peak force (F_{GT}), normalized GT relevant peak force (F_{GT}/m_{eff}) and the percent of total peak force directed to the GT relevant area ($F_{GT\%}$) correlated with the total contact area at peak force (*CA*), total body mass and

BMI. It was hypothesized that peak impact force (F_{max}) would be positively correlated with total body mass, BMI and *CA*. Normalized peak impact force (F_{max}/m_{eff}) would be significantly correlated with total body mass and BMI and *CA*. GT relevant force (F_{GT}), normalized GT relevant force (F_{GT}/m_{eff}) and the percent of total peak force directed to the GT relevant area ($F_{GT\%}$) would be correlated with the total contact area at peak force (*CA*), total body mass and BMI. Third, to determine if contact area at peak force and different anthropometric variables associated with hip fracture risk (effective mass, total body mass, BMI) were significantly correlated. It was hypothesized that contact area at peak force would be positively correlated with effective mass, total body mass and BMI.

4.2 **Methods**

4.2.1 **Participants**

Twenty women, aged 18-35, were recruited from the university population (Table 4-1). Participants completed a short health questionnaire regarding medical history and current health status, confirming the information provided to the researcher during the recruiting stage of the study. Participants were excluded if they: 1) had a history of fracture to the femur, pelvis or spine, or fractures to any bone within the past year; 2) had experienced any other musculoskeletal injury or physiological disorder within the past year; or 3) they had been diagnosed with osteopenia or osteoporosis.

Table 4-1: Anthropometrics for twenty female participants recruited in study.

	Age (years)	*Height (cm)*	*Mass (kg)*	*BMI (kg/m^2)*
Mean	24.3	167.0	67.2	24.1
SD	3.2	6.8	12.5	4.0
COV (%)	13.1	4.1	18.6	16.7

4.2.2 **Experimental Protocol**

This study utilized the "lateral pelvis release" experimental setup, which was developed by Robinovitch et al. (1991), and has subsequently used to study many factors associated with hip impact dynamics (Bhan et al., 2013; Choi et al., 2010a; Laing and Robinovitch, 2008a; Levine et al., 2013). A lateral impact trial required that the participant lay on their left side with their pelvis supported by a sling, which was raised above the impact surface (pressure plate), which was placed above the force plate (Figure 4.1). The participant's left arm was flexed overhead, with their right arm positioned across their chest to ensure that they would not contact the impact surface or provide any bracing during the trial. Participant hips were flexed to 70 º, and their knees flexed to 90 º, similar to the impact configuration mentioned in chapter three. The sling was attached to a height-adjustable turnbuckle, which was in-turn connected to an electromagnet. With the magnet engaged, the participant's pelvis was raised to a height of five cm above the impacting surface (pressure plate and force plate). This height was selected to allow for a safe, but clinically relevant impact velocity of 1.0 m/s (Feldman and Robinovitch, 2007; Nankaku et al., 2005). Once suspended in the sling, the participant was instructed to relax their core and extremity muscles. After reporting they

were ‘ready’, the magnet was subsequently disengaged, allowing the participant’s pelvis to fall onto the impact surface. This was repeated four times for each participant recruited for the study (n=20).

The deformation of the pelvis was measured simultaneously by two motion capture methods tracking the vertical displacement of an Optotrak smart marker (Northern Digital, Waterloo, Ontario, Canada) on the right hip of the participant (non-impacting hip). The motion of that one marker was collected simultaneously by both a three-dimensional motion-capture system (Optotrak, Northern Digital, Waterloo, Ontario, Canada) sampling at 1500 Hz, and a high speed camera (AOS Technologies, Cheshire, CT) sampling at a rate of 9000 Hz, for two seconds. The time-varying loads applied to the pelvis were measured by the force plate (model OR6-3, Advanced Medical Technology, Inc., Watertown, Massachusetts, USA), sampling at 36000 Hz. If the visibility of the hip marker was obscured or incompletely measured by one system, the redundant capturing of deflection by two systems allowed at least one set of complete data to be retained for that impact trial. Since, the initial study in this thesis (Chapter 2) found that both systems are comparable in measuring peak impact force and deflection, thus data from both systems were used interchangeably. This allowed for a greater number of impact trials to be used for analysis for each participant.

Force and deflection data sampled by the Optotrak system (OPT) was collected via NDI First Principles (Northern Digital, Waterloo, Ontario, Canada) software and outputted for analysis. The high speed camera video and force (HSV) was collected via AOS Imaging Studio (Baden, Switzerland) and MiDAS DA (Xcitex, Cambridge, MA), respectively. This video data was then post processed using the particle tracking feature of the ProAnalyst

software (Xcitex, Cambridge, Massachusetts). ProAnalyst is a full-featured auto-tracking software which can measure position of unique objects in the image window. All three systems were synchronized with an external trigger, which initiated a two-second collection of the impact event. Contact pressure was measured with a rigid pressure plate (RSscan International, Olen, Belgium) which contained 4096 sensors (arranged in a 64 x 64 matrix) with each resistive sensor having an area of 0.762 x 0.508 cm. The pressure range measurable for each sensor ranged from 0.27 - 200 N/cm^2, and was sampled at 500Hz. A 0 N threshold was used for each sensor.

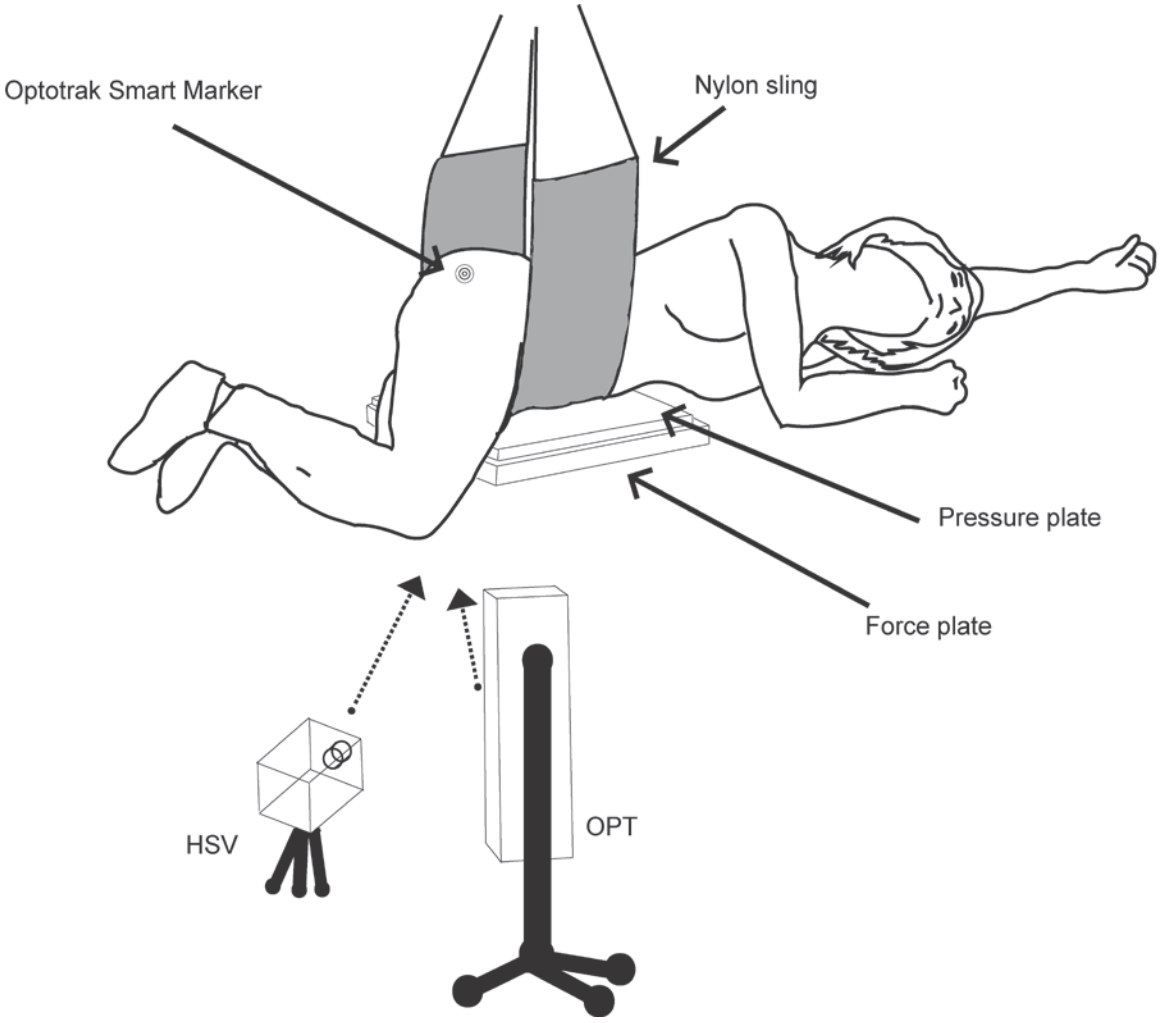

Figure 4.1: Visibility of the greater trochanter optical marker from the perspective of the HSV and OPT camera. The placement was determined to ensure the complete visibility of the marker throughout the entire impact trial by both motion capture systems. The participant was positioned on their left side with the pelvis supported by the nylon sling. The upper torso and shoulder, as well as the lower legs were contacting the ground, not impacting the pressure plate.

4.2.3 **Data Analysis**

Overall, 21 trials from the OPT system were analyzed, and the rest from the HSV (78 in total). All deflection and force data was downsampled to 500 Hz to match the sampling rate for the pressure data. Although, the initial study in this thesis showed a significant difference between data sampled at 9000 Hz and 500 Hz, the results showed a mean reduction of less than 0.5 %. Thus for the correlational purpose of this study, sampling at 500 Hz was deemed to not affect the results of this study. The synchronization of the two motion capture systems with the pressure plate was achieved by cross correlating the force signal measured by the pressure plate with that measured by the respective motion tracking system. To determine the compressive phase of the impact trial, the time of initial pelvic impact (T_{imp}) was identified. T_{imp} was defined as the time at which force exceeded twice the standard deviation of the previous 25 frames (unloaded) and T_{max} was the time at which peak force (F_{max}) occurred. The interval between T_{imp} and T_{max} was considered the loading phase of impact. This was also the interval where time-varying data (F_t ,D_t *and* C_t) were measured and analyzed. Peak impact force (F_{max}) was defined as the maximum vertical impact force measured by the force plate. The effective mass of the pelvis (m_{eff}) was calculated similarly to the method described by Levine et al. (2013) whereby the final twenty frames of the force plate signal were averaged to give an estimate of the mass interacting with the force plate, and dividing that force by gravity (9.81 m/s^2). The normalized peak impact force (F_{max}/m_{eff}) was then calculated by dividing F_{max} by m_{eff}. To calculate GT relevant force (F_{GT}), the pressure image sampled at T_{max} was obtained and the sensor with the highest measured force was assumed to be the center of the GT. A 5cm radius circle was then defined around this

sensor and those inscribed sensors established the GT relevant zone. The peak GT relevant force (F_{GT}) was measured as the sum of the forces measured by the sensors in the GT zone at T_{max}. The normalized GT relevant force (F_{GT}/m_{eff}) was calculated by dividing F_{GT} by m_{eff}. The percent of total peak force directed to the GT relevant area ($F_{GT\%}$) was calculated as the percent of total peak force measured in the GT relevant zone, divided by peak impact force (i.e. (F_{GT}/F_{max}) x 100%). The total contact area at peak force (*CA*) was calculated by the number of active sensors (> 0 N measured) by the active area of one sensor (0.387096 cm^2). All signal conditioning and data processing was performed using customized Matlab (Mathworks, Natick, Massachusetts, U.S.A.) routines.

4.2.4 **Statistics**

For the first purpose of this study, the time-varying contact area was plotted as a function of time-varying force and time-varying deflection (data from the interval between T_{imp} and T_{max}). The Pearson product-moment correlation coefficient (r) was calculated to assess the linear association between contact area and force, as well as contact area and deflection for each impact analyzed. An average correlation value was then calculated across impacts within each participant, for a total of twenty correlation coefficients for each of the three time varying relationships. As Hertzian contact model describes a power law relationship between contact area and force, time-varying force data was transformed to the power of 2/3 and the correlation coefficient (*r*) was then also calculated for this transformed relationship. This was also averaged across impacts within a participant. The average correlation coefficient was then calculated for each relationship of interest (F_t *to* C_t ,D_t *to* C_t , FT_t *to* C_t) using the average correlations calculated per participant. The average *r* for each

relationship (F_t *to* C_t ,D_t *to* C_t , FT_t *to* C_t) was then bootstrapped via bias corrected and accelerated (BCa) methods (5000 iterations) to obtain a 95% confidence interval. If the bootstrapped confidence interval did not contain zero, a significant correlation was deemed to exist between the variables.

For the second purpose of this study, separate Pearson product-moment correlations were calculated between the five measures of impact load (F_{max} , F_{max}/m_{eff} , F_{GT} , F_{GT}/m_{eff} , $F_{GT\%}$) and total contact area at peak force (*CA*), total body mass and BMI. Power sensitivity calculations determined that at a sample size of 20, a correlation with selected power of 0.8, required an effect size of 0.557 (with $\alpha = 0.05$). For the third purpose of this study, trial-specific dependent measures were averaged within participant (twenty participants overall). Separate Pearson product-moment correlations were calculated to assess the degree of linear association between *CA* and m_{eff}, total body mass, and BMI. All statistical analyses were performed with the SPSS software package (SPSS Version 20, SPSS Inc., Chicago, IL, USA), and power analysis was performed with G*Power 3.1 software (Faul et al., 2009).

4.3 **Results**

4.3.1 **Time-varying Contact Area**

Figure 4.2 shows how time-varying contact area and time-varying deflection for four separate participants. Additionally, Figure 4.3 shows how time-varying contact area and time-varying impact force for those same four subjects. All three time-varying signals ($F_{t,}$ FT_t and D_t) were significantly correlated with time-varying contact area (C_t) (Table 4-

2).There was a significant positive relationship between C_t and F_t, r = 0.94, 95% CI [0.90, 0.97]. C_t was also significantly related to FT_t, r = 0.94, 95% CI [0.90, 0.97], the same as the untransformed F_t. Time-varying deflection was also significantly correlated to C_t, r = 0.86, 95% CI [0.79, 0.92].

Table 4-2: Correlations between time-varying contact area with time varying-force, transformed time-varying force, and time varying deflection. Correlations were calculated for every impact trial, and then averaged within participants. Bootstrapped mean correlations (bias corrected and accelerated) were calculated through 5000 iterations to determine the 95% confidence interval. F_t signifies time varying force, FT_t is transformed time varying force and C_t is the time varying contact area. A significant correlation was concluded if the confidence interval did not include zero, and is denoted by *.

Relationship	*Pearson correlation*	*95% Confidence Interval*	
		Lower	*Upper*
F_t *to* C_t	0.94*	0.90	0.97
FT_t *to* C_t	0.94*	0.90	0.97
D_t *to* C_t	0.86*	0.79	0.92

4.3.2 **Contact Area and Force Distribution**

Average values for impact loading variables are shown in Table 4-5. Peak impact force (F_{max}) was significantly correlated with effective mass (r = 0.744, p < 0.001), total body mass (r = 0.744, p < 0.001) and BMI (r = 0.573, p = 0.008), but not contact area at peak force (p = 0.079). Greater trochanter relevant force (F_{GT}) was not significantly correlated with either total body mass (p = 0.278) or BMI (p = 0.865), but was significantly correlated with contact area at peak force (r = -0.544, p < 0.001). Normalized peak impact force (F_{max}/m_{eff}) was not significantly correlated with mass, BMI or contact area at peak force (all p > 0.5). Normalized GT relevant force (F_{GT}/m_{eff}) was significantly correlated with contact area at peak force (r = -0.785, p < 0.001), but not with mass (p = 0.329) nor BMI (r = -0.422, p = 0.064). The percent of total peak force directed to the GT relevant area ($F_{GT\%}$) was significantly correlated with BMI (r = -0.538, p = 0.014) and contact area at peak force (r = -0.963, p < 0.001), but not with total body mass (Table 4-6).

Table 4-3: Mean values for impact force measures in this study. Also reported are standard deviations (SD) and coefficient of variations (COV).

	F_{max} (N)	F_{GT} (N)	F_{max}/m_{eff} (N/kg)	F_{GT}/m_{eff} (N/kg)	$F_{GT\%}$ (%)
Mean	1278.2	1013.8	3.9	3.1	79.6
SD	220.6	220.8	0.5	0.7	13.8
COV	17.3	21.8	12.6	22.9	17.3

Table 4-4: Pearson product-moment correlations calculated between previously cited measures of hip fracture risk and five dependent variables of load distribution.

			Mass	*BMI*	*CA*
F_{max}	***Pearson Correlation***		0.744*	0.573*	0.402
	95% Confidence Interval	***Lower***	0.514	0.231	-0.118
		Upper	0.925	0.834	0.744
			p <0.001	*p=0.008*	*p=0.079*
F_{GT}	***Pearson Correlation***		0.255	-0.041	-0.544*
	95% Confidence Interval	***Lower***	-0.304	-0.560	-0.801
		Upper	0.659	0.488	-0.130
			p=0.278	*p=0.865*	*p=0.013*
$F_{GT\%}$	***Pearson Correlation***		-0.354	-0.538*	-0.963*
	95% Confidence Interval	***Lower***	-0.680	-0.827	-0.988
		Upper	0.118	-0.030	-0.909
			p=0.125	*p=0.014*	*p <0.001*
F_{max}/m_{eff}	***Pearson Correlation***		0.139	0.015	-0.076
	95% Confidence Interval	***Lower***	-0.500	-0.594	-0.675
		Upper	0.551	0.488	0.489
			p=0.559	*p=0.946*	*p=0.751*
F_{GT}/m_{eff}	***Pearson Correlation***		-0.230	-0.422	-0.785*
	95% Confidence Interval	***Lower***	-0.613	-0.769	-0.952
		Upper	0.250	0.119	-0.344
			p=0.329	*p=0.064*	*p <0.001*

4.3.3 **Contact Area and Anthropometrics**

The average values for contact area and anthropometry are shown in Table 4-3. Effective mass ($r = 0.455$, $p = 0.044$), total body mass ($r = 0.472$, $p < 0.036$) and body mass index ($r = 0.578$, $p < 0.008$) were positively correlated with contact area at peak force (*CA*) (Table 4-4). Overall, body mass index was correlated with contact area, where increases in BMI were correlated with increases in contact area. The same positive relationships were evident for total body mass and effective mass, although both of those were correlated to a lower degree.

Table 4-5: Mean contact area and body anthropometry measured across twenty participants. Also shown are standard deviations and coefficient of variations.

	Mass (kg)	***BMI (kg/m^2)***	***m_{eff} (kg)***	***CA (cm^2)***
Mean	67.2	24.1	34.2	139.1
SD	12.5	4.0	6.3	48.5
COV	18.6	16.7	18.4	34.9

Table 4-6: Correlations between contact area at peak force (CA) and three common variables associated with hip fracture risk: body mass (*Mass*); body mass index (*BMI*); effective mass (m_{eff}). Pearson correlations significant at the 0.05 level are denoted by *.

			CA
Mass	***Pearson Correlation***		0.472*
	95% Confidence Interval	***Lower***	0.069
		Upper	0.748
			p = 0.036
BMI	***Pearson Correlation***		0.578*
	95% Confidence Interval	***Lower***	0.133
		Upper	0.866
			p = 0.008
m_{eff}	***Pearson Correlation***		0.455*
	95% Confidence Interval	***Lower***	-0.003
		Upper	0.769
			p = 0.044

4.4 **Discussion**

This study utilized human participants in a lateral pelvis release paradigm to explore the associations between contact area and impact deflection, force, and anthropometry. As hypothesized, time varying-force (r = 0.94) and deflection (r = 0.86) was positively correlated with time-varying contact area. However, contrary to hypotheses derived from Hertzian contact theory, transformed impact force (to the 2/3 power) was not correlated higher with time-varying contact area when compared to the untransformed impact force (both r =0.94). The second purpose of this study explored the associations between distribution of impact load and body anthropometry, as well as contact area. As was expected, total body mass and BMI were positively correlated with peak impact force, where body mass explained 55 %, and BMI explained 33 %, of the variance in peak impact force. Surprisingly, contact area was not correlated with peak impact force (p = 0.08). Furthermore, when normalized by mass, peak impact force was not significantly correlated with body mass, BMI, or contact area (as was hypothesized). Interestingly, none of the greater trochanter relevant loading measures (F_{GT}, F_{GT}/m_{eff} or $F_{GT\%}$) were significantly correlated with total body mass. Only $F_{GT\%}$ was significantly correlated with BMI, where lower measures of BMI were associated with a higher percentage of total impact force directed to the GT relevant area (R^2= 0.29). Contact area, however, was significantly correlated with every measure of GT relevant loading. Larger measures of contact area were associated with lower values of GT relevant peak force (R^2= 0.30). After GT relevant peak force was normalized by total effective mass, smaller contact areas were associated with larger values of F_{GT}/m_{eff} (R^2= 0.62). The highest correlation measured in this study was between $F_{GT\%}$ and

contact area, whereby larger measures of contact area were associated with a smaller percent of total peak force directed to the GT relevant area (R^2= 0.93). Lastly, this study explored the association between anthropometry and contact area. As hypothesized, contact area at peak force (*CA*) was positively correlated with a participant's effective mass, total body mass and BMI, where each anthropometric variable accounted for 21, 22 and 33% of the variance in *CA*, respectively.

4.4.1 **Time-varying Contact Area**

The high level of correlation between all time-varying signals tested in this study (F_t *to* C_t ,D_t *to* C_t , FT_t *to* C_t) lends credence to the possibility of a hip specific contact model. However, applicability of a Hertzian model to lateral hip impact remains unclear. The Hertzian contact model referenced in equations 11 and 12 describe a linear relationship between contact area and deflection, and a non-linear power law relationship between contact area and impact force. However, results from this study show that in actuality F_t *was* correlated to a greater degree with C_t, as compared to D_t . Indeed, representative traces show this relationship between contact area and deflection (Figure 4.2) and contact area and force (Figure 4.3). However, transforming impact force did not increase the linear relationship between FT_t and C_t , as theorized by Hertzian models.

Nevertheless, a move to Hertzian contact models might be most appropriate when considering hip impact models for two reasons. Interestingly, for a Hertzian impact between an elastic sphere and an elastic plate, the initial contact between the two bodies will produce

a force of zero, which has proven to a difficulty with predictive lumped parameter models which include damping (especially Voigt models) of hip impact (Robinovitch et al., 1997). Regardless, this study does demonstrate the possibility for contact models as contact area shows an association with impact force and deflection, and further studies should attempt to better understand the true relationships between F_t and D_t in relation to C_t .

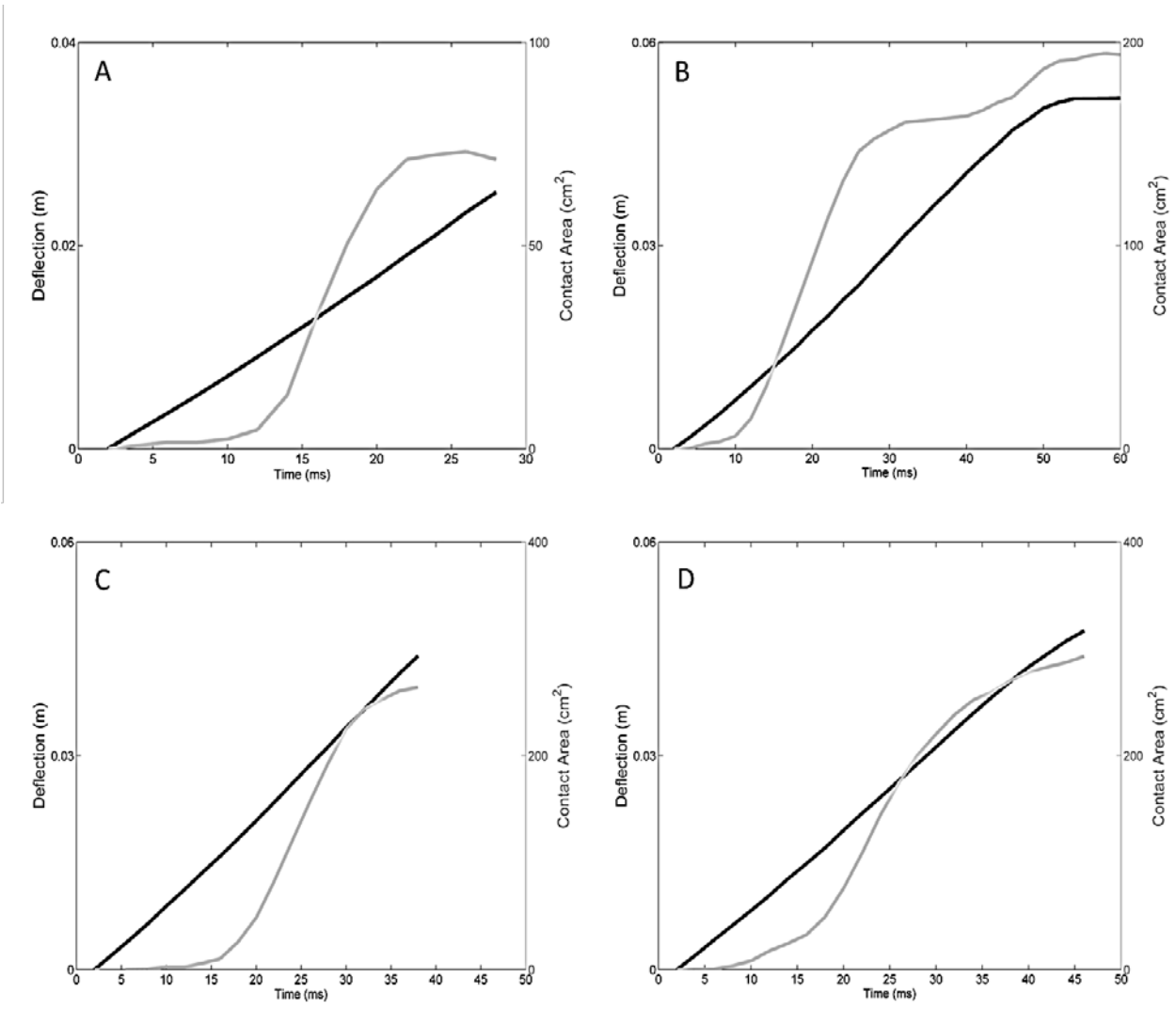

Figure 4.2: Selected deflection and contact area traces for four separate participants. The top two panels show participants from opposite ends of the BMI spectrum. A) Lower BMI participant (BMI=20.7 kg/m^2); B) higher BMI participant (BMI=30.8 kg/m^2). The bottom two panels show two participants with the highest two highest peak contact areas measured. A) lower BMI participant (BMI=22.5 kg/m^2) with a peak contact area of 251.3 cm^2; B) higher BMI participant (BMI=33.2 kg/m^2) with a peak contact area of 237.8 cm^2.

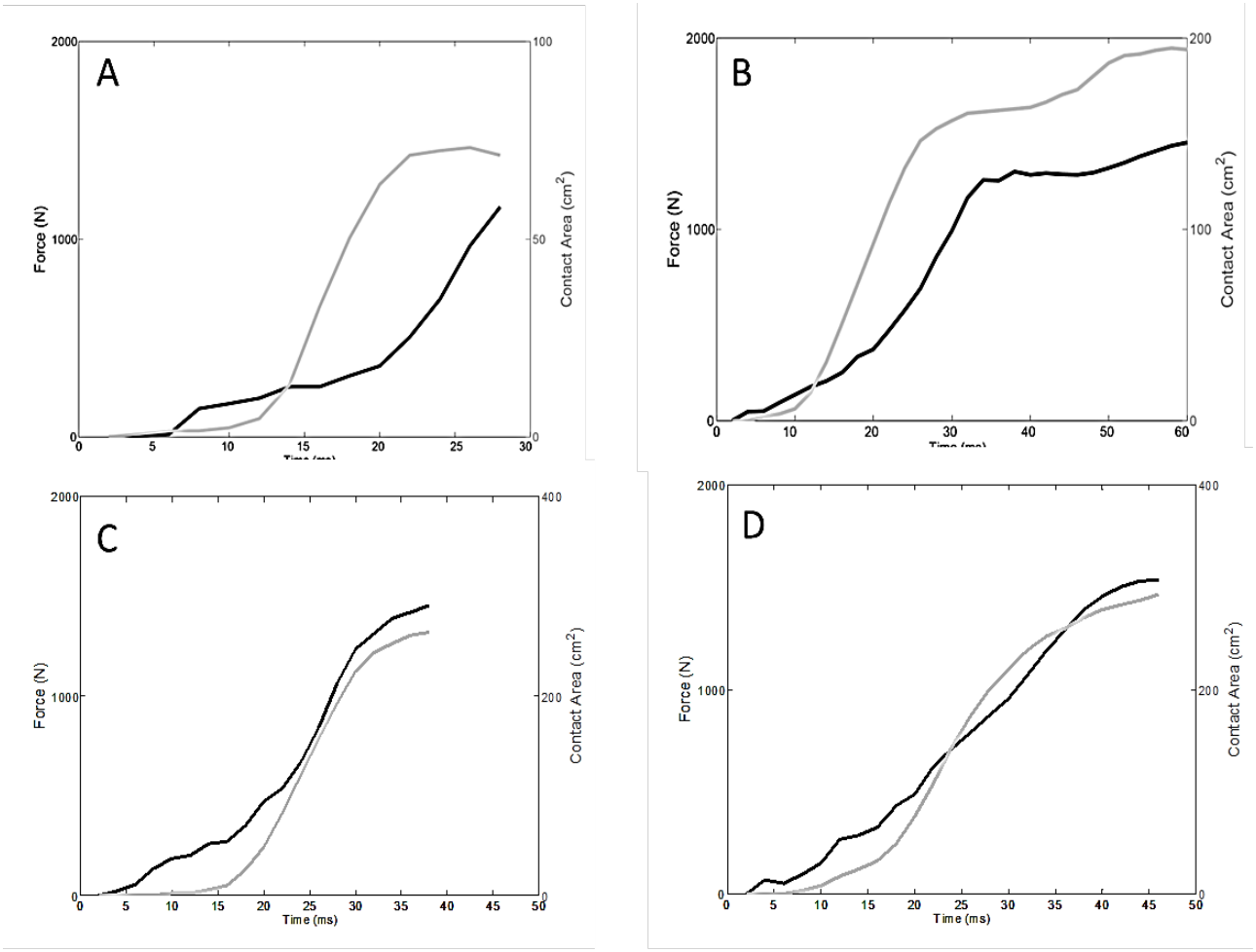

Figure 4.3: Selected force and contact area traces for four separate participants. The top two panels show participants from opposite ends of the BMI spectrum. A) Lower BMI participant (BMI=20.7 kg/m^2); B) higher BMI participant (BMI=30.8 kg/m^2). The bottom two panels show two participants with the highest two highest peak contact areas measured. A) lower BMI participant (BMI=22.5 kg/m^2) with a peak contact area of 251.3 cm^2; B) higher BMI participant (BMI=33.2 kg/m^2) with a peak contact area of 237.8 cm^2.

4.4.2 **Contact Area and Force Distribution**

These results differ somewhat from previously reported studies using extreme BMI subgroups. A study by Levine et al. (2013) found that total peak impact force was significantly higher for high BMI participants (BMI > 28) compared to low BMI participants (<22.5). However, when peak force was normalized to the effective mass of the pelvis, the relationship between low and high BMI participants was reversed. The normalized peak force was significantly lower for high BMI participants (2.82 (0.58) N/kg) compared to the low-BMI participants (4.09(0.80) N/kg). In my study, BMI was only correlated with peak impact force (F_{max}), explaining 33 % of the variance. But with normalized peak impact force (F_{max}/m_{eff}), no significant relationship existed. Additionally, Choi et al. (2010) found that neither total peak impact force nor the percent force that was applied to the danger zone (2.5 cm wide U-shaped regions oriented along the femoral diaphysis and centered at the GT) was associated with BMI. Although they did find that high BMI participants (BMI > 25) had 23.8 (SE=7) % of total impact force in the danger zone, while low BMI (BMI < 18.5) had 48.5 (SE=6) % of total peak force distributed to the danger zone; this relationship was not significant. In this current study, we found that BMI was significantly correlated with the percent of force applied to a 5cm diameter "danger zone" (defined as GT relevant area in this study), with higher BMI being associated with a lower percentage of total impact force applied to the GT (R^2=0.29). Interestingly, both of these previous studies used cohorts of differing BMI groups, for example in the Choi study the average body mass and height of the average body mass and height were 47 kg (SD 4) and 162 cm (SD 5) in the low BMI group, and 75 kg (SD 9) and 163 cm (SD 5) in the high BMI group. My study did not separate by

extreme BMI groups and as a result the sample of participants tested here overlap with the BMI subgroups of these previous studies while also spanning the range between these extremes. Nevertheless, it is possible that at the extreme ends of anthropometry, the biomechanically relevant risk factors (mass, contact area, pelvic geometry) become more varied within extreme subgroups of BMI, and this diminishes any expected differences.

This study also provides important insight into the relationship between reduced hip fracture risk and high BMI. Specifically, it shows that measures of body anthropometry (body mass and BMI), while correlating well with peak impact force, do not significantly correlate with actual loading distributed to the greater trochanter. In fact, contact area at peak force had the strongest relationship with GT relevant loading, where smaller values of *CA* were related with higher loading distributed to the greater trochanter (Figure 4.4 and 4.5). Although, BMI explained 33% of the variance in contact area it appears that the relationship between BMI and greater trochanter loading is not as well defined.

The difficulty with relating impact loads with simple anthropometrics is evident when considering three participants in this study. Figure 4.6 shows the load distribution for two participants collected in this study who had comparable contact areas. One participant has a relatively low BMI (Panel A=22.5 kg/m^2) and the other has a relatively high BMI (Panel B=33.2 kg/m^2), yet both have similar contact area (A=247.1 cm^2, B=237.8 cm^2). Furthermore, both participants have similar peak impact force (Panel A =1464.9 N; Panel B=1485.2 N). Still, the peak force distributed to the GT relevant area for participant B is just 10 % less than for participant A (A=770.4 N; B=688.7 N), even despite the fact that the mass of participant B is 21.5 % greater (A= 67.5 kg; B=86.0 kg). Alternatively, Figure 4.7 shows

the same participant from Figure 4.6 (A) compared to a participant with comparable BMI (Panel A=22.5 kg/m^2 and Panel B=20.7 kg/m^2), with stark differences in contact area (A=247.1 cm^2, B=62.3 cm^2), and force distributed to the GT relevant area (A=770.4 N; B=1184.0 N). Evidently, the relationship between BMI and mass with greater trochanter loading is not as simple as previously presumed.

It is possible that contact area at peak force could provide better prediction of hip impact loading to the greater trochanter. Previous models of hip fracture risk have associated total body mass as a significant predictor of impact loads, where by higher mass is associated with greater higher impact forces (Bouxsein et al., 2007; Dufour et al., 2012; Robinovitch et al., 1991; van den Kroonenberg et al., 1995). The results of this study show that this postulation is warranted when considering the total peak impact force measured by the entire force plate; but not as strongly supported when considering greater trochanter relevant loading. When considering the high correlation between total peak impact force and mass (r = 0.744), finding a good clinical predictor of *CA* could provide better estimates of hip fracture risk.

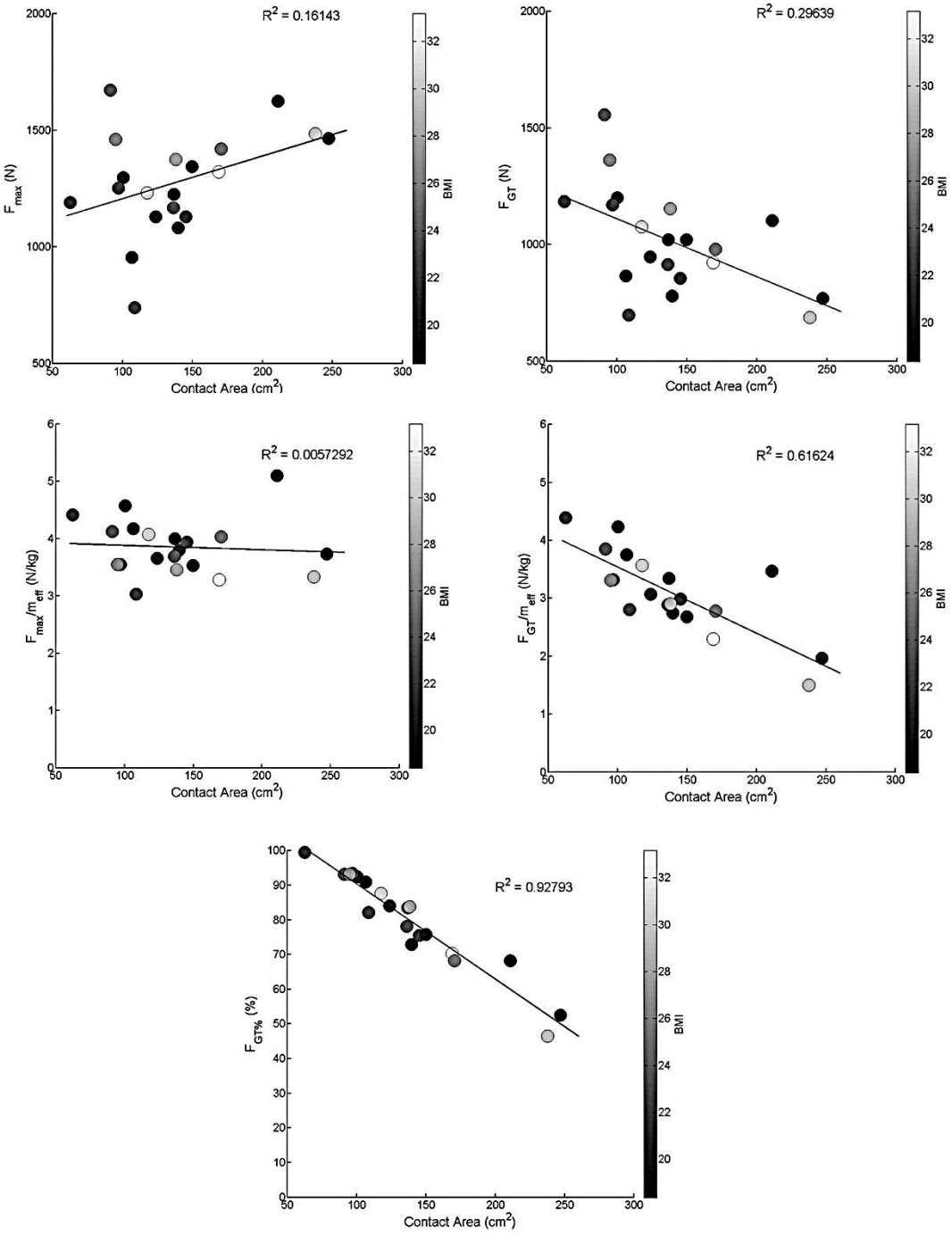

Figure 4.4: Correlations between loading parameters and contact area. The shade of each dot varies by the BMI of the participant according to the shade bar associated with each plot.

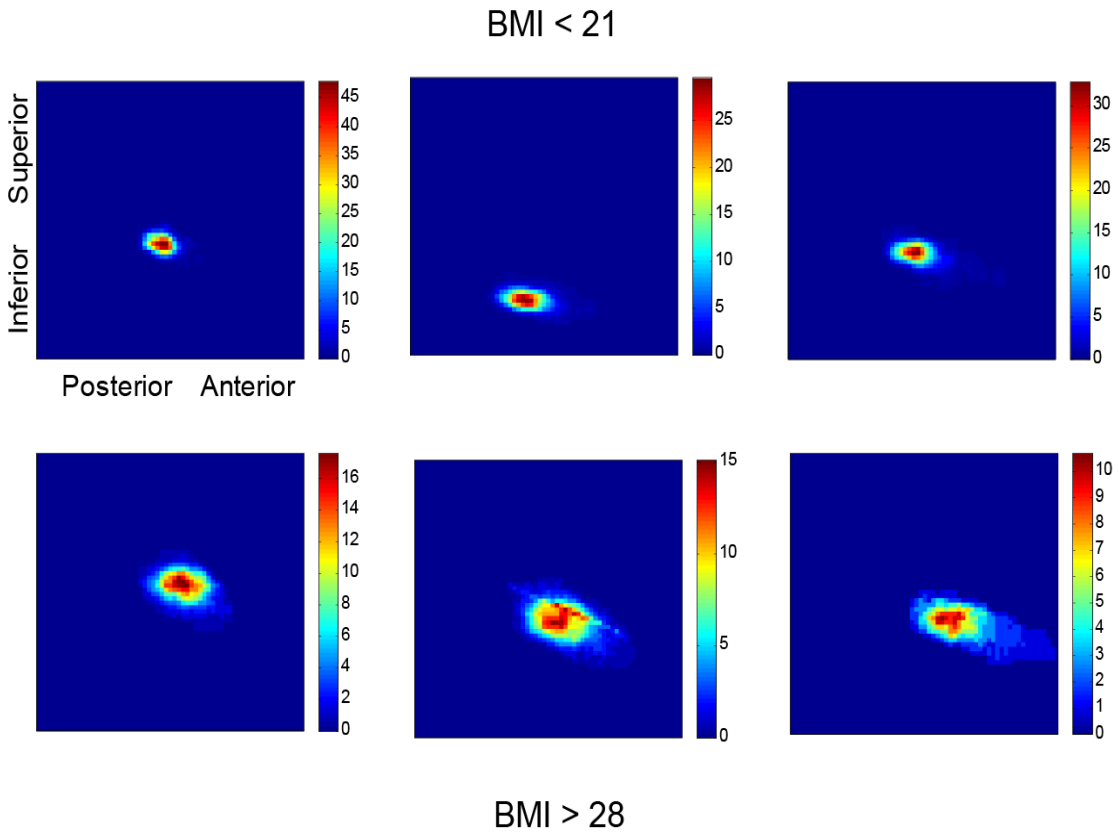

Figure 4.5: Load distribution images at peak force for six participants. The top three images are from three separate participants with a lower BMI (below 21 kg/m^2). The bottom three images are from three participants with a higher BMI (above 28 kg/m^2). Note the differences in contact area between participants of lower and higher BMI. Also of interest are the differences in the range of loads measured by each sensor in the pressure plate (evidenced from the range of the colour bars to the right of each image) between lower and higher BMI participants. Units for the colour bars are in Newtons, images depict each sensor of the pressure plate (64 x 64 =4096 sensors of 0.762 x 0.508 cm dimensions).

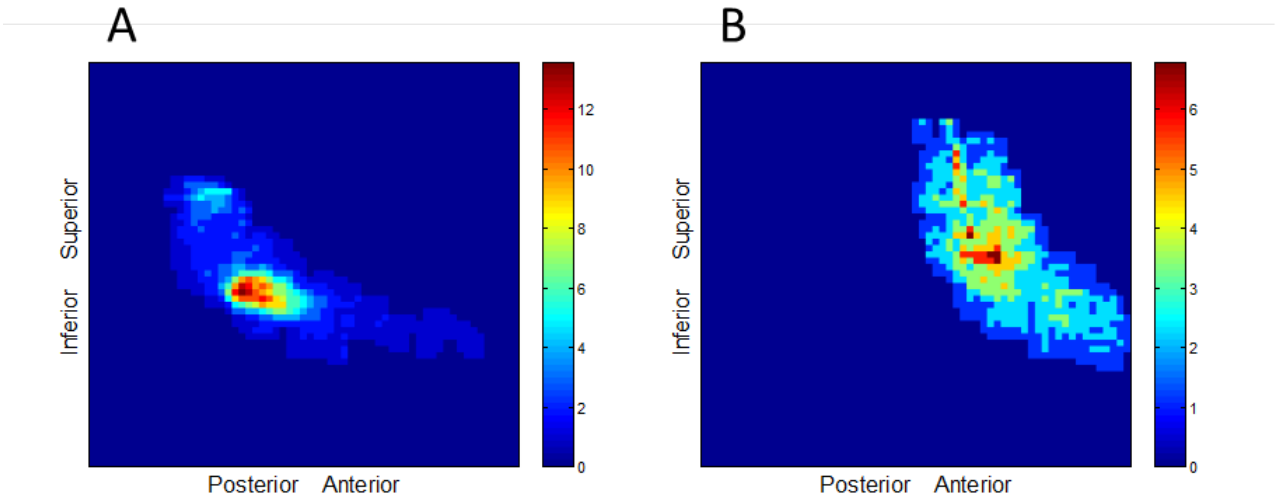

Figure 4.6: Pressure at peak force for two subjects who had relatively differing body mass indices (A=22.5 kg/m^2, B=33.2 kg/m^2), but similar contact area (A=247.1 cm^2, B=237.8 cm^2). Units for the colour bars are in Newtons, images depict each sensor of the pressure plate (64 x 64 =4096 sensors of 0.762 x 0.508 cm dimensions).

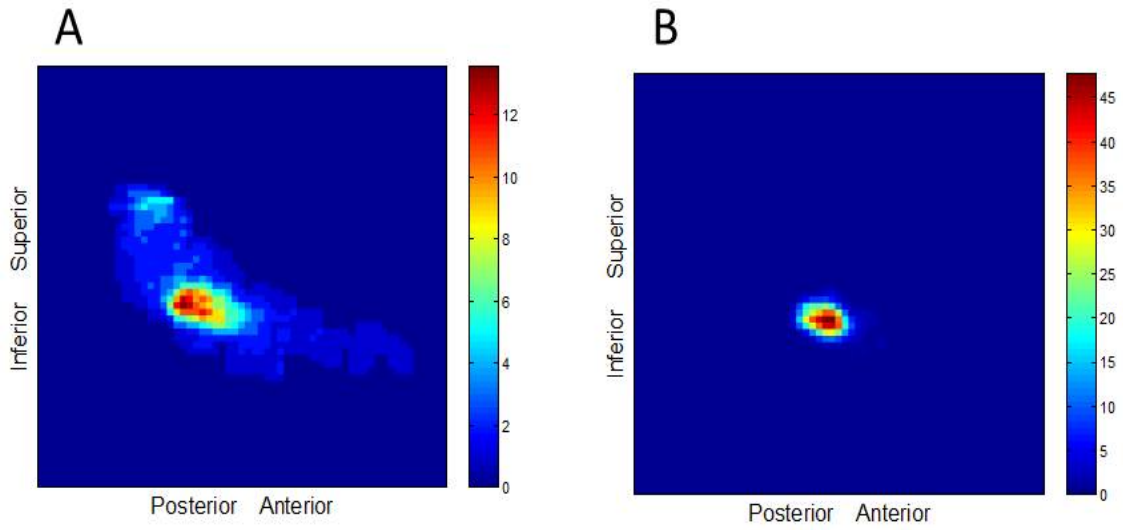

Figure 4.7: Pressure at peak force for two subjects who had comparable body mass indices (A=22.5 kg/m^2, B=20.7 kg/m^2), but starkly different contact area (A=247.1 cm^2, B=62.3 cm^2). Units for the colour bars are in Newtons, images depict each sensor of the pressure plate (64 x 64 =4096 sensors of 0.762 x 0.508 cm dimensions).

4.4.3 **Contact Area and Anthropometrics**

The relationships between contact area and body anthropometry explored in this study have never been reported previously for impact studies with humans, and offer some insight into the association between hip fracture risk and body composition (Figure 4.7). Previous work by Laing and Robinovitch (2008c) using a mechanical hip testing system, showed that the percentage of total force transmitted to the femoral neck during impact increased with decreases in pelvis size, and postulated that this was likely the result of a decrease in total contact area. Other studies have shown that although the soft tissue overlying the greater trochanter offers partial protection in a fall causing direct impact to the lateral aspect of the hip, energy absorption by this soft tissue is insufficient to prevent fracture regardless of the thickness (Robinovitch et al., 1995b). Thus, it has been postulated that alternative energy absorption mechanisms must be involved in the reduced risk of hip fracture present in high BMI individuals. The results of this study show that impacting the ground over a large contact area might be one of these alternative mechanisms. Clearly, contact area plays a role in the distribution of impact force to the greater trochanter (purpose 2), but BMI only explains 33% of the variation in contact area. Thus it appears that some other property is largely responsible for reduced hip fracture risk, most likely contact geometry.

Unlike the assumptions of Hertzian contact models, the lateral hip is neither a sphere, nor composed of elastic material. It is a slightly more complex geometry and heterogeneous in its material properties. Furthermore, the inherent viscoelasticity of biological tissue (Fung, 1993) implies spatiotemporal smoothness of biomechanical processes, and this smoothness

implies spatiotemporal correlation. For lateral hip impacts, the addition of soft tissue could increase this viscoelastic nature for the lateral hip. This increased viscoelasticity would then also reduce the spatial frequency of contact stresses applied to the hip during impacts (smaller changes in stress between adjacent contact regions). This reduction in spatial frequency implies a smaller concentration of total impact force to the greater trochanter. In simplest engineering terms “stiffness attracts load”, if there are two load paths and one is somewhat stiffer than the other, it will attract more load and hence its stress levels may be unacceptable. Unfortunately no study to date has addressed the relationship between regional material differences of the lateral hip and pressure distributions.

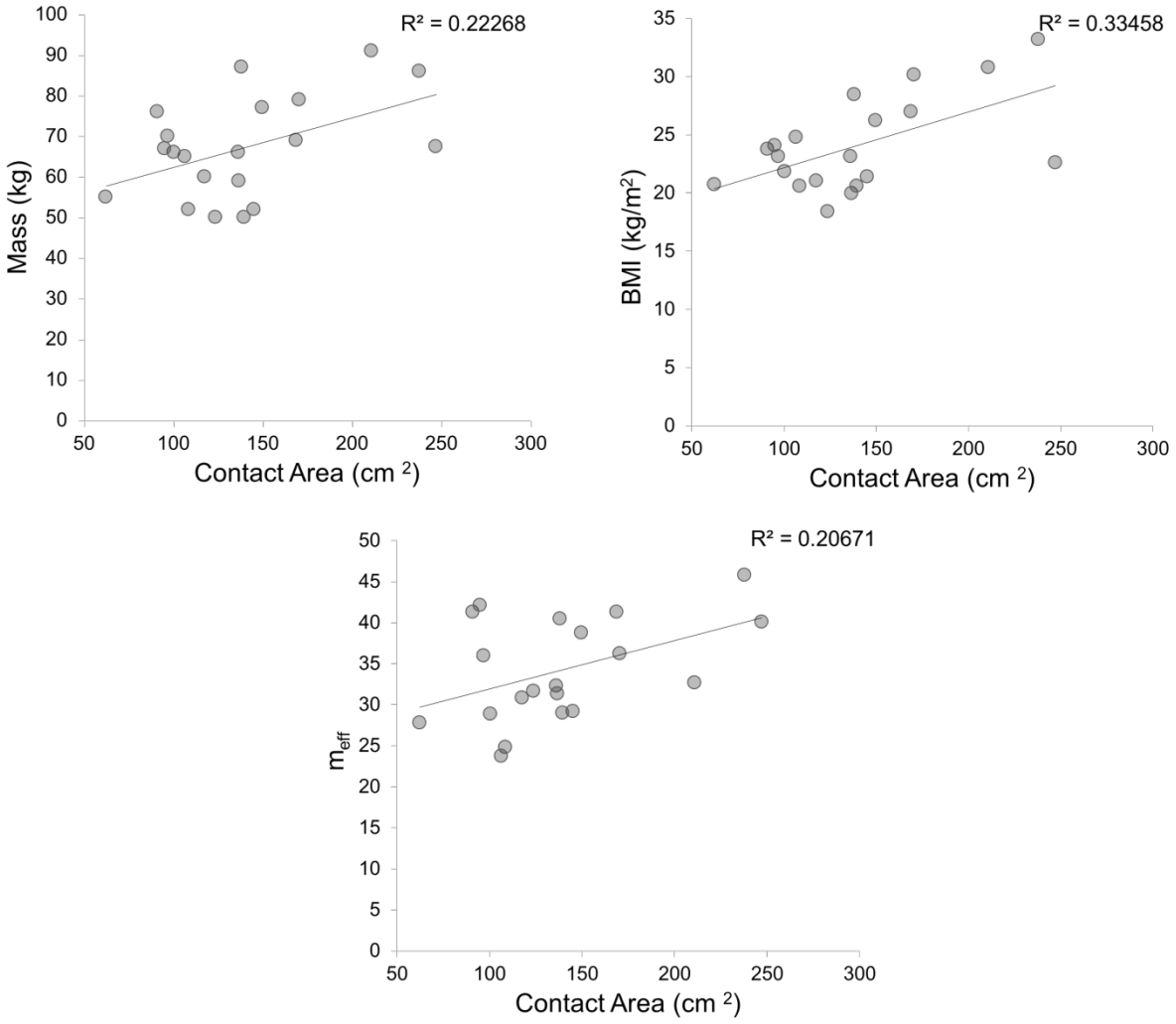

Figure 4.8: Correlations between body mass (*Mass*), body mass index (*BMI*) and effective mass (m_{eff}), with contact area (measured at peak force).

4.4.4 **Limitations**

This study had several limitations. First, due to safety concerns we did not use older adults as participants. It is possible that the relationships explored here might differ in older adults, who might have different contact geometries and soft tissue distribution. Although the mean (SD) BMI for adults > 65 years of age has been reported to be 26.4 (3.7) kg•m^2 for males and 25.1 (4.6) kg•m^2 for females, and the participants tested in my study had a mean (SD) BMI of 24.1 (4) kg•m^2, the contributions of fat, muscle and skeletal mass that contributes to BMI can have varied effects on the mechanical response across participants. Thus, directly extrapolating these results directly for older adults is cautioned, and warrants further study. Although BMI is commonly used as a surrogate measure of soft tissue thickness over the greater trochanter, it does not provide direct insights into the mechanisms by which impact dynamics are differentially influenced by BMI. Future work would absolutely benefit from directly measuring soft tissue thickness by ultrasound or diagnostic imaging.

Second, as noted above, due to safety issues, our impact velocity of approximately 1 m/s (based on a 5 cm drop height) is lower than the 3 m/s average impact velocity reported during unexpected falls from standing (Feldman and Robinovitch, 2007). However, our results show a high correlation between time-varying impact force and time-varying contact, as such higher velocity impacts are expected to also show similar relationships with contact area. Lastly, it is possible that the sample size in this study was too small to detect certain significant relationships tested here. A priori power calculations determined that at a sample size of 20, a correlation with selected power of 0.8, required an effect size of 0.557 (with α =

0.05). Agreeably, this lack of power requires further study into the relationships mentioned here, especially in regards to body anthropometry. However seeing as this is the first study to report relationships with contact area, further study was inevitable. It is worth mentioning that a study with more power could easily have failed to find a difference (e.g. because perhaps the true effect is smaller than I think), or it may as easily have found a difference. A study with more power is more likely to find a difference than one with less power, but as the effect size of the underlying relationship sinks it is worth considering how much it can add to estimates of hip fracture risk.

4.4.5 **Conclusions**

In summary, this study shows that all three time-varying signals (F_t, FT_t and D_t) were significantly correlated with time-varying contact area (C_t). These results lend support to the possibility of modeling lateral hip impacts with contact models, but provide little support for a Hertzian model adaptation. Analysis on the relationships between body mass and BMI found both anthropometric measures to correlate significantly with peak impact force, but not with peak impact force directed to the greater trochanter. These results bring into question the feasibility of modeling hip fracture risk with body mass or BMI as inputs, without further investigating the distribution of impact force to the greater trochanter. In this study only contact area was significantly correlated with all measures of GT specific loading, and has never before been implemented in predictive modelling of hip fracture risk. Finally, this study found that although effective mass, total body mass and BMI were significantly correlated with the contact area at peak force, they only accounted for 21, 22 and 33% of the variance in *CA*. Altogether, this study sheds new light on the role that contact area plays in

lateral hip impact loading and the importance of understanding load distribution during lateral hip impacts. It also highlights the importance of moving towards predictive models that incorporate more robust estimate of body material composition and geometry, with hopes that these will better help estimate the risk of hip fracture.

Chapter 5
Thesis Summary

The experiments presented in this thesis provide novel insight into two scarcely studied areas in the field lateral hip impact biomechanics. With respects to the effect of measurement technique, this study shows that 3D optical motion capture and 2D high-speed videography perform similarly in measuring the impact response of the human pelvis during lateral pelvis release impact trials. Although significant differences were seen between systems in measuring T_{Fmax} and E_{max}, the magnitude of differences were at or below 5% of the total magnitude of each measured variable. Furthermore, averaging impacts within a subject reduced the differences between systems for E_{max}. This study also showed the effect of sampling rate on measuring the impact response of the human pelvis, where the degree of effect that sampling rate had was contingent on the dependent variable measured. Sampling as low at 300 Hz, significantly reduced measures of F_{max} and D_{max}, but only by on average 0.7 and 0.5 %, respectively, whereas measures of T_{Fmax} and T_{Dmax} increased by on average 9.5 and 6.8 %. Sampling E_{max} at 500 Hz and 300 Hz increased measures of impact absorption by 2.2 and 2.8 % respectively. Sampling at 4500 Hz was the lowest sampling rate that was not significantly different from 9000 Hz across all dependent variables.

The second study of this thesis showed the influence of contact area on in load variables during lateral hip impacts. In particular, that all three time-varying signals (F_t, FT_t and D_t) were significantly correlated with time-varying contact area (C_t). These results lend support to the possibility of modeling lateral hip impacts with contact models, but provide little support for a Hertzian model adaptation. Analysis on the relationships between body mass and BMI found both anthropometric measures to correlate significantly with peak impact force, but not with peak impact force directed to the greater trochanter, bringing into question the feasibility of modeling hip fracture risk with body mass or BMI as inputs, without further investigating the distribution of impact force to the greater trochanter. Finally, this study found that although effective mass, total body mass and BMI were significantly correlated with the contact area at peak force, they only accounted for 21, 22 and 33% of the variance in *CA.* Altogether, this study sheds new light on the role that contact area plays in lateral hip impact loading and the importance of understanding load distribution during lateral hip impacts. It also highlights the importance of moving towards predictive models that incorporate more robust estimate of body material composition and geometry, with hopes that these will better help estimate the risk of hip fracture.

References

Aharonoff, G.B., Dennis, M.G., Elshinawy, A., Zuckerman, J.D., Koval, K.J., 1998. Circumstances of falls causing hip fractures in the elderly. Clinical orthopaedics and related research, 10-14.

Aharonoff, G.B., Koval, K.J., Skovron, M.L., Zuckerman, J.D., 1997. Hip fractures in the elderly: predictors of one year mortality. Journal of orthopaedic trauma 11, 162-165.

Andrews, D.M., Callaghan, J.P., 2003. Determining the minimum sampling rate needed to accurately quantify cumulative spine loading from digitized video. Appl Ergon 34, 589-595.

Arakaki, H., Owan, I., Kudoh, H., Horizono, H., Arakaki, K., Ikema, Y., Shinjo, H., Hayashi, K., Kanaya, F., 2011. Epidemiology of hip fractures in Okinawa, Japan. Journal of bone and mineral metabolism 29, 309-314.

Armstrong, M.E., Spencer, E.A., Cairns, B.J., Banks, E., Pirie, K., Green, J., Wright, F.L., Reeves, G.K., Beral, V., 2011. Body mass index and physical activity in relation to the incidence of hip fracture in postmenopausal women. Journal of bone and mineral research : the official journal of the American Society for Bone and Mineral Research 26, 1330-1338.

Askegaard, V., Lauritzen, J.B., 1995. Load on the hip in a stiff sideways fall. European Journal of Musculoskeletal Research 4, 111-116.

Beason, D.P., Dakin, G.J., Lopez, R.R., Alonso, J.E., Bandak, F.A., Eberhardt, A.W., 2003. Bone mineral density correlates with fracture load in experimental side impacts of the pelvis. J Biomech 36, 219-227.

Beillas, P., Helfenstein, C., Rongieras, F., Gennisson, J.L., Tanter, M., 2013. A new method to assess the deformations of internal organs of the abdomen during impact. Computer methods in biomechanics and biomedical engineering 16 Suppl 1, 202-203.

Bhan, S., Levine, I., Laing, A.C., 2013. The Influence of Body Mass Index and Gender on the Impact Attenuation Properties of Flooring Systems. Journal of applied biomechanics.

Bouxsein, M.L., Szulc, P., Munoz, F., Thrall, E., Sornay-Rendu, E., Delmas, P.D., 2007. Contribution of trochanteric soft tissues to fall force estimates, the factor of risk, and prediction of hip fracture risk. Journal of bone and mineral research : the official journal of the American Society for Bone and Mineral Research 22, 825-831.

Bruyere, O., Varela, A.R., Adami, S., Detilleux, J., Rabenda, V., Hiligsmann, M., Reginster, J.Y., 2009. Loss of hip bone mineral density over time is associated with spine and hip fracture incidence in osteoporotic postmenopausal women. European journal of epidemiology 24, 707-712.

Casalena, J.A., Badre-Alam, A., Ovaert, T.C., Cavanagh, P.R., Streit, D.A., 1998. The Penn State Safety Floor: Part II--Reduction of fall-related peak impact forces on the femur. J Biomech Eng 120, 527-532.

Cesari, D., Ramet, M., Clair, P., 1980. Evaluation of pelvic fracture tolerance in side impact.

Chapra, S.C., Canale, R., 2005. Numerical methods for engineers. McGraw-Hill, Inc.

Cheng, X.G., Lowet, G., Boonen, S., Nicholson, P.H., Brys, P., Nijs, J., Dequeker, J., 1997. Assessment of the strength of proximal femur in vitro: relationship to femoral bone mineral density and femoral geometry. Bone 20, 213-218.

Cho, S., Grazioso, R., Zhang, N., Aykac, M., Schmand, M., 2011. Digital timing: sampling frequency, anti-aliasing filter and signal interpolation filter dependence on timing resolution. Physics in medicine and biology 56, 7569-7583.

Choi, W.J., Hoffer, J.A., Robinovitch, S.N., 2010a. Effect of hip protectors, falling angle and body mass index on pressure distribution over the hip during simulated falls. Clin Biomech (Bristol, Avon) 25, 63-69.

Choi, W.J., Hoffer, J.A., Robinovitch, S.N., 2010b. The effect of positioning on the biomechanical performance of soft shell hip protectors. J Biomech 43, 818-825.

Cooper, G.J., Pearce, B.P., Stainer, M.C., Maynard, R.L., 1982. The biomechanical response of the thorax to nonpenetrating impact with particular reference to cardiac injuries. The Journal of trauma 22, 994-1008.

Cooper, G.J., Taylor, D.E., 1989. Biophysics of impact injury to the chest and abdomen. Journal of the Royal Army Medical Corps 135, 58-67.

Courtney, A.C., Wachtel, E.F., Myers, E.R., Hayes, W.C., 1994. Effects of loading rate on strength of the proximal femur. Calcified Tissue International 55, 53-58.

Courtney, A.C., Wachtel, E.F., Myers, E.R., Hayes, W.C., 1995. Age-related reductions in the strength of the femur tested in a fall-loading configuration. J Bone Joint Surg Am 77, 387-395.

Cummings, S.R., Melton, L.J., 2002. Epidemiology and outcomes of osteoporotic fractures. Lancet 359, 1761-1767.

Cummings, S.R., Nevitt, M.C., 1989. A hypothesis: the causes of hip fractures. J Gerontol 44, M107-111.

Cummings, S.R., Nevitt, M.C., 1994. Non-skeletal determinants of fractures: the potential importance of the mechanics of falls. Study of Osteoporotic Fractures Research Group. Osteoporosis international : a journal established as result of cooperation between the European Foundation for Osteoporosis and the National Osteoporosis Foundation of the USA 4 Suppl 1, 67-70.

De Laet, C., Kanis, J.A., Oden, A., Johanson, H., Johnell, O., Delmas, P., Eisman, J.A., Kroger, H., Fujiwara, S., Garnero, P., McCloskey, E.V., Mellstrom, D., Melton, L.J., 3rd, Meunier, P.J., Pols, H.A., Reeve, J., Silman, A., Tenenhouse, A., 2005. Body mass index as a predictor of fracture risk: a meta-analysis. Osteoporosis international : a journal established as result of cooperation between the European Foundation for Osteoporosis and the National Osteoporosis Foundation of the USA 16, 1330-1338.

DeGoede, K.M., Ashton-Miller, J.A., Liao, J.M., Alexander, N.B., 2001. How quickly can healthy adults move their hands to intercept an approaching object? Age and gender effects. The journals of gerontology. Series A, Biological sciences and medical sciences 56, M584-588.

Dhanwal, D.K., Cooper, C., Dennison, E.M., 2010. Geographic variation in osteoporotic hip fracture incidence: the growing importance of asian influences in coming decades. Journal of osteoporosis 2010, 757102.

Dhanwal, D.K., Dennison, E.M., Harvey, N.C., Cooper, C., 2011. Epidemiology of hip fracture: Worldwide geographic variation. Indian journal of orthopaedics 45, 15-22.

Dincel, V.E., Sengelen, M., Sepici, V., Cavusoglu, T., Sepici, B., 2008. The association of proximal femur geometry with hip fracture risk. Clin Anat 21, 575-580.

Dufour, A.B., Roberts, B., Broe, K.E., Kiel, D.P., Bouxsein, M.L., Hannan, M.T., 2012. The factor-of-risk biomechanical approach predicts hip fracture in men and women: the

Framingham Study. Osteoporosis international : a journal established as result of cooperation between the European Foundation for Osteoporosis and the National Osteoporosis Foundation of the USA 23, 513-520.

Durkin, J.L., Callaghan, J.P., 2005. Effects of minimum sampling rate and signal reconstruction on surface electromyographic signals. Journal of electromyography and kinesiology : official journal of the International Society of Electrophysiological Kinesiology 15, 474-481.

Efron, B., 1987. Better bootstrap confidence intervals. J Am Stat Assoc 82, 171-185.

Empana, J.P., Dargent-Molina, P., Breart, G., 2004. Effect of hip fracture on mortality in elderly women: the EPIDOS prospective study. J Am Geriatr Soc 52, 685-690.

Esses, S.I., Lotz, J.C., Hayes, W.C., 1989. Biomechanical properties of the proximal femur determined in vitro by single-energy quantitative computed tomography. Journal of bone and mineral research : the official journal of the American Society for Bone and Mineral Research 4, 715-722.

Etheridge, B.S., Beason, D.P., Lopez, R.R., Alonso, J.E., McGwin, G., Eberhardt, A.W., 2005. Effects of trochanteric soft tissues and bone density on fracture of the female pelvis in experimental side impacts. Ann Biomed Eng 33, 248-254.

Faul, F., Erdfelder, E., Buchner, A., Lang, A.G., 2009. Statistical power analyses using G*Power 3.1: tests for correlation and regression analyses. Behavior research methods 41, 1149-1160.

Feldman, F., Robinovitch, S.N., 2007. Reducing hip fracture risk during sideways falls: evidence in young adults of the protective effects of impact to the hands and stepping. Journal of Biomechanics 40, 2612-2618.

Ford, C.M., Keaveny, T.M., Hayes, W.C., 1996. The effect of impact direction on the structural capacity of the proximal femur during falls. Journal of bone and mineral research : the official journal of the American Society for Bone and Mineral Research 11, 377-383.

Fregly, B.J., Bei, Y., Sylvester, M.E., 2003. Experimental evaluation of an elastic foundation model to predict contact pressures in knee replacements. J Biomech 36, 1659-1668.

Fung, Y.C., 1993. Biomechanics : mechanical properties of living tissues, 2nd ed. Springer-Verlag, New York.

Gefen, A., 2007. Risk factors for a pressure-related deep tissue injury: a theoretical model. Medical & biological engineering & computing 45, 563-573.

Gnudi, S., Ripamonti, C., Lisi, L., Fini, M., Giardino, R., Giavaresi, G., 2002. Proximal femur geometry to detect and distinguish femoral neck fractures from trochanteric fractures in postmenopausal women. Osteoporosis international : a journal established as result of cooperation between the European Foundation for Osteoporosis and the National Osteoporosis Foundation of the USA 13, 69-73.

Greenspan, S.L., Myers, E.R., Maitland, L.A., Resnick, N.M., Hayes, W.C., 1994. Fall severity and bone mineral density as risk factors for hip fracture in ambulatory elderly. Journal of the American Medical Association 271, 128-133.

Grisso, J.A., Kelsey, J.L., Strom, B.L., Chiu, G.Y., Maislin, G., O'Brien, L.A., Hoffman, S., Kaplan, F., 1991. Risk factors for falls as a cause of hip fracture in women. The Northeast Hip Fracture Study Group. N Engl J Med 324, 1326-1331.

Haentjens, P., Autier, P., Barette, M., Venken, K., Vanderschueren, D., Boonen, S., 2007. Survival and functional outcome according to hip fracture type: a one-year prospective

cohort study in elderly women with an intertrochanteric or femoral neck fracture. Bone 41, 958-964.

Hayes, W., Myers, E., 1997. Biomechanical considerations of hip and spine fractures in osteoporotic bone. Instructional course lectures 46, 431.

Hayes, W.C., Myers, E.R., Robinovitch, S.N., Van Den Kroonenberg, A., Courtney, A.C., McMahon, T.A., 1996. Etiology and prevention of age-related hip fractures. Bone 18, 77S-86S.

Hayes, W.C., Piazza, S.J., Zysset, P.K., 1991. Biomechanics of fracture risk prediction of the hip and spine by quantitative computed tomography. Radiol Clin North Am 29, 1-18.

Hirokawa, S., 1991. Three-dimensional mathematical model analysis of the patellofemoral joint. J Biomech 24, 659-671.

Hopkins, R.B., Tarride, J.E., Leslie, W.D., Metge, C., Lix, L.M., Morin, S., Finlayson, G., Azimaee, M., Pullenayegum, E., Goeree, R., Adachi, J.D., Papaioannou, A., Thabane, L., 2012. Estimating the excess costs for patients with incident fractures, prevalent fractures, and nonfracture osteoporosis. Osteoporosis international : a journal established as result of cooperation between the European Foundation for Osteoporosis and the National Osteoporosis Foundation of the USA.

Horsman, A., Marshall, D.H., Peacock, M., 1985. A stochastic model of age-related bone loss and fractures. Clinical orthopaedics and related research, 207-215.

Howland, J., Lachman, M.E., Peterson, E.W., Cote, J., Kasten, L., Jette, A., 1998. Covariates of fear of falling and associated activity curtailment. Gerontologist 38, 549-555.

Hsiao, E.T., Robinovitch, S.N., 1998. Common protective movements govern unexpected falls from standing height. J Biomech 31, 1-9.

Ioannidis, G., Papaioannou, A., Hopman, W.M., Akhtar-Danesh, N., Anastassiades, T., Pickard, L., Kennedy, C.C., Prior, J.C., Olszynski, W.P., Davison, K.S., Goltzman, D., Thabane, L., Gafni, A., Papadimitropoulos, E.A., Brown, J.P., Josse, R.G., Hanley, D.A., Adachi, J.D., 2009. Relation between fractures and mortality: results from the Canadian Multicentre Osteoporosis Study. CMAJ 181, 265-271.

Ishimaru, D., Ogawa, H., Wakahara, K., Sumi, H., Sumi, Y., Shimizu, K., 2012. Hip pads reduce the overall risk of injuries in recreational snowboarders. British journal of sports medicine.

Jarvinen, T.L., Sievanen, H., Khan, K.M., Heinonen, A., Kannus, P., 2008. Shifting the focus in fracture prevention from osteoporosis to falls. Bmj 336, 124-126.

Jayne, B.C., Lauder, G.V., Reilly, S.M., Wainwright, P.C., 1990. The effect of sampling rate on the analysis of digital electromyograms from vertebrate muscle. The Journal of experimental biology 154, 557-565.

Jellesmark, A., Herling, S.F., Egerod, I., Beyer, N., 2012. Fear of falling and changed functional ability following hip fracture among community-dwelling elderly people: an explanatory sequential mixed method study. Disabil Rehabil.

Johnson, K.L., 1985. Contact mechanics. Cambridge University Press, Cambridge Cambridgeshire ; New York.

Kanis, J.A., Oden, A., McCloskey, E.V., Johansson, H., Wahl, D.A., Cooper, C., 2012. A systematic review of hip fracture incidence and probability of fracture worldwide. Osteoporosis international : a journal established as result of cooperation between the

European Foundation for Osteoporosis and the National Osteoporosis Foundation of the USA 23, 2239-2256.

Kannus, P., Parkkari, J., Poutala, J., 1999. Comparison of force attenuation properties of four different hip protectors under simulated falling conditions in the elderly: an in vitro biomechanical study. Bone 25, 229-235.

Keene, G.S., Parker, M.J., Pryor, G.A., 1993. Mortality and morbidity after hip fractures. Bmj 307, 1248-1250.

Kenzora, J.E., McCarthy, R.E., Lowell, J.D., Sledge, C.B., 1984. Hip fracture mortality. Relation to age, treatment, preoperative illness, time of surgery, and complications. Clinical orthopaedics and related research, 45-56.

Kessler, S.L., ASTM Committee D-20 on Plastics., 1987. Instrumented impact testing of plastics and composite materials : a symposium sponsored by ASTM Committee D-20 on Plastics, Houston, TX, 11-12 March 1985. ASTM, Philadelphia, PA.

Kim, J.E., Hsieh, M.H., Soni, B.K., Zayzafoon, M., Allison, D.B., 2013. Childhood obesity as a risk factor for bone fracture: a mechanistic study. Obesity (Silver Spring) 21, 1459-1466.

Koike, T., Orito, Y., Toyoda, H., Tada, M., Sugama, R., Hoshino, M., Nakao, Y., Kobayashi, S., Kondo, K., Hirota, Y., Takaoka, K., 2009. External hip protectors are effective for the elderly with higher-than-average risk factors for hip fractures. Osteoporosis international : a journal established as result of cooperation between the European Foundation for Osteoporosis and the National Osteoporosis Foundation of the USA 20, 1613-1620.

Koivumaki, J.E., Thevenot, J., Pulkkinen, P., Salmi, J.A., Kuhn, V., Lochmuller, E.M., Link, T.M., Eckstein, F., Jamsa, T., 2010. Does femoral strain distribution coincide with the

occurrence of cervical versus trochanteric hip fractures? An experimental finite element study. Medical & biological engineering & computing 48, 711-717.

Laing, A., Tootoonchi, I., Robinovitch, S., 2004. Design of compliant floors to reduce impact forces during falls on the hip. Proceedings of the 26th Annual Meeting of the American Society for Bone and Mineral Research, Oct 1-5, Seattle, WA.

Laing, A.C., Feldman, F., Jalili, M., Tsai, C.M., Robinovitch, S.N., 2011. The effects of pad geometry and material properties on the biomechanical effectiveness of 26 commercially available hip protectors. J Biomech 44, 2627-2635.

Laing, A.C., Robinovitch, S.N., 2006a. Hip protector biomechanical effectiveness: the influence of soft tissue stiffness. Osteoporosis International 17, Supplement 2, S107.

Laing, A.C., Robinovitch, S.N., 2006b. Soft shell hip protectors absorb energy and shunt impact force away from the trochanter during a fall. Journal of Biomechanics 39, Supplement 1, S90.

Laing, A.C., Robinovitch, S.N., 2008a. Effect of soft shell hip protectors on pressure distribution to the hip during sideways falls. Osteoporosis International 19, 1067-1075.

Laing, A.C., Robinovitch, S.N., 2008b. The force attenuation provided by hip protectors depends on impact velocity, pelvic size, and soft tissue stiffness. J Biomech Eng 130, 061005-061009.

Laing, A.C., Robinovitch, S.N., 2009. Low stiffness floors can attenuate fall-related femoral impact forces by up to 50% without substantially impairing balance in older women. Accid Anal Prev 41, 642-650.

Laing, A.C., Robinovitch, S.N., 2010. Characterizing the effective stiffness of the pelvis during sideways falls on the hip. J Biomech 43, 1898-1904.

Laing, A.C., Tootoonchi, I., Hulme, P.A., Robinovitch, S.N., 2006. Effect of compliant flooring on impact force during falls on the hip. J Orthop Res 24, 1405-1411.

Lauritzen, J.B., 1997. Hip fractures. Epidemiology, risk factors, falls, energy absorption, hip protectors, and prevention. Dan Med Bull 44, 155-168.

Lauritzen, J.B., Askegaard, V., 1992. Protection against hip fractures by energy absorption. Dan Med Bull 39, 91-93.

Lauritzen, J.B., Petersen, M.M., Lund, B., 1993. Effect of external hip protectors on hip fractures. Lancet 341, 11-13.

Lawton, J.O., Baker, M.R., Dickson, R.A., 1983. Femoral neck fractures--two populations. Lancet 2, 70-72.

Leslie, W.D., Metge, C.J., Azimaee, M., Lix, L.M., Finlayson, G.S., Morin, S.N., Caetano, P., 2011. Direct costs of fractures in Canada and trends 1996-2006: a population-based cost-of-illness analysis. Journal of bone and mineral research : the official journal of the American Society for Bone and Mineral Research 26, 2419-2429.

Leslie, W.D., O'Donnell, S., Jean, S., Lagace, C., Walsh, P., Bancej, C., Morin, S., Hanley, D.A., Papaioannou, A., 2009. Trends in hip fracture rates in Canada. Jama 302, 883-889.

Levine, I.C., Bhan, S., Laing, A.C., 2013. The effects of body mass index and sex on impact force and effective pelvic stiffness during simulated lateral falls. Clinical Biomechanics 28, 1026-1033.

Levine, I.C.L., 2011. The Effects of Body Mass Index and Gender on Pelvic Stiffness and Peak Impact Force During Lateral Falls. Univeristy of Waterloo.

Lotz, J.C., Hayes, W.C., 1990. The use of quantitative computed tomography to estimate risk of fracture of the hip from falls. J Bone Joint Surg Am 72, 689-700.

Maitland, L.A., Myers, E.R., Hipp, J.A., Hayes, W.C., Greenspan, S.L., 1993. Read my hips: measuring trochanteric soft tissue thickness. Calcif Tissue Int 52, 85-89.

Majumder, S., Roychowdhury, A., Pal, S., 2007. Simulation of hip fracture in sideways fall using a 3D finite element model of pelvis-femur-soft tissue complex with simplified representation of whole body. Medical engineering & physics 29, 1167-1178.

Majumder, S., Roychowdhury, A., Pal, S., 2008. Effects of trochanteric soft tissue thickness and hip impact velocity on hip fracture in sideways fall through 3D finite element simulations. J Biomech 41, 2834-2842.

Maki, B.E., Fernie, G.R., 1990. Impact attenuation of floor coverings in simulated falling accidents. Applied Ergonomics 21, 107-114.

Marks, R., Allegrante, J.P., Ronald MacKenzie, C., Lane, J.M., 2003. Hip fractures among the elderly: causes, consequences and control. Ageing research reviews 2, 57-93.

Matsui, Y., Kajzer, J., Wittek, A., Ishikawa, H., Schroeder, G., Bosch, U., 2003. Injury pattern and tolerance of human pelvis under lateral loading simulating simulating car-pedestrian impact. SAE Technical Series - 2003-01-0165, 1-10.

Mautalen, C.A., Vega, E.M., 1993. Different characteristics of cervical and trochanteric hip fractures. Osteoporosis international : a journal established as result of cooperation between

the European Foundation for Osteoporosis and the National Osteoporosis Foundation of the USA 3 Suppl 1, 102-105.

McColl, A., Roderick, P., Cooper, C., 1998. Hip fracture incidence and mortality in an English Region: a study using routine National Health Service data. Journal of public health medicine 20, 196-205.

Melton, L.J., 3rd, 1993. Hip fractures: a worldwide problem today and tomorrow. Bone 14 Suppl 1, S1-8.

Melton, L.J., 3rd, 2000. Who has osteoporosis? A conflict between clinical and public health perspectives. Journal of bone and mineral research : the official journal of the American Society for Bone and Mineral Research 15, 2309-2314.

Meyer, H.E., Falch, J.A., O'Neill, T., Tverdal, A., Varlow, J., 1995a. Height and body mass index in Oslo, Norway, compared to other regions of Europe: do they explain differences in the incidence of hip fracture? European Vertebral Osteoporosis Study Group. Bone 17, 347-350.

Meyer, H.E., Tverdal, A., Falch, J.A., 1995b. Body height, body mass index, and fatal hip fractures: 16 years' follow-up of 674,000 Norwegian women and men. Epidemiology 6, 299-305.

Meyer, H.E., Tverdal, A., Falch, J.A., Pedersen, J.I., 2000. Factors associated with mortality after hip fracture. Osteoporosis International 11, 228-232.

Morin, S., Tsang, J.F., Leslie, W.D., 2009. Weight and body mass index predict bone mineral density and fractures in women aged 40 to 59 years. Osteoporosis international : a journal established as result of cooperation between the European Foundation for Osteoporosis and the National Osteoporosis Foundation of the USA 20, 363-370.

Nabhani, F., Bamford, J., 2002. Mechanical testing of hip protectors. J Mater Process Tech 124, 311-318.

Nahum, A.M., Gadd, C.W., Schneider, D.C., Kroell, C.K., 1971. The biomechanical basis for chest impact protection. I. Force-deflection characteristics of the thorax. The Journal of trauma 11, 874-882.

Nankaku, M., Kanzaki, H., Tsuboyama, T., Nakamura, T., 2005. Evaluation of hip fracture risk in relation to fall direction. Osteoporosis international : a journal established as result of cooperation between the European Foundation for Osteoporosis and the National Osteoporosis Foundation of the USA 16, 1315-1320.

Nevitt, M.C., Cummings, S.R., 1993. Type of fall and risk of hip and wrist fractures: the study of osteoporotic fractures. The Study of Osteoporotic Fractures Research Group. J Am Geriatr Soc 41, 1226-1234.

Nilson, F., Moniruzzaman, S., Gustavsson, J., Andersson, R., 2012. Trends in hip fracture incidence rates among the elderly in Sweden 1987-2009. J Public Health (Oxf).

Norton, R., Butler, M., Robinson, E., Lee-Joe, T., Campbell, A.J., 2000. Declines in physical functioning attributable to hip fracture among older people: a follow-up study of case-control participants. Disabil Rehabil 22, 345-351.

Omsland, T.K., Holvik, K., Meyer, H.E., Center, J.R., Emaus, N., Tell, G.S., Schei, B., Tverdal, A., Gjesdal, C.G., Grimnes, G., Forsmo, S., Eisman, J.A., Sogaard, A.J., 2012. Hip fractures in Norway 1999-2008: time trends in total incidence and second hip fracture rates. A NOREPOS study. European journal of epidemiology.

Pande, I., O'Neill, T.W., Pritchard, C., Scott, D.L., Woolf, A.D., 2000. Bone mineral density, hip axis length and risk of hip fracture in men: results from the Cornwall Hip Fracture Study.

Osteoporosis international : a journal established as result of cooperation between the European Foundation for Osteoporosis and the National Osteoporosis Foundation of the USA 11, 866-870.

Papadimitropoulos, E.A., Coyte, P.C., Josse, R.G., Greenwood, C.E., 1997. Current and projected rates of hip fracture in Canada. CMAJ 157, 1357-1363.

Partanen, J., Jamsa, T., Jalovaara, P., 2001. Influence of the upper femur and pelvic geometry on the risk and type of hip fractures. Journal of bone and mineral research : the official journal of the American Society for Bone and Mineral Research 16, 1540-1546.

Pinilla, T.P., Boardman, K.C., Bouxsein, M.L., Myers, E.R., Hayes, W.C., 1996. Impact direction from a fall influences the failure load of the proximal femur as much as age-related bone loss. Calcif Tissue Int 58, 231-235.

Pruzansky, M.E., Turano, M., Luckey, M., Senie, R., 1989. Low body weight as a risk factor for hip fracture in both black and white women. J Orthop Res 7, 192-197.

Pulkkinen, P., Eckstein, F., Lochmuller, E.M., Kuhn, V., Jamsa, T., 2006. Association of geometric factors and failure load level with the distribution of cervical vs. trochanteric hip fractures. Journal of bone and mineral research : the official journal of the American Society for Bone and Mineral Research 21, 895-901.

Robinovitch, S.N., Feldman, F., Wan, D., Aziz, O., Sarraf, T., 2009. Video recording of real-life falls in long term care provides new insight on the cause and circumstances of falls in older adults. In: Proceedings of the 19th Annual Meeting of the International Society for Posture and Gait. June 21-25. Bologna, Italy.

Robinovitch, S.N., Hayes, W.C., McMahon, T.A., 1991. Prediction of femoral impact forces in falls on the hip. J Biomech Eng 113, 366-374.

Robinovitch, S.N., Hayes, W.C., McMahon, T.A., 1995a. Energy-shunting hip padding system attenuates femoral impact force in a simulated fall. J Biomech Eng 117, 409-413.

Robinovitch, S.N., Hayes, W.C., McMahon, T.A., 1997a. Distribution of contact force during impact to the hip. Annals of Biomedical Engineering 25, 499-508.

Robinovitch, S.N., Hayes, W.C., McMahon, T.A., 1997b. Predicting the impact response of a nonlinear single-degree-of-freedom shock-absorbing system from the measured step response. J Biomech Eng 119, 221-227.

Robinovitch, S.N., McMahon, T.A., Hayes, W.C., 1995b. Force attenuation in trochanteric soft tissues during impact from a fall. J Orthop Res 13, 956-962.

Robinovitch, S.N., Normandin, S.C., Stotz, P., Maurer, J.D., 2005. Time requirement for young and elderly women to move into a position for breaking a fall with outstretched hands. The journals of gerontology. Series A, Biological sciences and medical sciences 60, 1553-1557.

Sandler, R., Robinovitch, S., 2001. An analysis of the effect of lower extremity strength on impact severity during a backward fall. J Biomech Eng 123, 590-598.

Sattin, R.W., 1992. Falls among older persons: a public health perspective. Annual review of public health 13, 489-508.

Schmitt, K.U., Schlittler, M., Boesiger, P., 2010. Biomechanical loading of the hip during side jumps by soccer goalkeepers. Journal of sports sciences 28, 53-59.

Sellier, K., 1965. [On the mechanics of bone fracture]. Deutsche Zeitschrift fur die gesamte gerichtliche Medizin 56, 341-348.

Shannon, C.E., 1949. Communication in the Presence of Noise. Proceedings of the IRE 37, 11.

Simpson, A.H., Lamb, S., Roberts, P.J., Gardner, T.N., Evans, J.G., 2004. Does the type of flooring affect the risk of hip fracture? Age Ageing 33, 242-246.

Siris, E.S., Chen, Y.T., Abbott, T.A., Barrett-Connor, E., Miller, P.D., Wehren, L.E., Berger, M.L., 2004. Bone mineral density thresholds for pharmacological intervention to prevent fractures. Arch Intern Med 164, 1108-1112.

SMARTRISK, 2009. The Economic Burden of Injury in Canada. SMARTRISK: Toronto, ON.

Song, E., Trosseille, X., Baudrit, P., 2009. Evaluation of thoracic deflection as an injury criterion for side impact using a finite elements thorax model. Stapp car crash journal 53, 155-191.

Sran, M.M., Robinovitch, S.N., 2008. Preventing fall-related vertebral fractures: effect of floor stiffness on peak impact forces during backward falls. Spine 33, 1856-1862.

Stolee, P., Poss, J., Cook, R.J., Byrne, K., Hirdes, J.P., 2009. Risk factors for hip fracture in older home care clients. The journals of gerontology. Series A, Biological sciences and medical sciences 64, 403-410.

Thelen, D.G., Wojcik, L.A., Schultz, A.B., Ashton-Miller, J.A., Alexander, N.B., 1997. Age differences in using a rapid step to regain balance during a forward fall. The journals of gerontology. Series A, Biological sciences and medical sciences 52, M8-13.

Tinetti, M.E., Speechley, M., Ginter, S.F., 1988. Risk factors for falls among elderly persons living in the community. New England Journal of Medicine 319, 1701-1707.

van den Kroonenberg, A.J., Hayes, W.C., McMahon, T.A., 1995. Dynamic models for sideways falls from standing height. J Biomech Eng 117, 309-318.

van den Kroonenberg, A.J., Hayes, W.C., McMahon, T.A., 1996. Hip impact velocities and body configurations for voluntary falls from standing height. Journal of Biomechanics 29, 807-811.

van Schoor, N.M., van der Veen, A.J., Schaap, L.A., Smit, T.H., Lips, P., 2006. Biomechanical comparison of hard and soft hip protectors, and the influence of soft tissue. Bone 39, 401-407.

Viano, D.C., 1988. Cause and control of automotive trauma. Bulletin of the New York Academy of Medicine 64, 376-421.

Viano, D.C., Lau, I.V., Andrzejak, D.V., Asbury, C., 1989a. Biomechanics of injury in lateral impacts. Accident; analysis and prevention 21, 535-551.

Viano, D.C., Lau, I.V., Asbury, C., King, A.I., Begeman, P., 1989b. Biomechanics of the human chest, abdomen, and pelvis in lateral impact. Accident; analysis and prevention 21, 553-574.

Viano, D.C., Lau, V.K., 1983. Role of impact velocity and chest compression in thoracic injury. Aviation, space, and environmental medicine 54, 16-21.

Visschedijk, J., Achterberg, W., Van Balen, R., Hertogh, C., 2010. Fear of falling after hip fracture: a systematic review of measurement instruments, prevalence, interventions, and related factors. J Am Geriatr Soc 58, 1739-1748.

Wainwright, S.A., Marshall, L.M., Ensrud, K.E., Cauley, J.A., Black, D.M., Hillier, T.A., Hochberg, M.C., Vogt, M.T., Orwoll, E.S., 2005. Hip fracture in women without osteoporosis. J Clin Endocrinol Metab 90, 2787-2793.

Winter, D.A., 2005. Biomechanics and motor control of human movement, 3rd ed. John Wiley & Sons, Hoboken, New Jersey.

Winter, D.A., Patla, A.E., 1997. Signal processing and linear systems for the movement sciences. Waterloo Biomechanics.

Wojcik, L.A., Thelen, D.G., Schultz, A.B., Ashton-Miller, J.A., Alexander, N.B., 1999. Age and gender differences in single-step recovery from a forward fall. The journals of gerontology. Series A, Biological sciences and medical sciences 54, M44-50.

Wojcik, L.A., Thelen, D.G., Schultz, A.B., Ashton-Miller, J.A., Alexander, N.B., 2001. Age and gender differences in peak lower extremity joint torques and ranges of motion used during single-step balance recovery from a forward fall. J Biomech 34, 67-73.

Wolinsky, F.D., Fitzgerald, J.F., Stump, T.E., 1997. The effect of hip fracture on mortality, hospitalization, and functional status: a prospective study. Am J Public Health 87, 398-403.

Yoon, H.K., Park, C., Jang, S., Lee, Y.K., Ha, Y.C., 2011. Incidence and mortality following hip fracture in Korea. Journal of Korean medical science 26, 1087-1092.

Zuckerman, J.D., 1996. Hip fracture. N Engl J Med 334, 1519-1525.

Appendix A

Synchronization and Drift Between OPT and HSV

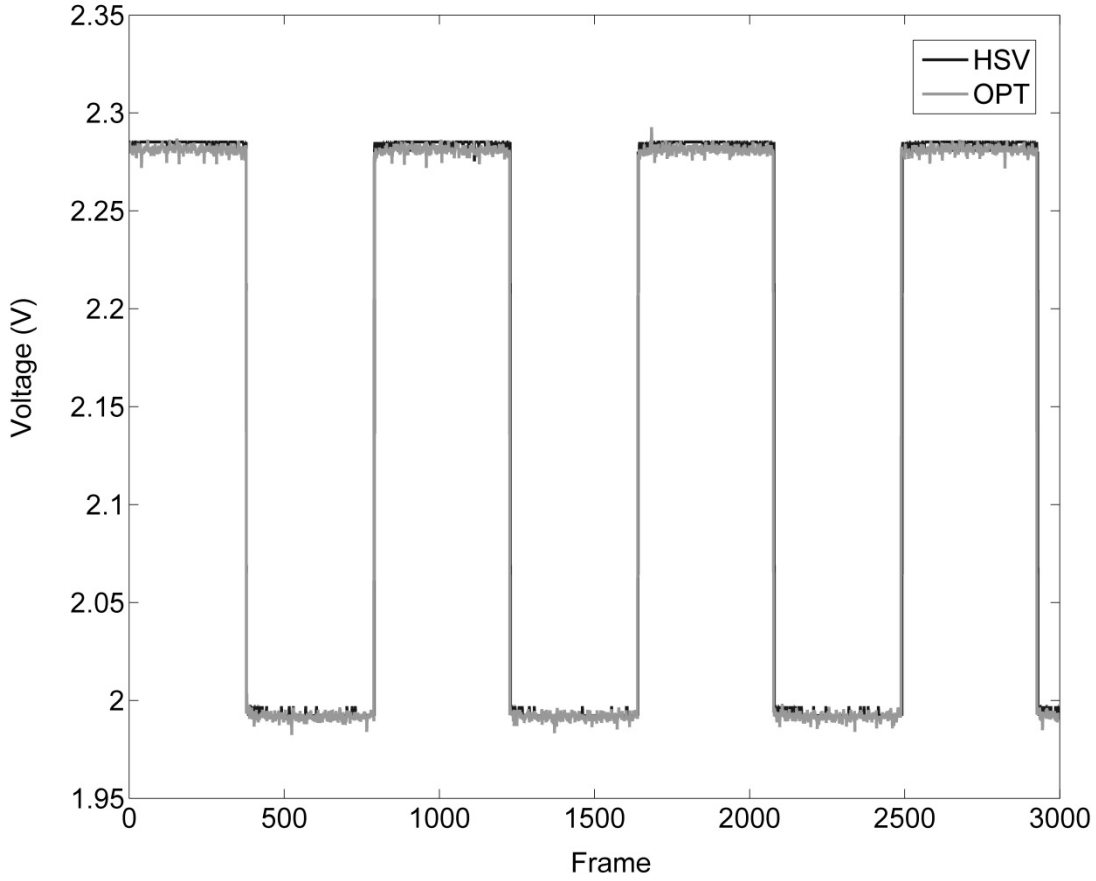

Figure 0.1: Representative square wave trial used to assess the synchronization of the OPT and HSV system by external trigger. Black tracing shows the square wave as measured by HSV, while the grey tracing shows that measured by the OPT.

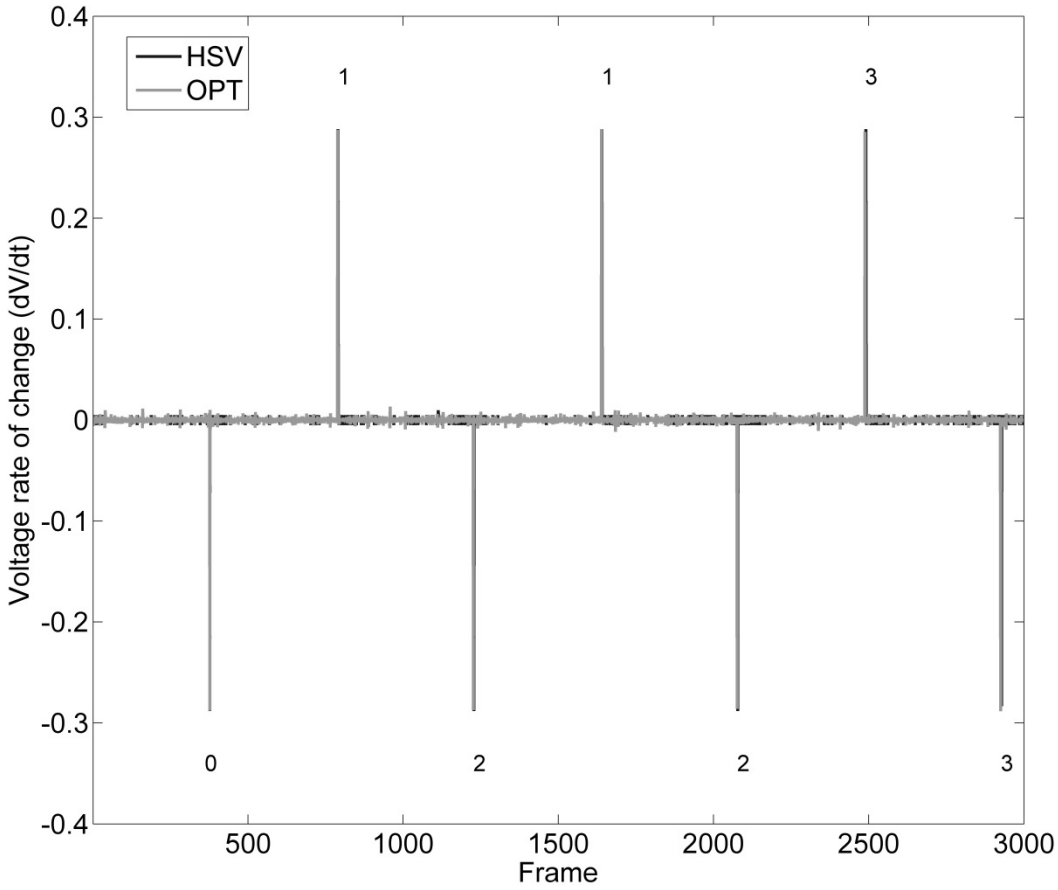

Figure 0.2: Representative derivatives of the square wave trials shown in Figure 5.1. The spikes indicate where the square wave changed levels. Numbers indicate the difference in time of pulse measured between systems (by frame). Positive numbers indicate that the HSV measured a change in the square wave later than the OPT. Black tracing shows the square wave as measured by HSV, while the grey tracing shows that measured by the OPT.

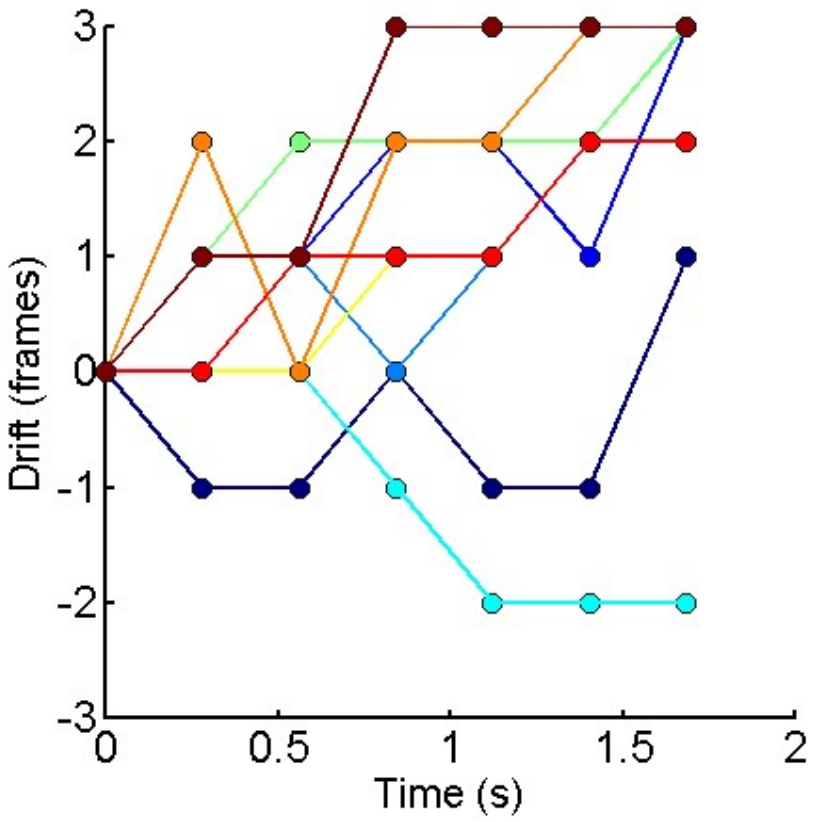

Figure 0.3: Change in agreement between systems as a function of collection duration. Each trace is from a separate pilot trial (colour coded). Positive values indicate that HSV measured a change in square wave voltage later than the OPT (vice versa for the negative values). Notice how drift increases as a function of time, but the direction of the drift is not systematic, meaning in some trials the OPT was faster (negative values), while in other the HSV was faster.

Appendix B

Empirical Cumulative Distributions

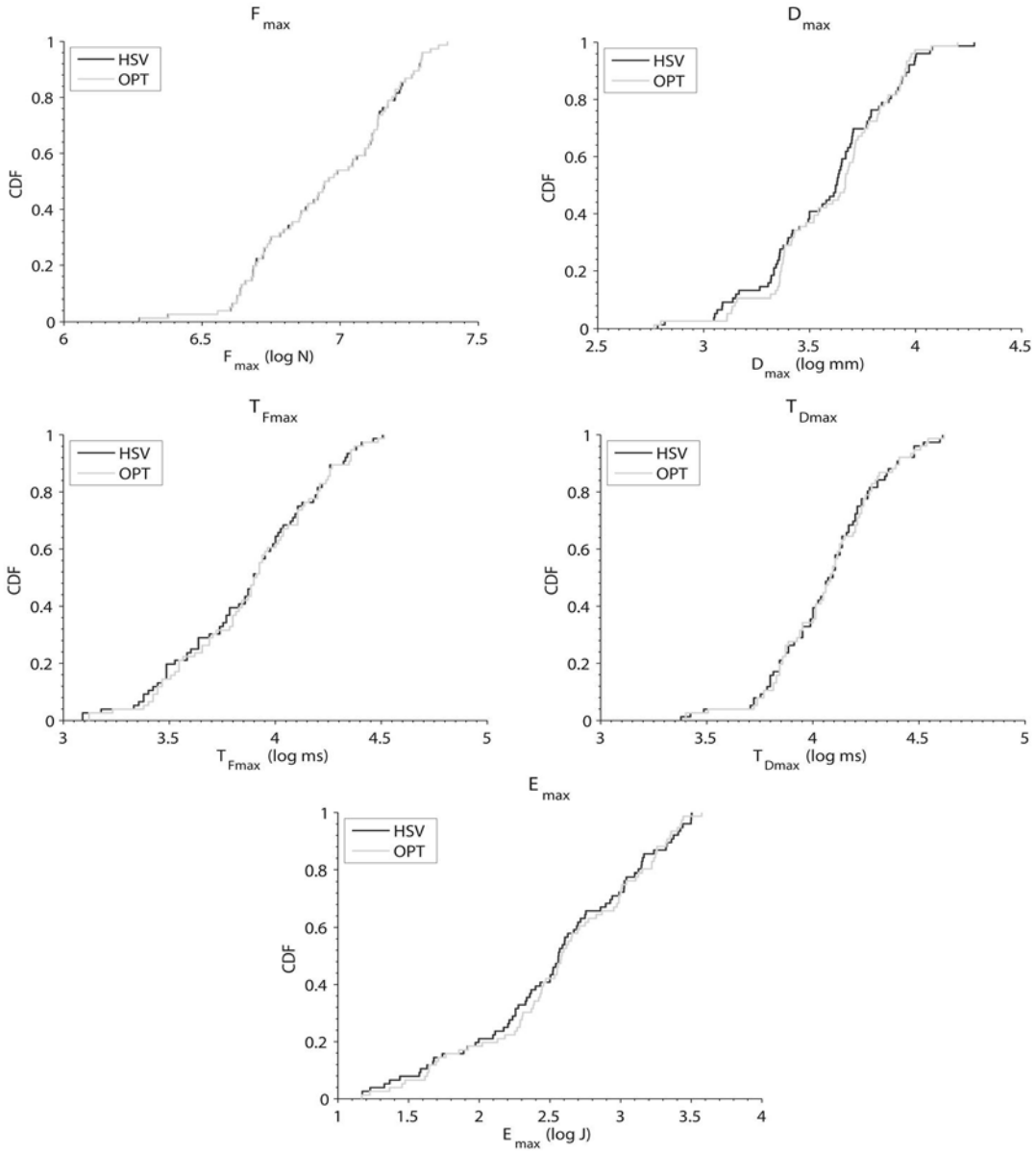

Figure 0.4: Empirical cumulative distributions for each dependent variable of interest. The abscissa of each plot is logarithmic to allow for better visualization of the differences between systems at end ranges. Dark black lines depict measurements from the HSV system, and grey lines depict the OPT.

Appendix C

Contingency Table Analysis

	Negative T_{Fmax}	Non-negative T_{Fmax}	Total
Negative E_{max}	42	19	61
Non-negative E_{max}	14	14	28
Total	56	33	89

There was not a significant association between a negative T_{Fmax} value and a negative E_{max} (χ^2 (1) = 2.92, p = 0.10). In this analysis, "Negative" values were defined as those which were below zero. Values that were defined as "non-negative" made up all other measurements (including those which were zero). The assumption was that if a difference in measured energy absorption was directly due to an increased time to peak force, then there would be a significant association between the two. However, in this first level analysis it seems that the additional energy absorption measured by the Optotrak system is not related to the increased time to peak force measured by Optotrak.

Appendix D

Non-constant Errors in Deflection and Trapezoidal Integration

A possible cause of disagreement between both motion capture systems for energy absorption can arise when the differences between systems in measuring deflection are non-constant—i.e. the differences change over the duration of the deflection. To illustrate this, three separate theoretical difference traces were created to mimic some of the extreme time-varying differences seen between systems in this thesis (Figure 3.10). Each one of these traces was added to a deflection trial from a participant in this study (5cm drop height). Subsequently, the energy absorption was calculated for this altered trace and the energy absorbance was compared to the unadjusted trace. The overall peak differences for each "error" trace are not relatively high (0.25, 0.68, 1.31 mm), but the resulting energy differences can lead to similar disagreement to that seen between OPT and HSV.

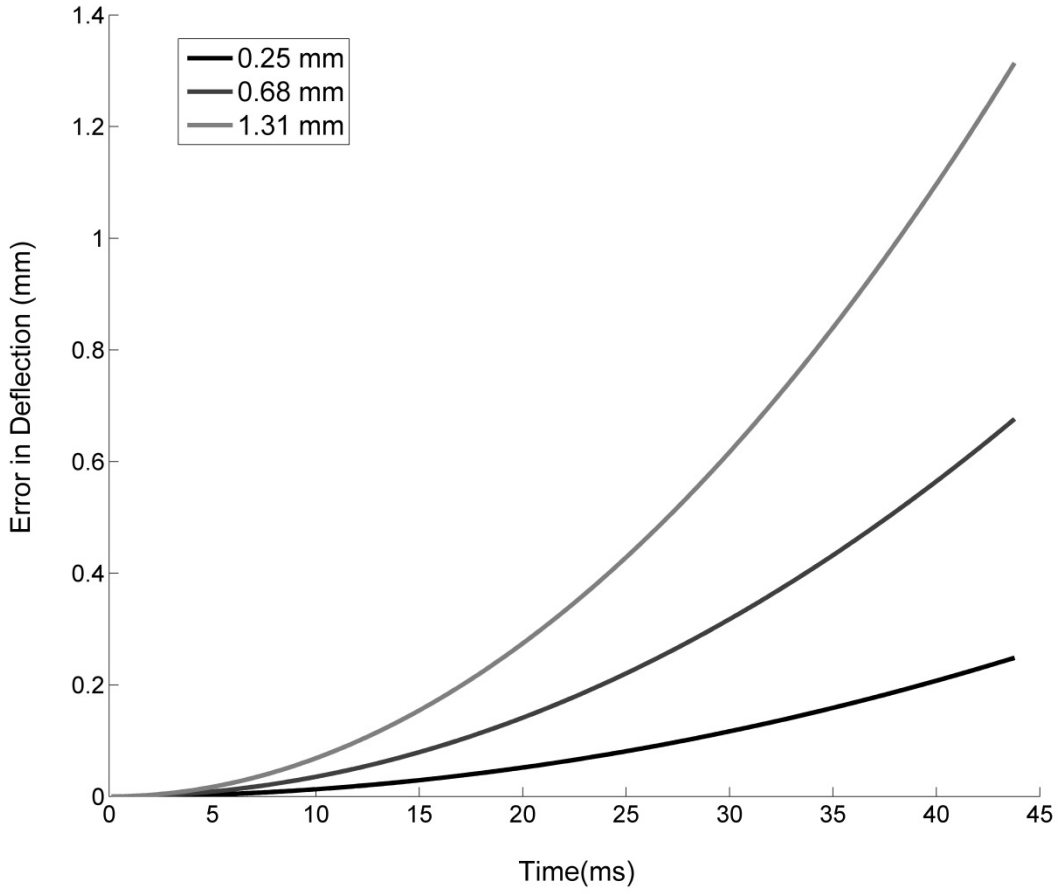

Figure 0.5: Three difference traces that were created to simulate non-constant difference between systems. Separately, each one of these traces was added to an actual collected deflection trial from a participant. Subsequently, the energy absorbance was calculated. This was then compared to the energy calculated for the unadjusted force deflection trial (See Figure 4.13).

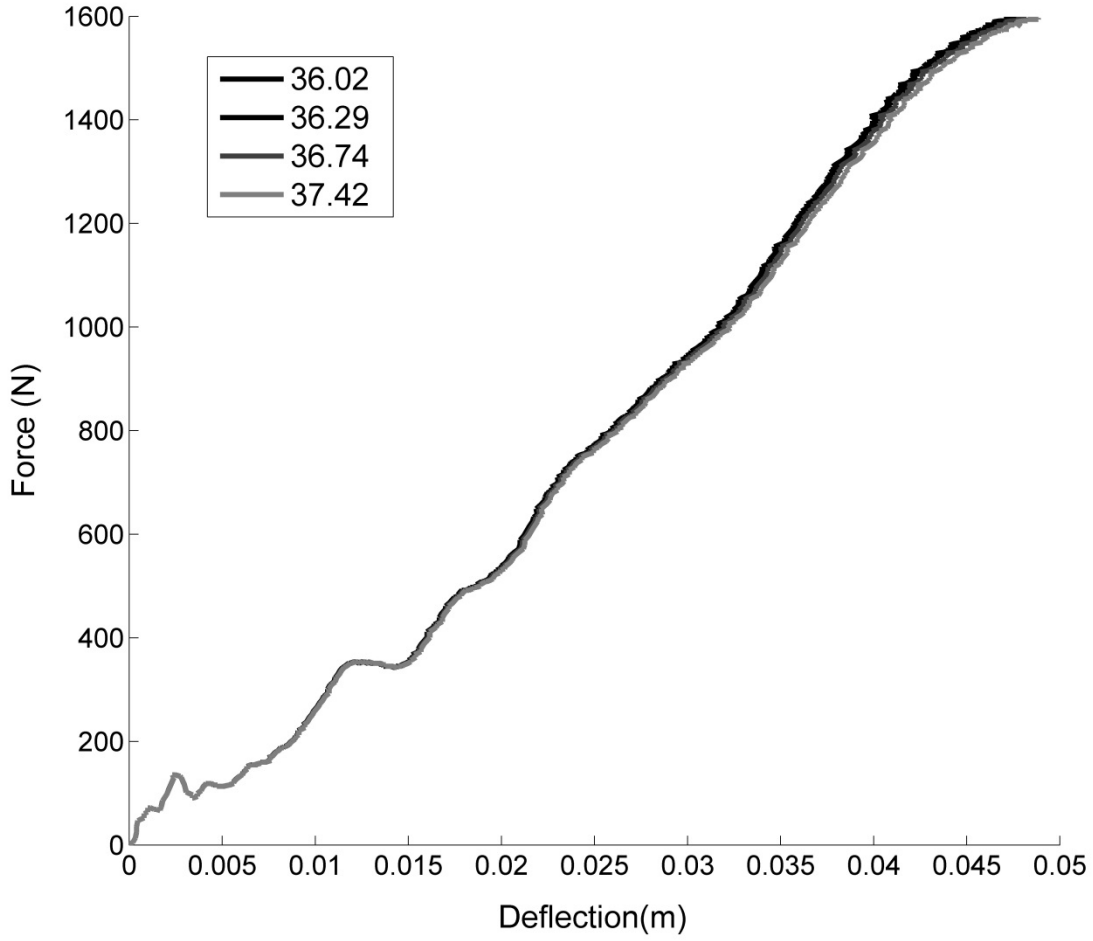

Figure 0.6: Force deflection tracings for four separate trials. The black trial is an actual impact trial measured in this study. The rest of the trials (three in total) are hypothetical force deflection tracings if the deflection had an additional error in it. The peak deflection error for each force deflection trace corresponds with the trace in Figure 4.12. Values in the legend are energy calculations for that corresponding force deflection trace.

Table 0-1: Anthropometrics for every participant in collected in this study. Also reported are mean, standard deviation (SD) and coefficient of variation (COV) for each anthropometric measure.

Participant	*Age*	*Height (cm)*	*Mass (kg)*	*BMI (kg/m^2)*	*M_{eff} (kg)*
1	20	174.0	66.0	21.8	12.5
2	31	165.0	50.0	18.4	11.1
3	21	169.0	60.0	21.0	12.4
4	23	179.0	76.0	23.7	13.3
5	23	169.0	66.0	23.1	13.7
6	21	172.0	91.0	30.8	17.9
7	26	173.0	67.5	22.6	13.0
8	26	156.0	52.0	21.4	13.7
9	25	159.0	52.0	20.6	12.9
10	22	167.0	67.0	24.0	14.4
11	28	174.0	70.0	23.1	13.3
12	29	162.0	65.0	24.8	15.3
13	23	160.0	69.0	27.0	16.8
14	21	172.0	59.0	19.9	11.6
15	25	163.0	55.0	20.7	12.7
16	22	161.0	86.0	33.2	20.6
17	28	175.0	87.0	28.4	16.2
18	28	171.5	77.0	26.2	15.3
19	22	156.0	50.0	20.5	13.2
20	22	162.0	79.0	30.1	18.6
Mean	24.3	167.0	67.2	24.1	14.4
SD	3.2	6.8	12.5	4.0	2.5
COV	13.1	4.1	18.6	16.7	17.2